DEPARTMENT OF THE AIR FORCE

AIR UNIVERSITY

AIR FORCE INSTITUTE OF TECHNOLOGY

Wright-Patterson Air Force Base, Ohio

AFIT/GE/ENG/88D-19

FLIGHT CONTROLLER DESIGN WITH NONLINEAR AERODYNAMICS, LARGE PARAMETER UNCERTAINTY, AND PILOT COMPENSATION

THESIS

Thomas John Kobylarz
First Lieutenant, USAF

AFIT/GE/ENG/88D-19

Approved for public release; distribution unlimited

AFIT/GE/ENG/88D-19

FLIGHT CONTROLLER DESIGN WITH NONLINEAR AERODYNAMICS, LARGE PARAMETER UNCERTAINTY, AND PILOT COMPENSATION

THESIS

Presented to the Faculty of the School of Engineering
of the Air Force Institute of Technology
Air University
In Partial Fulfillment of the
Requirements for the Degree of
Master of Science in Electrical Engineering

Thomas John Kobylarz, B.S.E.E.
First Lieutenant, USAF

December, 1988

Accession For	
NTIS GRA&I	X
DTIC TAB	☐
Unannounced	☐
Justification	
By	
Distribution/	
Availability Codes	
Dist	Avail and/or Special
A-1	

Acknowledgments

I would like to thank all my instructors at AFIT for providing me with the foundation for completing this research, especially my thesis committee, Dr. Constantine Houpis, Dr. Issac Horowitz and Lt Col Zdzislaw Lewantowicz. Without them this thesis would have never been completed. The weekend *discussions* with Dr. Horowitz were invaluable for the insight into the problem they provided to both of us, thanks again. Thanks to Finley Barfield whose guidance kept these results in line with reality.

Never ending thanks goes out to my beautiful wife [redacted] for forcing me to sit down and complete this work, as well as providing me with a list of home improvements to breakup the monotony of such a large task. Of course a can't leave out the kids; thanks [redacted] and [redacted] and to all the guys on the Hockey, Football, and Softball teams, thanks for letting me bang my head a little.

To my classmates Captains Kurt Neumann and Daryl Hammond a special thanks goes out for the enlightening conversions at the annex. To Ron L, Larry, Dave, Brian, Steve, and Chuck, what's life without a little fun.

Finally, I would like to dedicate this work to my loving mother [redacted] for 25 years of inspiration.

Thomas John Kobylarz

Table of Contents

List of Figures

List of Tables

Abstract

Nonlinear Quantitative Feedback Theory (QFT), developed by Dr. Isaac Horowitz, is used to design a flight control system for the YF-16 aircraft. Upon completing this stability augmentation system (SAS) additional compensation is added to reduce pilot workload while improving handling qualities.

The YF-16 uncertain plant is simulated with C^* (a blend of normal acceleration at pilot station and pitch rate) as the controlled output. The simulation includes the full six degree of freedom nonlinear dynamic equations of motion and aerodynamic data throughout the entire subsonic flight envelope. A technique is presented which enables the uncertain nonlinear YF-16 to be represented as a set of linear time-invariant plants which is equivalent to the nonlinear plant with respect to the set of acceptable outputs. Once this set of plants is obtained, a linear QFT controller is synthesized yielding fixed compensation which is extremely insensitive to varying flight conditions.

Given the aircraft and resulting flight controller, additional compensation is generated which accounts for the man-in-the-loop. The Neal-Smith pilot model for a compensatory tracking task is used to develope a technique which allows the designer to synthesize compensation which minimizes pilot workload, increases system bandwidth, and improves handling qualities ratings. The presented technique is applicable to other aircraft and pilot tasks, possessing a similar pilot model, given the desired standards of performance. This technique can be used at the earliest stages of flight control design phase thus saving time and money over the current practice.

Simulations in the time and frequency domains demonstrate that the desired performance is attained. Further work with real-time man-in-the-loop simulations should be accomplished to expand the area of pilot compensation.

FLIGHT CONTROLLER DESIGN WITH NONLINEAR AERODYNAMICS, LARGE PARAMETER UNCERTAINTY, AND PILOT COMPENSATION

I. Background

Introduction

The design of a flight control system which allows the pilot to maneuver an aircraft to desired flight paths is a major task. The maneuverability and speeds required of modern aircraft place forces on the airframe that are too large for the pilot to control. Also, the dynamic responses of the basic airframe are usually unsatisfactory, even to the point of being so unstable that the aircraft is totally uncontrollable by the pilot alone. The flight controller aids the pilot in performing the tasks which allow him to accomplish the mission.

In order to design the controller, extensive modeling of the aircraft dynamics is required, including the aerodynamic forces. The parameters in these models vary drastically from one flight condition to another and are not precisely known for any given flight condition. Research has shown that the flight controller design must be sufficiently robust to handle these parameter variations if the desired performance is to be obtained over a variety of flight conditions [19].

For certain missions the models of the aircraft system are also highly nonlinear, with uncertain model parameters which challenges the engineer because the mathematical analysis tools available are limited. Nonlinear quantitative feedback theory allows the controls engineer to take both of these aspects into account at the onset of the design and guarantees that the design will be acceptable for the stated problem.

Problem Statement

This thesis uses nonlinear quantitative feedback theory to design a controller for the YF-16 allowing the pilot to control C^*, which is a handling qualities measure of the normal acceleration felt at the pilot station blended with pitch rate. The controller is to provide an acceptable output to a given set of inputs regardless of the aircraft parameters. In addition to this stability augmentation system (SAS) an outer loop consisting of compensation to reduce pilot work load is designed. The addition of this compensation is to yield good handling quality ratings and increase the bandwidth of the pilot-aircraft system.

Review of Current Literature

The design of a flight controller for an aircraft is a problem of regulation and control, despite parameter uncertainty and disturbances [8]. The mathematical relationships between the pilot's inputs and the output variables are highly nonlinear as well as possessing parameters that are functions of the aircraft's flight conditions. These parameters vary significantly throughout a flight regime and in this study it is assumed that air data measurements are not being made to determine their values. These values would not be precisely known even if such measurements are made during flight, but the resulting residual uncertainty would be much less then in the former case. [3]. There is also the existence of unknown external disturbances, such as wind gusts, whose effect on the aircraft performance must be suitably small [14].

Current Approach. Presently, there is no complete synthesis theory for this problem. Barfield [1] stated that existing flight controllers are based upon various design techniques depending on the task. Most of the controller is designed around approximated linear, time-invariant models of the aircraft. A large number of these models are then generated to approximate various flight conditions which

the aircraft experiences while in flight. A flight controller is designed for each of these models and stored in the on-board memory of the plane's computers. While in flight, the computer chooses the controller designed for the model that is closest to the current flight conditions [1]. Houpis [14] has indicated that describing function theory has been used for nonlinearities only to test for overall system stability. The bottom line is that current, highly nonlinear aircraft are treated as linear systems in the hope that the aircraft flight condition does not deviate too far from the approximations [14]. Quinlivan has demonstrated that during violent maneuvering, the approximations are violated. The current solution to this problem is to define even more models for the aircraft during maneuvers in air-to-air scenarios. The extra models add to the number of controllers to be designed to the point that different flying modes must be selected by the pilot to achieve acceptable responses for different tasks [19].

Current Techniques. Given the chosen models to represent the aircraft, many techniques exist to solve the resulting linear, time-invariant problem. Horowitz and Shaked concluded that the superiority of the transfer function over the state- variable method explains why most designs are accomplished using classical techniques. Bode plots and root locus analysis give insight to the engineer which is hidden in the state space representation [9].

Although the added insight gained through the use of classical analysis reduces iterations, both approaches require extensive simulation and trial-and-error modifications. Horowitz, *et al.*, claimed existing designs, "...have worked because of the ingenuity of practical designers and the inherent power of feedback; but a great deal of cut and try design is essential" [8].

Uncertain vs. Deterministic Models. Horowitz, *et al.*, suggested that the situation is caused by an almost total neglect of quantitative feedback synthesis theory (QFT) in current designs [8]. Both classical and modern state-variable

techniques concentrate on a design to achieve the desired output for a fixed, or deterministic, model which represents the aircraft. The QFT technique provides a single design to give an acceptable range of outputs over the entire range of uncertainty of the model parameters [14].

For example, consider the following transfer function model for a system:

$$P(s) = \frac{K}{As^2 + Bs + C} \tag{1.1}$$

where A, B, C and K are the model's parameters. Using classical or modern techniques requires all parameters to be constants. If a single parameter changes, a new design is required. Using QFT, all four parameters have a specified range. A design is generated with fixed compensators that is guaranteed to work for any combination of the parameters over their individual intervals, allowing for an infinite number of possibilities [13].

The Quantitative Approach. The QFT technique is summarized in a technical report [13] for Air Force Wright Aeronautical Labs (AFWAL) which provides a single document from which future designs can be referenced. The entire design procedure is performed in the complex frequency domain to provide insight as to the requirements placed on the feedback elements [13]. However, the most direct and useful form of specifications on a system are those on the time responses. Krishnan and Cruickshanks provided a simple and rational means of translating time domain specifications to the frequency domain, which can then be used in QFT synthesis [17]. East has demonstrated an algorithmic approach to calculate boundaries on the loop transmission for given frequency domain specifications for the system. These specifications include both the tracking of a commanded input as well as attenuating any unwanted disturbances [4].

Houpis suggested a methodological approach [13] to designing the controller once the above mentioned boundaries are obtained. A design which does not

violate any of the boundaries is guaranteed to meet the desired frequency domain specifications over the entire range of uncertainty for both tracking and disturbance attenuation [13]. Once the choice of using quantitative feedback theory has been made, there exist two logical paths to take — linear or nonlinear synthesis.

Linear Time-Invariant QFT. The simplest application of quantitative feedback synthesis is an extension of the current flight control procedures; that is to take the approximate linear models of the aircraft and replace the constant parameters with a range of values. The resulting designs then operate at larger deviations from the deterministic model.

Although this technique is an improvement over other prominent techniques, it is still based upon the approximate linear model. However, Hamilton [5] has shown that a single fixed design can be sufficiently robust to allow for a combination of total surface failures, yet still maintain the flyability of an unmanned research vehicle. Simulations of the design included nonlinearities which were not designed for; however there was no guarantee that the design would work with the nonlinear elements included. Hamilton noted that the QFT procedure eliminates the trial and error portion of design, but was still very tedious due to the lack of computer aided design programs specifically written for QFT design [5]. Walke and Horowitz extended QFT to uncertain MIMO plants whose determinant had right half plane poles and zeros and, applied it to the experimental X-29 aircraft over the entire range of uncertainty after contracted designers abandoned the attempt to independently control two of the output variables [11].

Yaniv has stated that the lack of a generic computer aided design (CAD) package has kept QFT from being used by industry; most work is being done by graduate students [21]. Houpis has noted that AFIT produced ICECAP and introduced MATRIX_X packages are part of an ongoing effort to create a QFT CAD package but are not as yet complete [14].

Non-Linear QFT. Horowitz was the first to present a quantitative procedure of synthesis for nonlinear, time-varying systems with large uncertainty. The work of Porter and other modern theorists at the time dealt only with the qualitative properties of nonlinear design [10]. Since that time, the theory has continued to expand and prove itself. Golubev applied the nonlinear QFT technique to control a modified Air Force F-4 to an angle of attack reaching 35 degrees, an extremely nonlinear case [8].

The above nonlinear design technique is based on conversion of the nonlinear models to "equivalent linear" models with the appropriate uncertainty. This could lead to much larger equivalent linear uncertainty than inherently needed. This is attributed to the manner in which the "equivalent linear" models were obtained. Use of nominal nonlinear plant cancellation, involving a nonlinear network of the same complexity as the plant overcomes this problem [6]. At a chosen nominal plant value, the combination of the two behaves like a linear time-invariant network for all inputs and allows the designer to greatly reduce over design [6]. The large "saving" thereby obtained was vividly demonstrated in a highly nonlinear uncertain 2×2 MIMO problem [7].

Barfield points out the need for nonlinear uncertainty models in early flight control simulations. Current practice is to adjust for the pilot dynamics after the aircraft is in the advanced simulation testing phase where modifications are expensive [1]. QFT may prove to be a valuable design tool when working with nonlinear pilot models that are highly uncertain. Parameters in such models change, not only from person to person, but from day to day. Taking this into account early in the design may account for less need, if any at all, of fine tuning in the later stages of simulation.

Summary. The foundation has been laid to make the design of a flight control system quantitative in nature. The technique still requires a large amount of

designer interaction, resulting in the requirement for a QFT CAD package. The development of such a package will no doubt increase the use of the technique throughout the control industry.

Robustness is inherent in QFT. There is no need to examine system robustness after a design has been made, as is the case in much of modern control methods.

The nonlinear QFT techniques lend themselves directly to early man-in- the-loop simulations and may save money in the design process.

Finally, it is obvious that the modern control statement that frequency response methods are only valid for linear time-invariant systems, is false [6,7,8,10].

Assumptions

The following assumptions are made in the design problem of this thesis.

1. All parameters contain finite uncertainty.
2. All commanded inputs and desired outputs are Laplace transformable.
3. All aircraft models (plants) have a unique inverse. This assumption excludes the case of hard saturation of elevator deflection.
4. The set of commanded inputs describes the range of the actual inputs to the aircraft.
5. The design is only in the longitudinal axis, therefore the only independent command input is the elevator.

It should be noted that assumptions 3 and 5 are added here only to reduce the scope of the thesis and, in theory, can be relaxed. QFT has been extended to handle the hard saturation problem, but the *usual* QFT can be applied only if the inverse range is finite. For example given an output $y(t)$, there is only a finite

number of inputs $x_i(t)$ which can generate this $y(t)$ [8]. In actuality, uncertainty can be semi-infinite, *i.e.* a gain factor from 1 to ∞ but not from $-\infty$ to $+\infty$ [8].

Scope

The foundation of this thesis is laid in nonlinear quantitative feedback theory. This thesis applies the technique to a single input, single output (SISO) nonlinear system with large parameter uncertainty. There is an inner stability augmentation system (SAS) loop involving a nonlinear airframe model and, an outer loop containing the pilot, where the model contains a pure time delay.

The full, nonlinear six degrees of freedom equations of motion are used to generate the plants, although the design is done only for the longitudinal axis.

The only commanded input to the system is a symmetric elevator deflection and the commanded output is C^*: normal acceleration at the pilot station blended with pitch rate.

The completed design is simulated as a linear system using MATRIX$_X$ and on a Fortran simulator using the six degrees of freedom, nonlinear equations of motion. The validation of the design is to demonstrate that all of the output responses are within acceptable limits.

Approach

The first step in the design procedure is to obtain linear time-invariant models which are rigorously equivalent to the nonlinear plant with respect to the defined set of desired outputs. These equivalent plants are generated from time histories of the input and output from simulator data supplied by AFWAL. This data is used in a program, developed by Golubev [8] and provided by Dr. Horowitz, to generate linear time-invariant (LTI) plants that are equivalent to the nonlinear plant in that both models give the same output for the given input. This procedure is repeated for the set of inputs and outputs that are to exist in the operating region of the

system. The result is a set of LTI equivalent plants which are used in the design process.

Next, the boundaries on acceptable outputs provided by AFWAL are translated from the time domain to the frequency domain. At this point, a decision can be made whether the specifications are reasonable and attainable by any design method. QFT or other. The generation of bounds on a nominal loop in the frequency domain are obtained, which must be satisfied in order that the output is in the acceptable set over the entire set P. When the design is completed without violating any boundary, the controller is guaranteed to work, not only for the nominal plant, but also for the entire nonlinear plant set over its range of uncertainty.

The controller design is linearly simulated on MATRIX_X as a first validation and a design tool. The final validation is performed on an existing nonlinear YF-16 simulator using the full six degree of freedom equations.

Presentation

This thesis has seven chapters. Chapter II develops the nonlinear QFT theory. Chapter III presents the generation of the linear time-invariant plants. Chapter IV explains the development of the SAS compensation of the inner loop. Chapter V presents the MATRIX_X linear and Fortran nonlinear simulations of the inner loop excluding pilot compensation. Chapter VI explains the development of the additional single degree of freedom pilot compensation, as well as its simulation, while Chapter VII contains the conclusions and recommendations for future study. Appendix A includes the LTI set P derived from Golubev's program along with plots validating these transfer functions. Appendix B presents the plant templates of interest and frequency domain tracking bounds. Appendix C contains simulations of the inner loop SAS along with the data used to obtain the prefilter, while Appendix D derives the fourth order Padé approximation of a pure time delay used in the Fortran simulations.

II. Nonlinear QFT Theory

Introduction

This chapter presents the theory behind controller design for a nonlinear uncertain plant. A brief overview of linear SISO QFT design is presented. The reader is referred to a technical report [13] for a comprehensive presentation of the design process.

Linear SISO Case

In the design of a controller for a linear model the technique begins with a set of linear differential equations whose parameters are uncertain, giving a set of plant transfer functions $\mathcal{P} = \{P\}$. Every possible combination of parameters gives a different plant contained in the set $\mathcal{P}$.

It is desired that the final closed loop tracking response be within given or desired acceptable bounds, for any possible combination of parameters and therefore any $P \in \mathcal{P}$. If the acceptable bounds are given in the time domain they can be converted to equivalent frequency domain bounds [13]. Once the closed loop frequency response bounds are obtained, the compensator $G(s)$ of Figure 2.1 is used to insure that the variation in the closed loop response is less than or equal to that of the bounds. However, this is insufficient to guarantee that the closed loop tracking response for every $P \in \mathcal{P}$ lies within the tracking bounds. The prefilter $F(s)$ of Figure 2.1 is used in this final task.

The designs of the compensators $G(s)$ and $F(s)$ are based upon boundaries that are derived for a set of frequencies. Similar bounds on $G(s)$ can be obtained for the response of the system to external disturbances. All of the bounds mentioned above can be generated manually on the Nichols chart [13] or the same concepts can be programed on a computer for automation as described in Chapter IV.

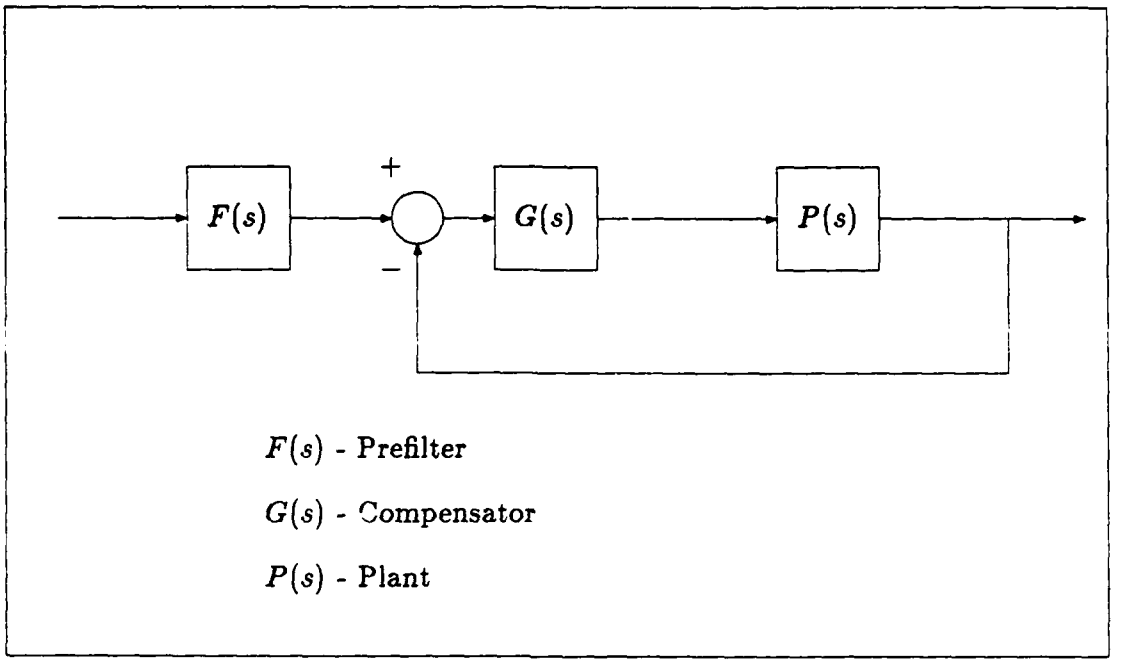

Figure 2.1. QFT Compensated Block Diagram

Nonlinear SISO Case

The problem with the nonlinear case is at the onset of the design. The differential equations are nonlinear and therefore transfer functions may not be used in the usual sense. There exists a set of nonlinear plants $\mathcal{W}$ due to every possible combination of parameter values. It is still desired that all system outputs due to realistic inputs lie within an acceptable set $\mathcal{A}$.

It is necessary to find a set of linear time-invariant plants $\mathcal{P}$ that is precisely equivalent to the nonlinear set $\mathcal{W}$ with respect to the acceptable output set $\mathcal{A}$. A rigorously proven technique for this problem, using Schauder's fixed point theorem, shows that a design meeting specifications for the set $\mathcal{P}$ will also satisfy the nonlinear problem with $\mathcal{W}$ [10].

Direct Analytical Model. For the nonlinear plant of Figure 2.2 having the input $x(t)$, and the output $y(t)$ is of the form:

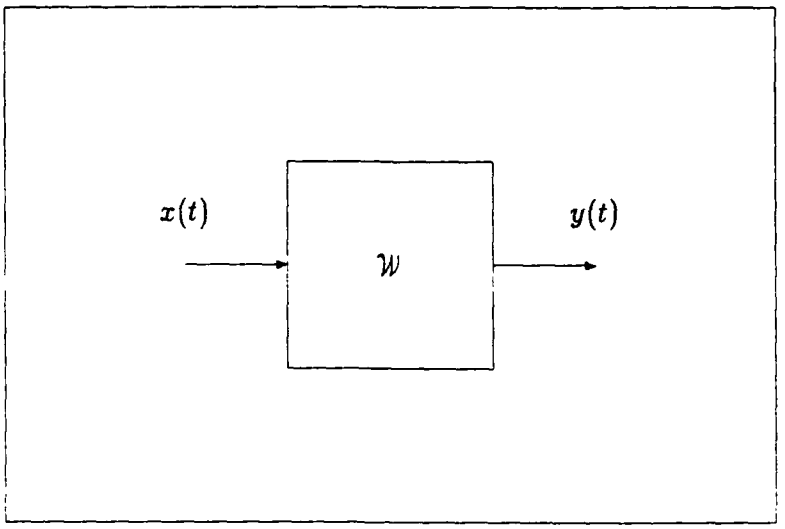

Figure 2.2. Nonlinear Plant Set

$$y(t) = w(x(t)) \tag{2.1}$$

Given any $a_i \in \mathcal{A}$ and any plant $w^j \in \mathcal{W}$, then the problem becomes one of determining the input to w^j which gives the output a_i by solving Eq (2.1) for x given y. The resulting x is denoted by x_i^j. It is necessary to find a linear time-invariant plant P_i^j which is equivalent to w^j for this one case. That is, the output of P_i^j is $a_i(t)$ when its input is $x_i^j(t)$. When $a_i(t)$ and $x_i^j(t)$ are Laplace transformable, a difficult condition to violate, one can write [8]:

$$P_i^j(s) = \frac{\mathcal{L}a_i(t)}{\mathcal{L}x_i^j(t)} \tag{2.2}$$

The linear time-invariant $P_i^j(s)$ is precisely equivalent to the nonlinear w^j only when the input is x_i^j. In order to describe the nonlinear set $\mathcal{W}$ with a linear set P, a set of outputs and corresponding inputs is required. This can be accomplished by repeating the above technique over all the $w \in \mathcal{W}$, for the same output $a_i(t)$. Then repeating the above steps for all of the desired outputs $a \in \mathcal{A}$, generates a set of $\{P_i^j\} \equiv P$ [8].

Non-Direct Analytical Model. Another technique, based in theory on the above procedure, is very useful for nonlinear plants that have extremely complicated analytic models. This technique requires either the physical availability of the plant or a nonlinear simulation of the plant. In this thesis a simulation of the YF-16 aircraft using the nonlinear equations of motion, complete with a large data base of aerodynamic data, is used. A stabilizing controller is first obtained, by "intelligent" cut and try, around the plant with the only goal being that the acceptable range of outputs can be obtained; no attempt is made at a reasonable design. The simulator is then run, with the operator supplying the "input" as needed to obtain one acceptable output. A record is kept of the input signal to the plant and the plant's output. This can be done by writing the two time histories to data files. The simulation is repeated until a set of acceptable outputs is obtained that fills the envelope of acceptable responses. The set of plant output and corresponding input time history points is then used to generate the set of linear equivalent plants P.

Summary

This chapter presents an overview of the continuous SISO QFT design technique, with extension to the nonlinear case. Two techniques for obtaining the linear time-invariant equivalent plants are presented, either of which may be used to accomplish the task.

III. Derivation of the LTI Equivalent Plants

Introduction

As noted in the previous chapter this thesis does not solve the analytical model backwards to obtain the linear time-invariant equivalent plants. Instead a simulator provided by Tom Cord of AFWAL is used. The simulator was originally developed for studying the high angle of attack and the spin characteristics of the YF-16.

The Simulator

The following modifications are made to the original simulator in order to aid in obtaining the desired data:

1. Longitudinal stick force shaping compensation is removed.
2. The commanded output C^* is generated as an output variable.
3. Various output files for transfer function generation and MATRIX_X graphics are added.
4. Normal acceleration feedback is replaced with C^* feedback.
5. Prefiltering of input signals is added.

The simulator is a Fortran implementation of the actual control laws as well as the six degree of freedom nonlinear equations of motion for the aircraft. The aerodynamic derivatives for the equations of motion are supplied from data tables covering the entire flight envelope, including high angle of attack. During the simulation, the equations of motion are solved using a Runge-Kutta integration scheme with the states updated every 5 msec. Reduction of the update interval shows no improvement in the accuracy obtained as compared to actual flight test data.

Each time the simulation is started, a prompt for load factor in g's and angle of attack in degrees is used to trim the aircraft to its nominal flight condition. This thesis has the nominal condition of straight and level flight at 0.9M and 20,000 ft in the derivation of the equivalent plants.

The input to the plant is considered to be the sum of the actuating signals to the two elevators of Figure 3.1, which are always symmetric since the elevator is the only commanded input. The output is C^* in g's which for the YF-16 is

$$C^* = A_{n_p} + 12.4q \tag{3.1}$$

where A_{n_p} is the normal acceleration at the pilot station in g's, and q is the pitch rate in rad/sec. By specifying the above input and output the plant is defined as the airframe with actuators, including the position and rate limiters of the actuators. Also included are the dynamics of the aircraft's leading edge flaps of Figure 3.1. Since this thesis is restricted to a single input, the two available choices are to either disable the flaps entirely in the trailing position, or make them a dependent input. The latter is chosen by commanding the leading edge flaps with an angle of attack plus pitch rate schedule. This not only gives an input totally dependent upon the commanded elevator input, but also has a stabilizing effect on the aircraft.

The Equivalent Plants

In order to adequately represent $\mathcal{W}$ with the set $\mathcal{P}$ it is necessary to know the range of acceptable outputs a priori and drive the simulator to outputs that adequately represent that envelope. In Figure 3.2 are the proposed normalized bounds on a C^* response to a step input used in this study. The lower boundary is modified from that proposed by Tobie [20]. The bottom of this envelope does not allow a higher order response and specifies a minimum greater than zero for the first 0.2 seconds. This modification makes the lower bound more severe then the original. The purpose behind the modification is to provide a smoother lower

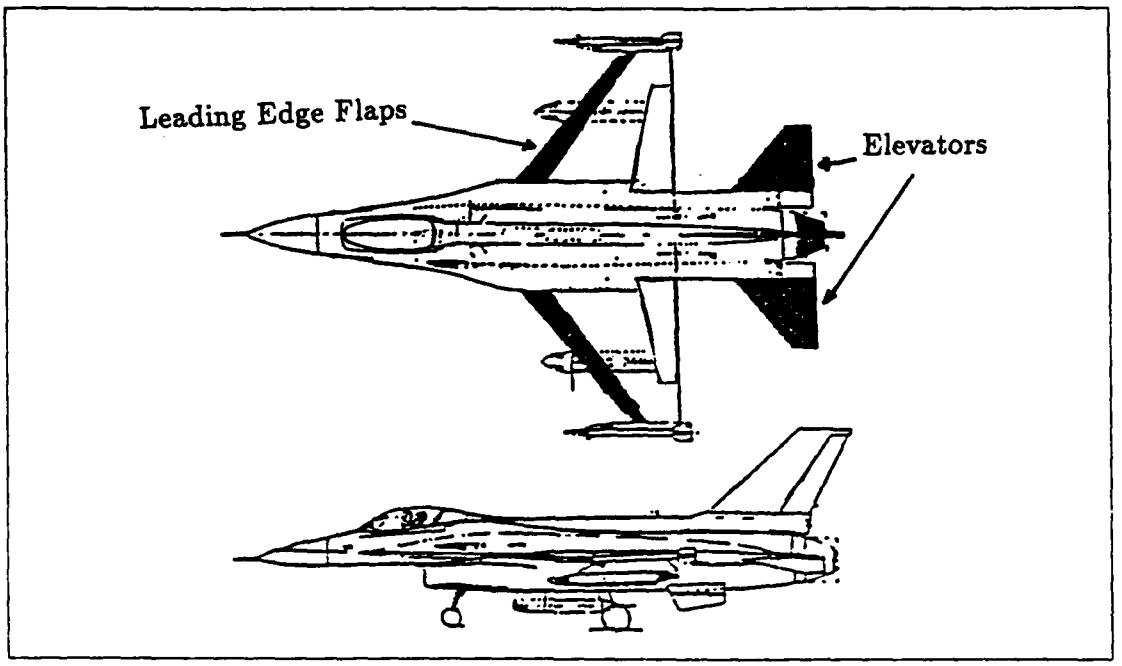

Figure 3.1. YF-16 and Control Surfaces

bound on the closed loop response in the frequency domain, as well as to disallow non-minimum phase responses, with no sacrifice to the time response.

The objective of the simulations is to drive a set of outputs that fill the envelope of Figure 3.2. This is accomplished with 8 outputs for a 1g envelope and 7 cases for a 2g envelope, all 15 normalized cases are shown in Figure 3.3 superimposed upon the normalized bounds and are judged to populate them very well.

The next objective is to find 15 linear time-invariant transfer functions, one for each input/output pair, given the time histories obtained from the simulator. Golubev's Fortran subroutine provided by Dr. Isaac Horowitz is used to help accomplish this task. By providing a vector of the plant's input, output, and time of occurrence the subroutine utilizes the Numerical Algorithms Group (NAG) Fortran Library and Crout's factorization method to obtain a linear transfer function equivalent to the nonlinear plant for that one specific input. The subroutine re-

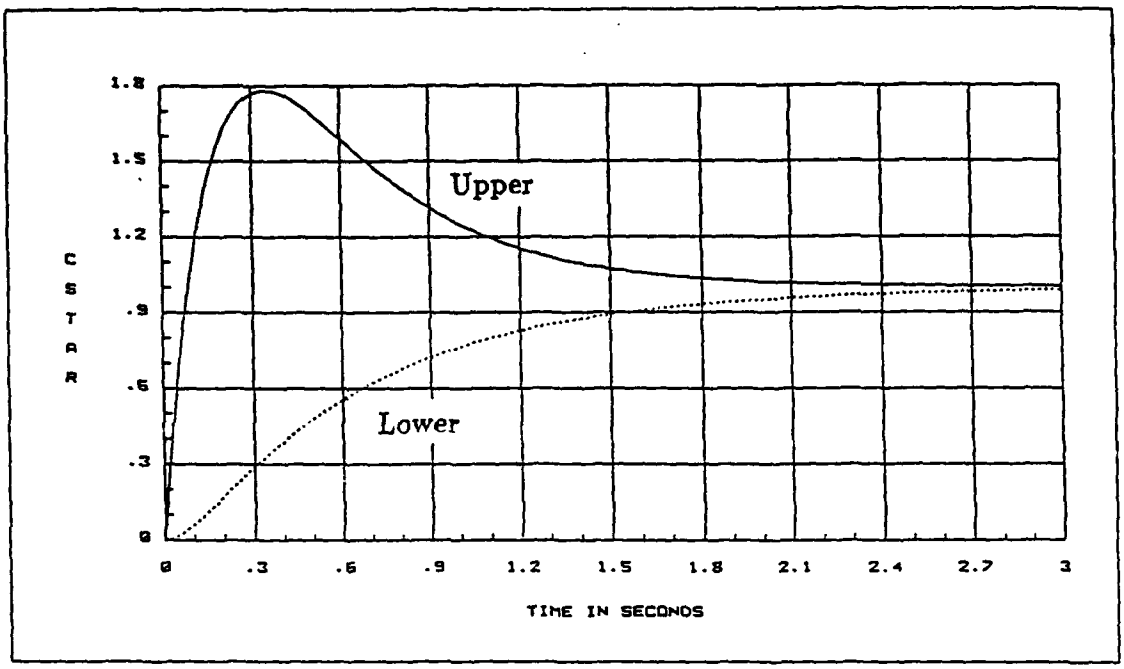

Figure 3.2. Normalized Bounds on the Output C^*

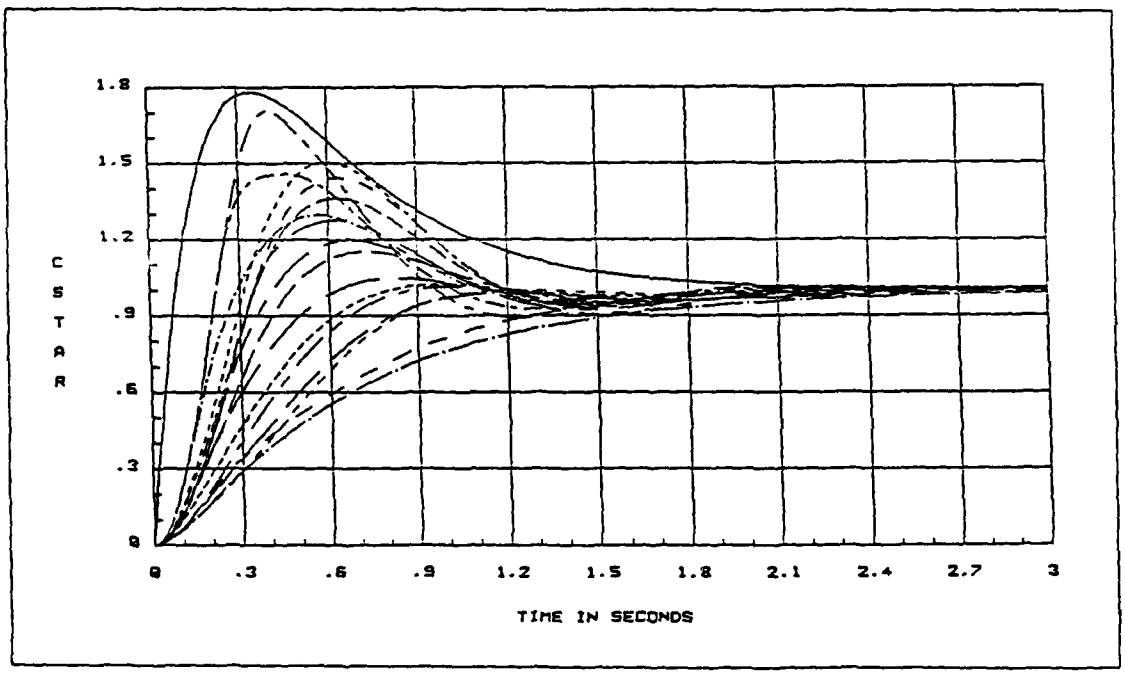

Figure 3.3. Simulator Outputs used to Generate Plants

quires the user to specify the order of both the numerator and denominator; a small amount of experience in analyzing the time responses of transfer functions allows the user to eliminate most of the trial and error in finding a suitable fit. The decision is made to fit the time histories with transfer functions that all have the same number of excess poles over zeros, while placing no constraint on the order of the system model. Thus causing the plant templates to have no uncertainty in phase angle at $\omega = \infty$. Analyzing the initial 10 msec of the response gives good insight into selection of the actual number of excess poles. An excess of two poles is chosen.

In addition to validating the program with the input/output time histories of known transfer functions, known test cases are run on the simulator. The simulator is given a step input with the leading edge flaps frozen and the output recorded. This data is then fitted with a transfer function that matches that of a linearized YF-16, without leading edge flaps, at the same nominal flight condition. The final transfer function fits are validated by reapplying the original input to the proposed transfer function and comparing this output with the original output. The two outputs are then plotted along with their error. Excellent results are obtained as shown in Figure 3.4. The results of all 15 cases along with the transfer functions obtained are contained in Appendix A.

Summary

This chapter presents the derivation of the set of plant linear time-invariant equivalent transfer functions used to represent the nonlinear YF-16. The simulator is described in detail, as well as the modifications made to it. The tracking response bounds on which the final design is evaluated, are presented for the first time. The use of the response bounds in operating the simulator is explained and examples presented. Converting time histories into transfer functions, along with a validation technique are both presented.

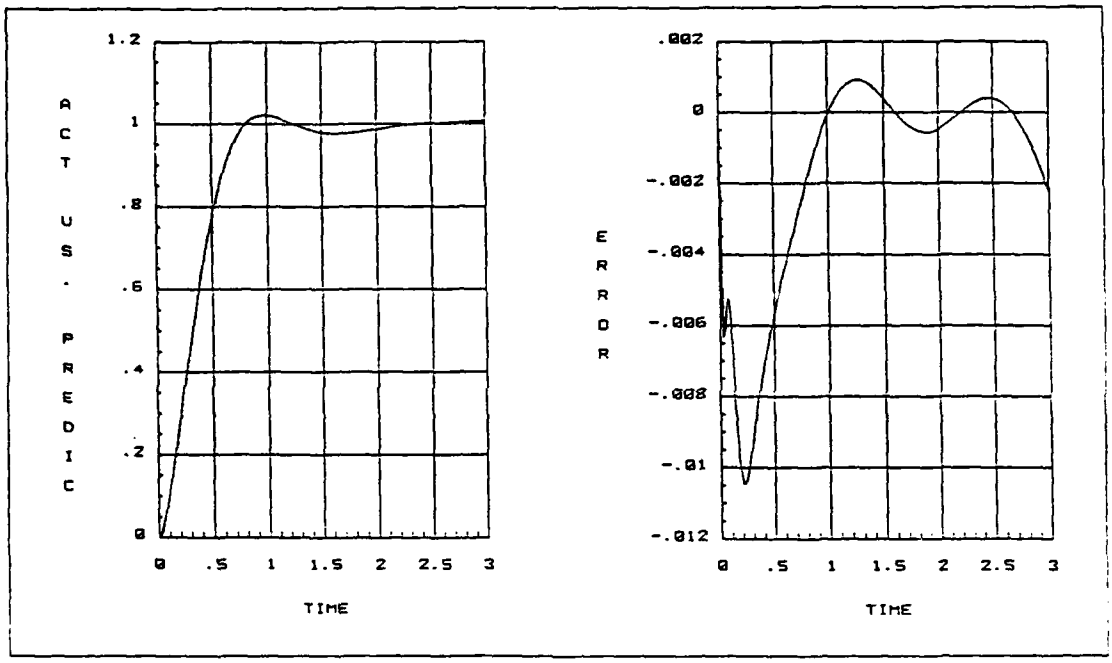

Figure 3.4. Response of YF-16 and Equivalent Plant to the Same Input

IV. Design of the Inner Loop Controller

Introduction

This chapter discusses the design of the compensators $F(s)$ and $G(s)$ shown in Figure 2.1. The bounds on the nominal loop transmission $L_o(s)$ are modified slightly from those obtained in the usual QFT problem, due to different responses obtained from 1g and 2g commands. After the modified bounds are established, the nominal loop is shaped on the Nichols chart. Once the closed loop is completed, bounds on the prefilter $F(s)$ are derived and the compensator designed.

Bounds on $L_o(s)$

The first step in generating the bounds on the nominal loop transmission is converting the time domain bounds of Figure 3.2 into bounds on the closed loop response in the frequency domain as shown in Figure 4.1. This is usually performed using standard figures of merit along with some trial and error; however, the program used to generate the equivalent plants can also be used.

In obtaining the equivalent plants, it is noted that the 2g responses alone do not populate an area of the envelope very well due to inertia of the aircraft and use of the same bounds for 1g and 2g commands. To make the amount of uncertainty more realistic an additional, more severe, upper bound is placed on the normalized 2g responses (see Appendix B). Since for all cases the output is a minimum phase response, only the magnitudes of the frequency domain bounds are required to generate the bounds on $L_o(s)$.

The transfer functions used to model the 1g upper bound, 2g upper bound, and common lower bound are respectively:

$$\frac{15.8965(s+0.9022)}{(s+2.6342)(s+5.439)} \tag{4.1}$$

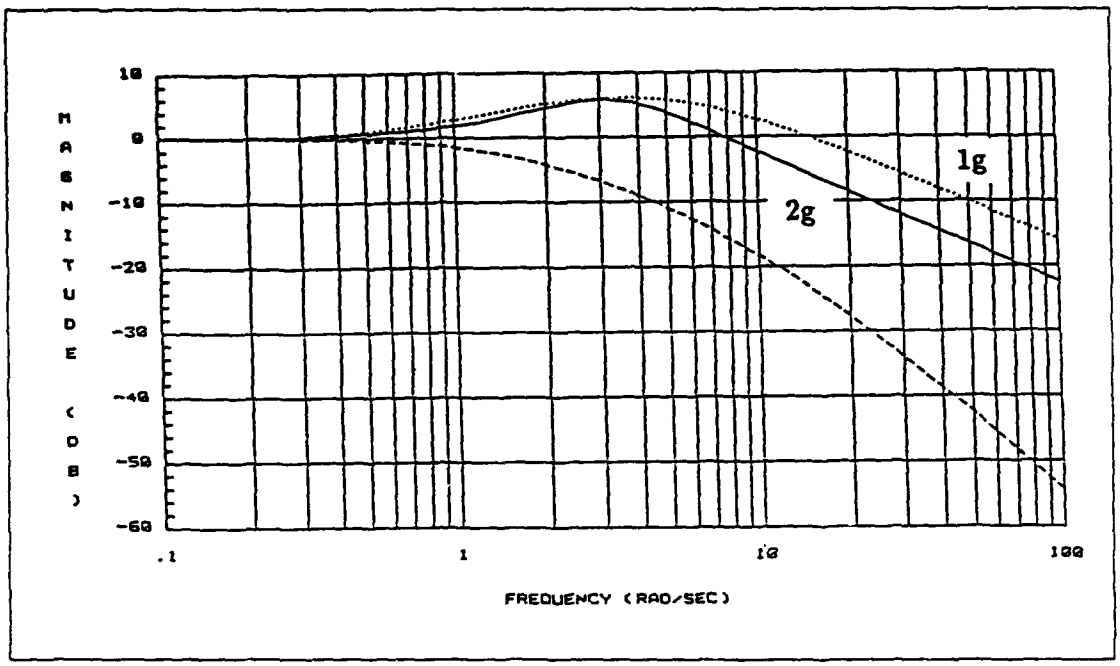

Figure 4.1. Closed Loop Tracking Bounds in the Frequency Domain

$$\frac{7.4435(s+1.5262)}{(s+2.112 \pm j2.5852)} \tag{4.2}$$

$$\frac{19.2109}{(s+1.5942)(s+12.088)} \tag{4.3}$$

For every frequency there is a maximum allowable variation in the magnitude of the response due to the set of plants P. The change in the calculation of the bounds on $L_o(j\omega)$ mentioned earlier is handled in the manner described next.

Modified Tracking Bounds. A plant template, consisting of the magnitude and phase angle of each of the 15 plants, at a frequency $\omega = \omega_i$, is generated in the usual manner [13]. However on this *combined* template, two subtemplates should also be distinctly marked, along with a single nominal plant's magnitude and phase. One subtemplate consist of only the points due to the 1g response (which contains the nominal plant), while the other is for the 2g response. Examples of two *combined* templates, each representing a different magnitude but the same phase angle of the nominal plant, are shown in Figure 4.2. The 1g subtemplate consists

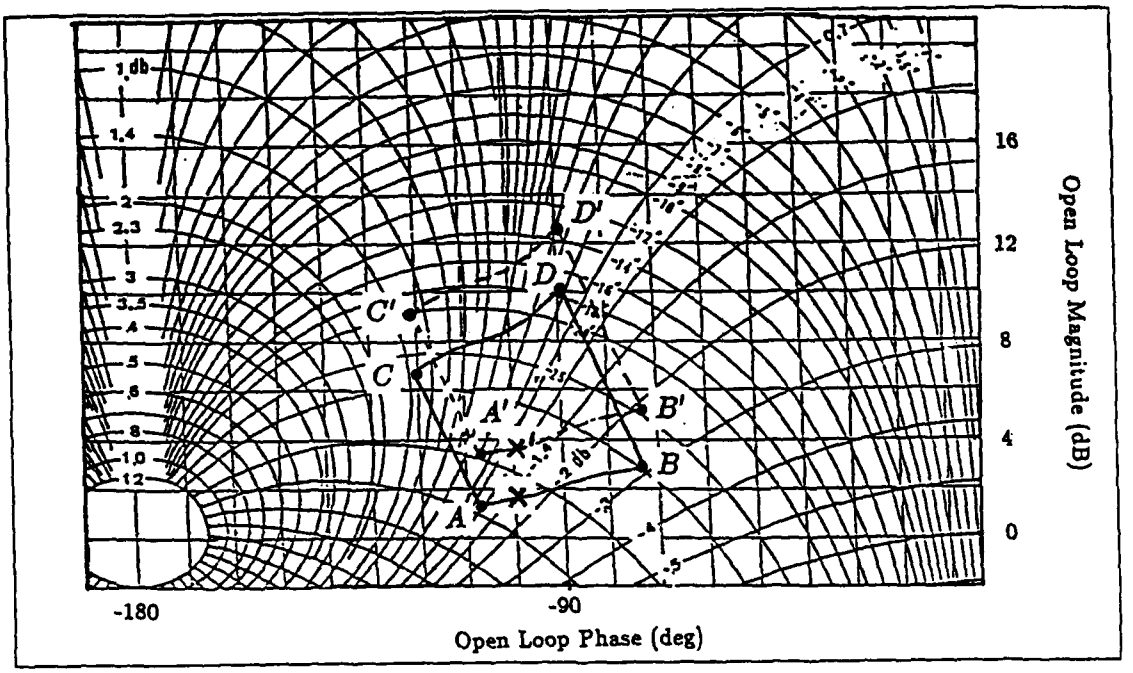

Figure 4.2. Example of Modified Tracking Bounds at $\omega = 1$ rad/sec

of the eight plant points between A (A') and B (B') while the 2g subtemplate consists of the seven plant points between C (C') and D (D').

The combined 1g and 2g template ($ABCD$) is then placed on the Nichols chart to locate a point on the boundary of $L_o(j\omega_i)$, using the allowable variation in magnitude from the 1g bounds in accordance with the technique for obtaining tracking bounds given by linear continuous QFT. For the remainder of this thesis unmodified QFT techniques are referred to as the usual case. The usual bound at $-100°$ for 1 rad/sec is given by the position of the template $ABCD$ in Figure 4.2 where the nominal point is indicated by $\times$. The maximum closed loop magnitude of 1.399 dB occurs at point C and the minimum of -2.864 dB occurs at point B, giving a variation of 4.263 dB for the *combined* 1g and 2g template. The allowable variation at 1 rad/sec for the 1g bound is 4.264. The allowable variations can be obtained from Figure 4.1 or Tables B.1 and B.2. Thus, the nominal point of the template would be marked as a point on the bound of $L_o(j1)$;

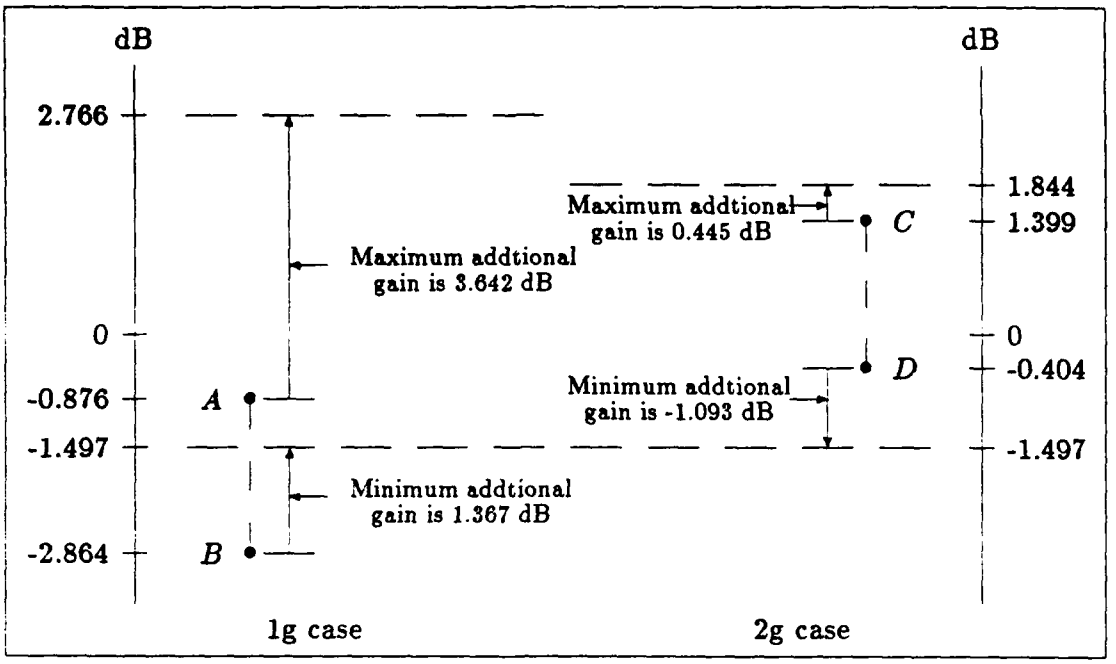

Figure 4.3. Calculation of Bounds on $F(j1)$ for the $ABCD$ Template

however, instead of marking the nominal plant's position, one more check must be performed. Note the maximum and minimum closed loop magnitudes due to the *1g subtemplate only*, in Figure 4.2 these are -0.876 db at point A and -2.864 dB at point B. Compare these two extreme values with the maximum and minimum allowed by the *1g tracking* response bound of 2.766 dB and -1.497 dB from Figure 4.1. Next calculate the range of additional magnitude required to meet the bounds at $\omega = 1$. The maximum gain that can be added by $F(j1)$ to lie within the bounds of Figure 4.1 is $2.766 - (-0.876) = 3.642$ dB while the minimum is $-1.497 - (-2.864) = 1.367$ dB as illustrated in Figure 4.3. Thus the range of allowable gain increase is from 1.367 dB to 3.642 dB. This range of magnitudes is the bound on the prefilter $F(j1)$ if the nominal loop is actually at 1.47 dB and $-100°$ at $\omega = 1$ rad/sec, i.e. $L_o(j1) = 1.47\text{dB}\angle -100°$.

Next repeat the same calculation on the bounds of $F(j1)$ except this time use the ***2g subtemplate and 2g closed loop tracking bounds.*** For the 2g subtemplate

the maximum closed loop magnitude is 1.399 dB at point C while the minimum is -0.404 dB at point D. Figure 4.1 (also see Table B.2) gives the maximum allowable closed loop magnitude 1.844 dB and the minimum of -1.497 dB. Calculating the acceptable bounds on $F(j1)$ gives a maximum of $1.844 - 1.399 = 0.445$ dB and a minimum of $-1.497 - (-0.404) = -1.093$ dB. Compare the two sets of bounds on $F(j1)$ thus obtained. The goal of this check is to have one prefilter $F(j\omega)$ to meet system specifications. Therefore, if there is some overlap between the two sets of bounds on $F(j\omega_i)$ there exists a single $F(j\omega)$ which meets both bounds, and the boundary location is a valid boundary point of $L_o(\omega_i)$. If there is no overlap between the two sets of bounds on $F(j\omega_i)$ then the open loop gain must be increased at this phase value, moving the *combined* template up the Nichols chart until an acceptable point is located. For the template $ABCD$ in Figures 4.2 and 4.3 the ranges of 3.642 dB to 1.367 dB and 0.445 dB to -1.093 dB have no overlap. This is graphically depicted in Figure 4.3 where for the 1g subtemplate the minimum increase in gain of 1.367 dB is greater then the maximum allowable of 0.445 dB for the 2g subtemplate. Therefore, the gain of the plant at $-100°$ must be increased raising the *combined* template.

If the nominal point of the template is raised to 3.82 dB the template $A'B'C'D'$ of Figure 4.2 is obtained. Since the allowable variation is met at the previous lower gain no additional check is required. Points A' and B' have the closed loop magnitudes of -0.134 dB and -2.09 dB respectively giving an acceptable 1g range on $|F(j1)|$ of $2.766 - (-0.134) = 2.9$ dB to $-1.497 - (-2.09) = 0.593$ dB. Points C' and D' have the magnitudes 1.248 dB and -0.241 dB respectively giving an acceptable 2g range on $|F(j1)|$ of $1.844 - 1.248 = 0.596$ dB to $-1.497 - (-0.241) = -1.256$ dB. There now exists an overlap between the ranges on $|F(j1)|$, thus 3.82 dB at $-100°$ is a valid boundary point of $L_o(j1)$. This process is repeated at various values of open loop phase angle for $\omega = 1$ rad/sec and then for various values of ω_i.

Finding the closed loop magnitude M, for the form of Figure 2.1 without the prefilter $F(s)$, when given the open loop magnitude m and phase angle θ, i.e. $L(j\omega) = m\angle\theta$, can be easily automated by solving for the magnitude of the closed loop transfer function:

$$|M(j\omega)| = \left|\frac{L(j\omega)}{1 + L(j\omega)}\right| \tag{4.4}$$

When both M and m are in arithmetic units not decibels, then

$$M = \frac{m}{\sqrt{1 + m^2 + 2m\cos\theta}} \tag{4.5}$$

This method is used to obtain the magnitudes of the above example and through the remainder of this thesis.

Stability Bounds. The modified tracking bounds are obtained for templates up to a frequency for which the allowable closed loop variation is sufficiently greater then the variation in the templates's magnitude. In this thesis a frequency of $\omega_h = 10$ rad/sec is sufficient. Above this frequency, only stability bounds exist representing the maximum allowable closed loop magnitude [13]. This thesis uses a stability or M contour of 3 dB. The boundaries on the nominal loop transmission, $L_o(j\omega)$ are shown on the Nichols chart in Figure 4.4.

The Shaping of $L_o(s)$

Next the nominal loop $L_o(j\omega)$ is shaped by choosing an appropriate $G(s)$ such that $L_o(j\omega_i)$ remains ***outside*** the boundary $B(\omega_i)$ for each $\omega_i = \omega$. Since $L_o(s) = G(s)P_o(s)$. This is accomplished by choosing the poles, zeros, and gain of $G(s)$. The optimal loop transmission L_{opt} lies on $B(\omega)$ at all ω and not only exists but is unique [8]. The design of a practical $L_o(s)$ is somewhat of an art. The greater the number of poles and zeros of $G(s)$ that are chosen, the closer to the optimum $L_o(s)$ is realized, thus there exists a tradeoff between complexity and bandwidth [8].

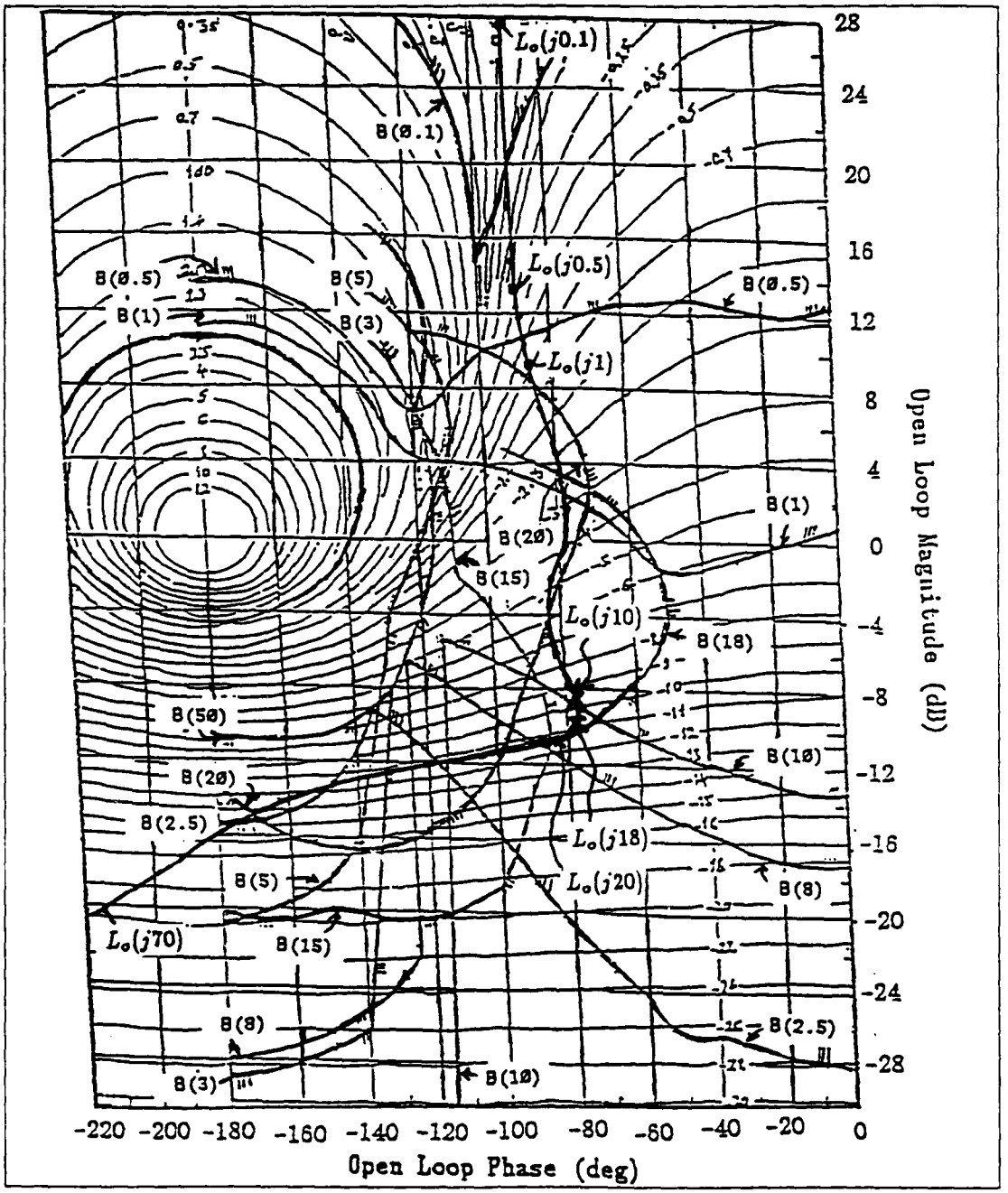

Figure 4.4. Bounds $B(\omega)$ on $L_o(j\omega)$ and Response of Proposed Design

Template Magnitude Variation Greater Than Allowed by Bounds	Template Magnitude Variation Less Than Allowed by Bounds	
Frequency Ranges		
$0 \leq \omega < \omega_l$	$\omega_l \leq \omega \leq \omega_h$	$\omega_h < \omega \leq \infty$
on or above and stability	on or above and on or below	stability only

Table 4.1. Frequency Ranges of Various Boundaries

Interpretation of the Boundaries. The reader is cautioned on the interpretation of "remaining outside the boundaries". Most of the literature breaks down the bounds, $B(s)$, into two subsets as is done here. However, one may be led to believe that the loop transmission must be outside the stability bounds but "on or above" the tracking bounds. This is not necessarily the case. There exits a range of frequencies where $L_o(j\omega)$ may have to be below a certain boundary to meet tracking bounds. The boundary $B(8)$ in Figure 4.4 shows this exception. In cases where $\angle L_o(j8) > -125°$, the magnitude of $L_o(j8)$ must be greater than the point on the $B(8)$ boundary at that phase. This is the normal case, $L_o(j8)$ must be on or above $B(8)$ on the Nichols chart. However, for $\angle L_o(j8) < -125°$ the magnitude must be less than the point on the boundary at that phase to insure that the closed loop variation in magnitude is less than that allowed at $\omega = 8$ rad/sec in Figure 4.1. Therefore there exists a region where $L_o(j\omega)$ must be "on or below" $B(\omega)$. It is emphasized that the entire boundary $B(8)$ is a tracking bound, not partly tracking bound and partly stability bound as in the case for $B(2.5)$.

The range of frequencies of interest, where one must check for the *on or below* condition, begins at the frequency $\omega = \omega_l$ where the magnitude variation of the template first becomes less than the variation allowed by the closed loop frequency bounds of Figure 4.1. The range ends at $\omega = \omega_h$. The definition of this range results in a quantitative method of obtaining ω_h as the highest frequency for which there exists an *on or below* region of the tracking boundary. Therefore,

for frequencies above ω_h only stability bounds exist. These frequency ranges are summarized in Table 4.1. A quick method to check if a frequency has an *on or below* boundary is to place the template at the bottom of the M contour on the Nichols chart, as if determining stability bounds, and checking the actual variation in closed loop magnitude. Since the closed loop contours are the closest together near the 0 dB, $-180°$ point, then this region on the chart is where the largest variation in the closed loop magnitude exists while meeting the stability bound. If the closed loop variation is satisfied, the stability bound dominates. If the closed loop variation is not met, the template on the Nichols chart must be lowered until the variation is satisfied and the resulting boundary is an "on or below" boundary. For this thesis the region to check is approximately $3 \leq \omega \leq 10$ rad/sec.

Proposed $G(s)$. The first design of $G(s)$ is accomplished using the bounds on $L_o(j\omega)$ of Figure 4.4 on page 4-7 with the exception of $B(18)$, and is shown superimposed upon these bounds. A prefilter $F(s)$ is then designed in the usual manner [13]. This design is then examined using linear simulation on MATRIX_X by obtaining the responses of each of the 15 LTI plants in P using the fixed $G(s)$ and $F(s)$. All responses are within the specified boundaries and all except one are judged to be satisfactory. The response which uses plant 15 has a lightly damped sinusoidal component of approximately 16 rad/sec superimposed upon an acceptable first order response. Plots of the closed loop frequency responses give immediate insight into the problem as can be seen in Figures 4.5 and 4.6.

The decision is made to proceed to the nonlinear simulation based upon the following reasoning. The *commanded inputs* to the simulator that produced the time histories to form plant 15 are extremely erratic, worse than any other case. It is felt that this plant represents a very unlikely operating condition for the aircraft and is therefore ignored for the time being. The error in this reasoning is that. the signal to be analyzed in making the judgement of erratic response is the input signal to the aircraft actuators which, in fact, is rather well behaved. The nonlinear

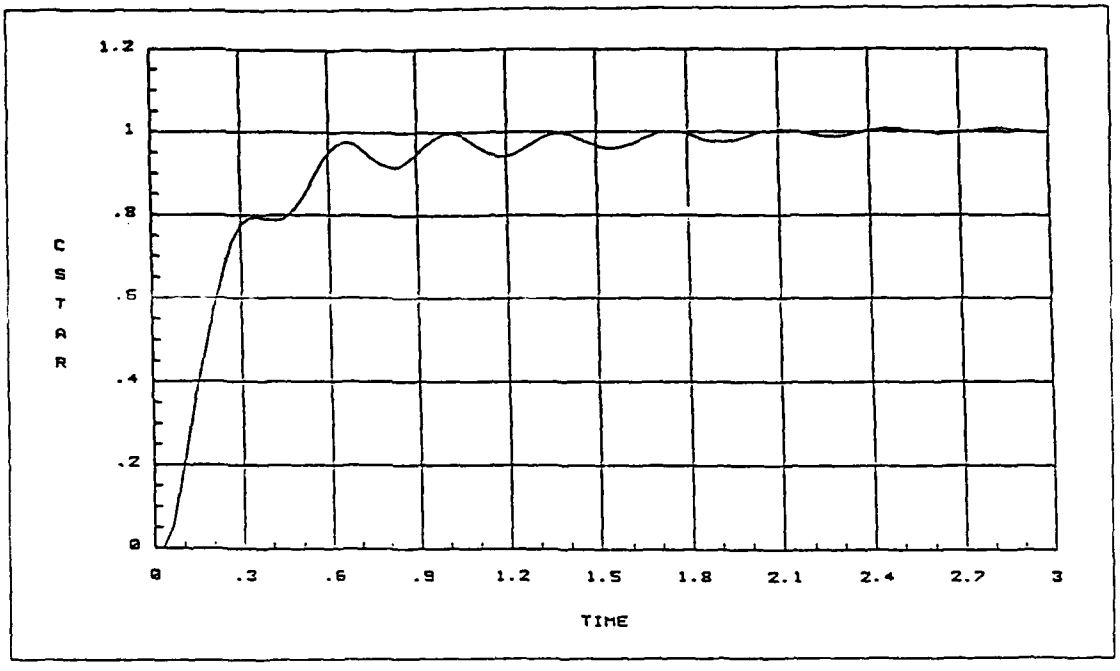

Figure 4.5. Response of Plant # 15 for Initial Design

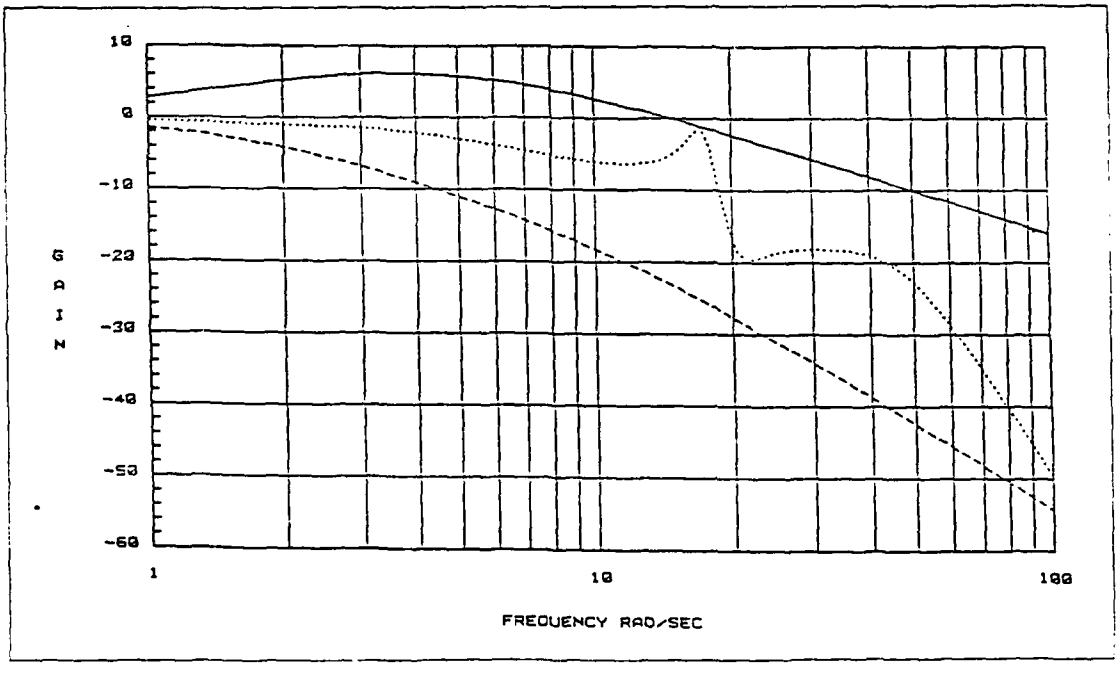

Figure 4.6. Closed Loop Frequency Response of Plant # 15

simulation points this out by exciting a limiting cycle, while attempting to trim, at $\omega \approx 16$ rad/sec. This agrees with the resonant peaks seen in the linearly simulated frequency response of plant 15 in Figure 4.6. A closer examination of the bounds for $15 \leq \omega \leq 20$ rad/sec from which the boundary $B(18)$ in Figure 4.4 is obtained, makes very clear that this boundary is violated. This first design points out the drawbacks of representing the infinite number of boundaries with a finite set, but exemplifies the insight possible from working in the frequency domain.

Final Design of $G(s)$. Using the full set of bounds, $B(s)$, on $L_o(s)$ of Figure 4.4 a new nominal loop transmission is designed. The emphasis again is on minimizing the bandwidth of $G(s)$ while having $L_o(s)$ remain outside of the boundaries, and on accomplishing this with a practical $G(s)$. With the addition of the boundary $B(18)$, and the knowledge of similar boundaries in this frequency range, the following conditions become the dominant constraints on $L_o(j\omega)$.

The region near -10 dB at $-70°$ on the open loop grid of the Nichols chart in Figure 4.4 is the focal point. To meet specifications in this area; the magnitude of $L_o(j10)$ must be greater than the magnitude of $B(10)$, but there is also the bound at $\omega = 18$ rad/sec requiring $|L_o(j18)| \leq |B(18)|$. For an open loop phase angle of approximately $-70°$ the rate at which $L_o(j\omega)$ decreases in the frequency range is rather small. This results in a nearly horizontal segment of $L_o(j\omega)$ on the Nichols chart after suitable additional phase angle is contributed by $G(s)$. If additional phase lag is added at frequencies too near 18 rad/sec stability bounds similar to $B(18)$, unmarked in Figure 4.4, are violated. For this reason the additional phase lag to be added by $G(s)$, and required to decrease the magnitude $L_o(j\omega)$, is delayed until higher frequencies for a given complexity of $G(s)$. This results in a higher bandwidth of $G(s)$.

All designed $G(s)$ obtained, using the above reasoning, are felt to have excessive bandwidth and gain. This problem suggests that bounds on $G(j\omega)$, rather

than $L_o(j\omega)$, give more insight into the problem at hand. Bounds on $G(j\omega)$ are obtained by dividing out the nominal plant $P_o(j\omega)$ from the bounds on the nominal loop transmission $L_o(j\omega)$, that is $G(j\omega) = \frac{L_o(j\omega)}{P_o(j\omega)}$, and $G(s)$ is designed rather than $L_o(s)$. However, the decision is made to continue shaping $L_o(s)$ in the following manner. The major causes of excessive bandwidth and gain of $G(s)$ are the modified boundaries $B(8)$ and $B(10)$ of Figure 4.4. The normal tracking bounds at these frequencies for $\angle L_o(j\omega) > -100°$ are well below -40 dB. The decision is therefore made to intentionally violate these two modified bounds (obtained by the method in the *Modified Tracking Bounds* subsection of this chapter). The tracking boundary at $B(0.5)$ now becomes dominant along with the previously mentioned stability bounds, allowing for a much smaller gain and bandwidth required of $G(s)$.

The above reasoning leads to

$$G(s) = \frac{-2.6303 \times 10^3 (s+5)^2 (s+40)}{s(s+50)(s^2+70s+4900)} \tag{4.6}$$

with the frequency response of Figure 4.7, which results in a very modest bandwidth of $L_o(s)$ of $\omega_c \approx 1.5$ as shown in Figure 4.8. A more economical compensator can be chosen at the cost of greater complexity.

The Design of the Prefilter $F(s)$. The bounds on the prefilter $F(s)$ of Figure 2.1 can be generated from the plant templates and Nichols chart [13]; or by simulating each of the 15 plants, as $\frac{L(j\omega)}{1+L(j\omega)}$, and storing the maximum and minimum magnitudes at each frequency as the variation. The second technique is used in obtaining Figure 4.9. The constraints on $F(s)$ are the range of magnitudes, at each frequency, which ensures that the response of $\frac{F(j\omega)L(j\omega)}{1+L(j\omega)}$ is within the bounds of Figure 4.1. The resulting bounds on $F(s)$, as we. as the first $F(s)$ chosen,

$$F(s) = \frac{25(s+4)}{s^2 - 10s + 100} \tag{4.7}$$

are shown in Figure 4.10.

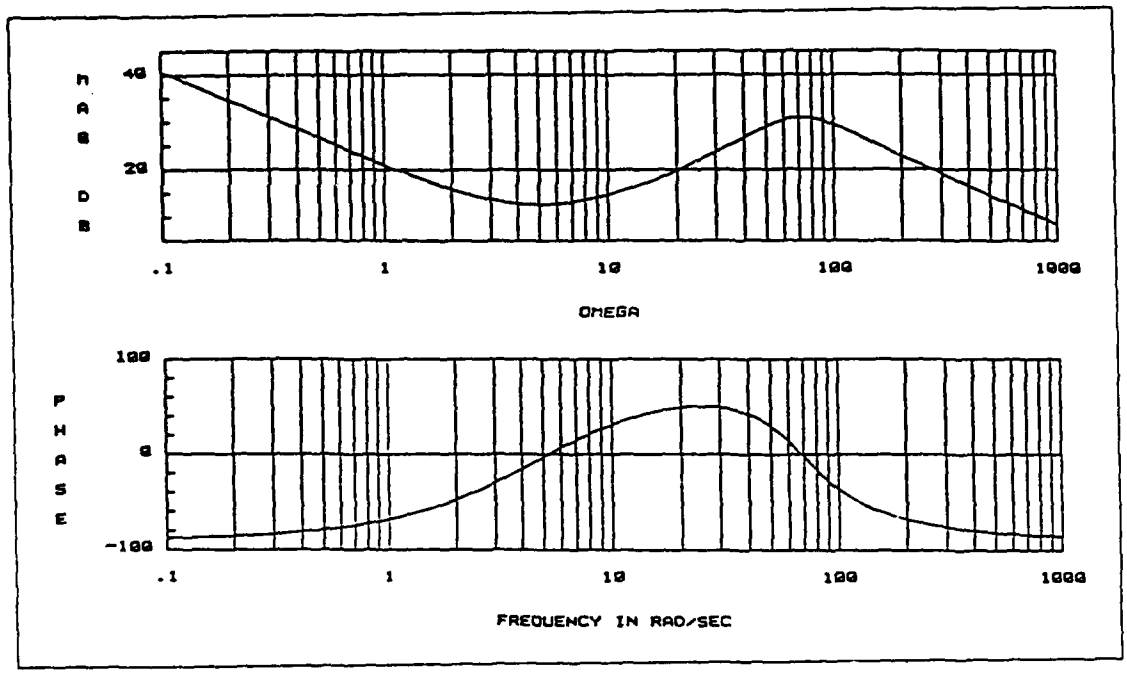

Figure 4.7. Frequency Response of $G(s)$

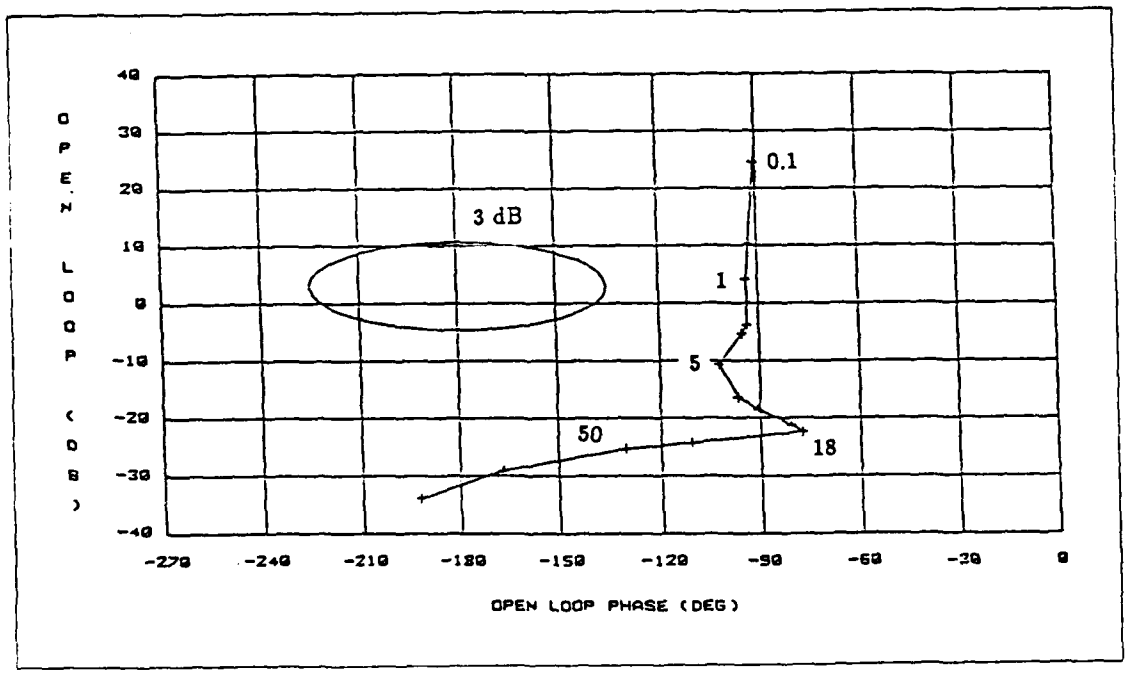

Figure 4.8. Nominal Loop Transmission $L_o(j\omega)$ Designed

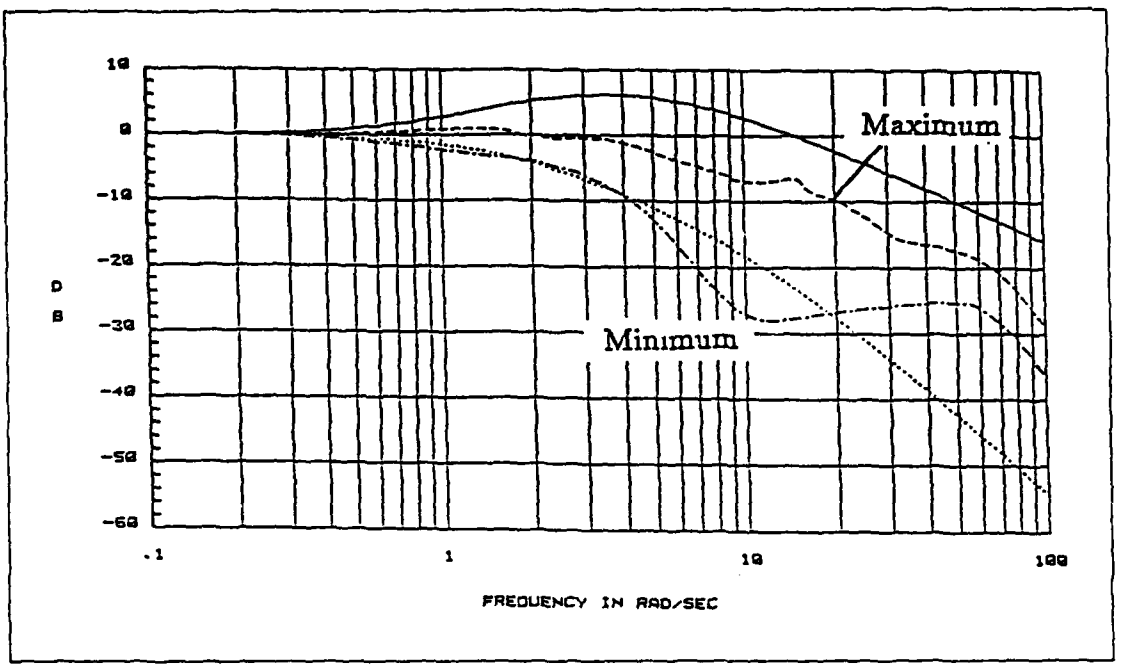

Figure 4.9. Desired and Actual Variation in Closed Loop Response without $F(s)$

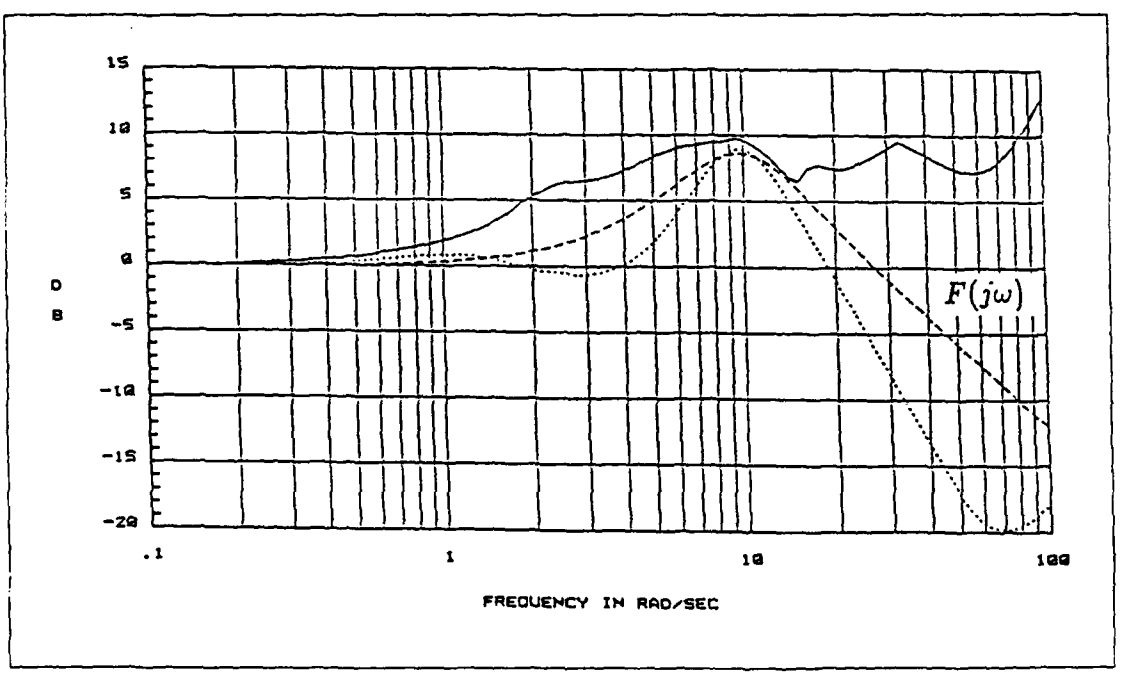

Figure 4.10. Bounds on Prefilter and Proposed $F(j\omega)$

It is obvious that satisfying the bounds on $F(s)$ for all frequencies results in an impractical prefilter; due to the fact that $\frac{L(s)}{1+L(s)}$ has a greater number of excess poles than the two of the lower frequency bound of Eq (4.3). The required amplification around 10 rad/sec may also cause problems for certain cases. One solution is to obtain another lower bound in the frequency domain with the same, or greater, number of excess poles than $\frac{L(s)}{1+L(s)}$ and the proper time response, but this extra effort is not necessary. It is noted that this could have been done at the onset of the problem. A simple tradeoff may be made between boundary violation on $F(s)$ and obtaining a practical prefilter. This tradeoff does not present a real problem since the violation of the boundaries can be deferred in frequency until the magnitude of $L(j\omega)$ is very small.

The MATRIX$_X$ linear simulation of the final design is presented in Chapter V along with the reasons behind modifying the prefilter. Acceptable time response is the final objective, therefore one technique is to use the slowest prefilter that results in acceptable responses. The following prefilter is chosen:

$$F(s) = \frac{8K_f}{s+8} \tag{4.8}$$

where K_f is a nonlinear gain function experimentally determined from nonlinear simulations (see Appendix C). This variable gain is used to minimize the step error coefficients of the nonlinear simulations over a large range of C^* commands, allowing for a more "linear" response for the system. The value of $K_f = 1$ is used in all the linear simulations of the inner loop SAS on MATRIX$_X$.

Summary

This chapter presents generation of the bounds on $L_o(s)$, and its shaping on the Nichols chart. The modification to the usual tracking bounds is described in detail and a graphical example presented. Two choices of $G(s)$ and their design are outlined, as well as the logic enabling the shortcomings of the first design to give

needed insight for the accepted second design. Finally, the prefilter is designed and a discussion on practical prefilters is presented.

V. *Simulation of the Inner Loop SAS*

Introduction

This chapter presents the linear and nonlinear simulations of the stability augmentation system (SAS) designed in Chapter IV. The design only guarantees satisfaction of responses for 1g and 2g C^* commands at the nominal flight condition of 0.9M at 20,000 ft; however, the inherent robustness of the technique is demonstrated by significantly varying the initial conditions. A demonstration of the linearizing effect of the feedback is included. The inner loop is then modeled as an equivalent LTI plant for use in the additional pilot compensation of Chapter VI.

MATRIX$_X$ Linear Simulation

The response of all 15 LTI equivalent plants are shown in Figure 5.1 using the compensator $G(s)$ of Eq (4.6) and the prefilter

$$F(s) = \frac{25(s+4)}{s^2 + 10s + 100}$$

of Figure 4.8.

The MATRIX$_X$ linear simulations are used only as a design aid while a satisfactory nonlinear response is the final goal. Therefore further inspection of the individual responses is required. In the proposed design of $G(s)$ outlined in Chapter IV, in which a limiting cycle of the nonlinear YF-16 is excited, it is found that the equivalent plant #15 best describes the nonlinear aircraft at this operating point. This conclusion is made based on the similarities in the responses of plant #15 and the nonlinear simulation for this first design of $G(s)$. The response of plant #15 has a lightly damped sinusoidal component while the nonlinear simulation's response shows no reduction in the oscillation's magnitude within 50 sec. For the final design the response of plant #15 in Figure 5.1 has a 30 % overshoot

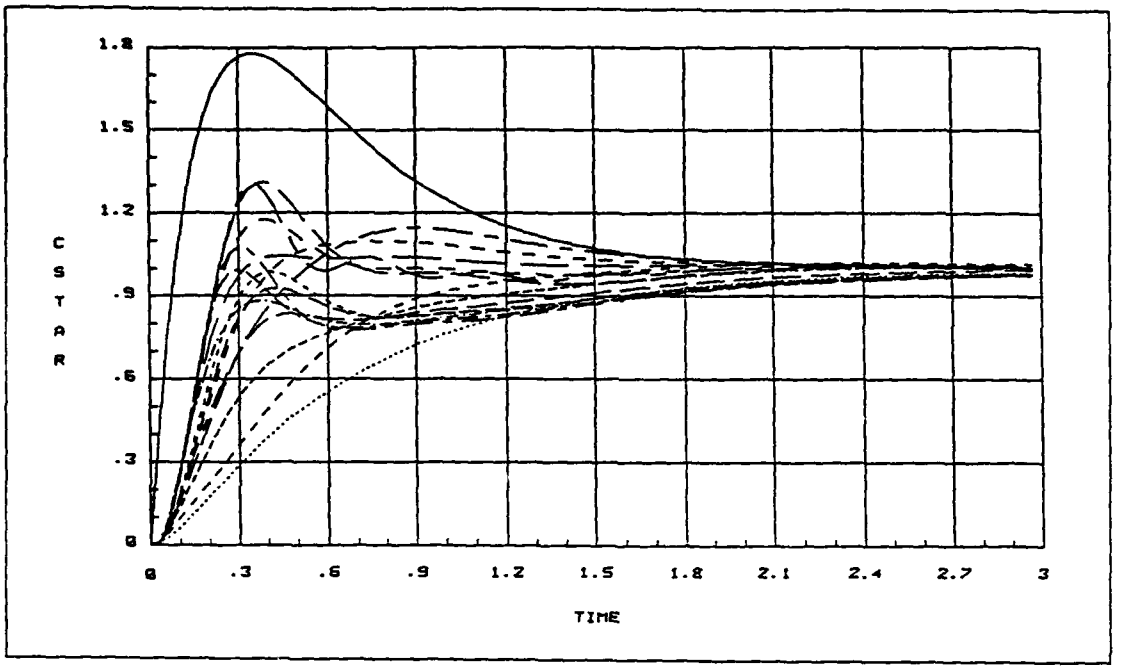

Figure 5.1. MATRIX$_X$ Simulation of SAS Over Range of Uncertainty

and a slight amount of oscillation before reaching its final value, as seen in trace #1 of Figure 5.2. From previous experience with the nonlinear simulation, it is expected that the response of the nonlinear aircraft would be worse. The decision is made to slow down the prefilter, specifically to remove the amplification around 10 rad/sec from Figure 4.8. The implementation of the final prefilter, $\frac{8}{s+8}$ gives the response of trace #2 in Figure 5.2 for plant #15. The slower prefilter causes several of the responses of the set P to violate the bounds on the output; however the nonlinear results are the end objective. The simulations are then continued using the first order prefilter.

Nonlinear Simulation

The compensation is then implemented in Fortran in the form of Figure 2.1 page 2-2 where the output of $G(s)$ is the actuating signal to the elevator's actuators and the feedback signal is C^*. The initial flight condition is specified and the program calculates the required thrust as well as the deflections of the elevators

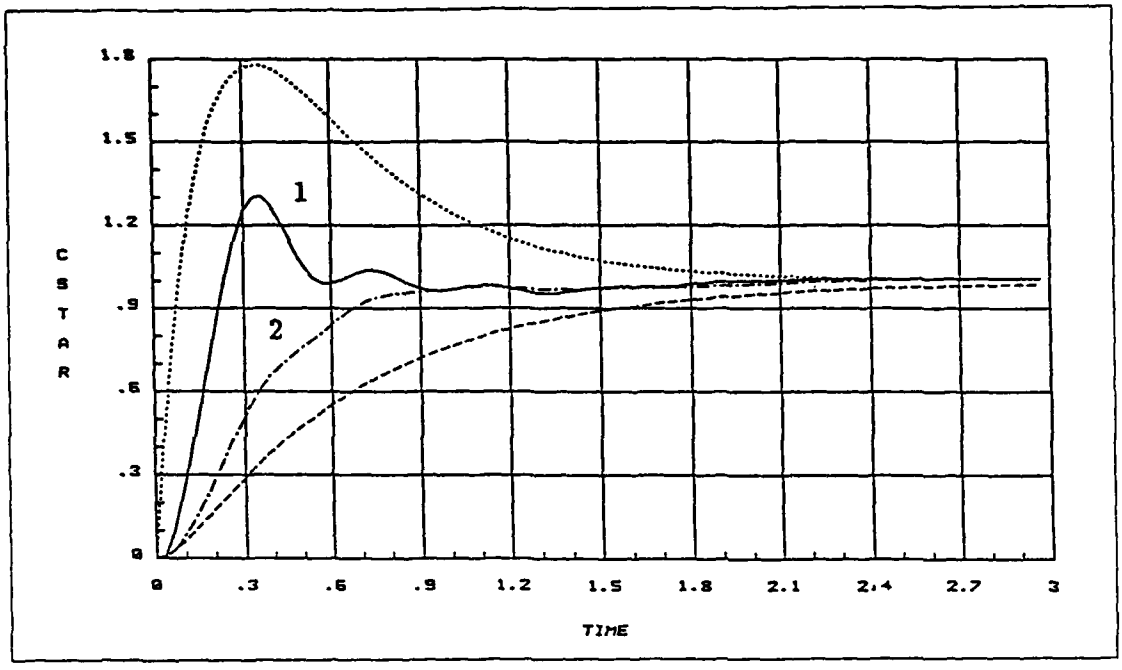

Figure 5.2. Response of Plant #15 for the two Prefilters

and leading edge flaps to maintain this condition. Once the equilibrium conditions are established, the internal states of the compensators are solved for their trim values. This is automatically completed prior to $t = 0$. The simulation is then run where commands are given as perturbations from the trim values and outputs are in full state values.

Nominal Flight Condition Simulation. The first run is a 1g commanded C^* at the nominal flight point of 0.9M and 20,000 ft, as shown in Figure 5.3. Comparison of this nonlinear response with the MATRIX$_X$ linear response of plant #15 for the same prefilter validates the use of the first order prefilter for this case. It is yet to be determined if the slower prefilter adversely affects other operating points.

The design guarantees acceptable responses for 1g to 2g commands at the nominal flight condition and Figure 5.4 shows this to be the case. The responses are normalized to the commanded input over the range of 0.5g to 2.5g steps at increments of 0.1g.

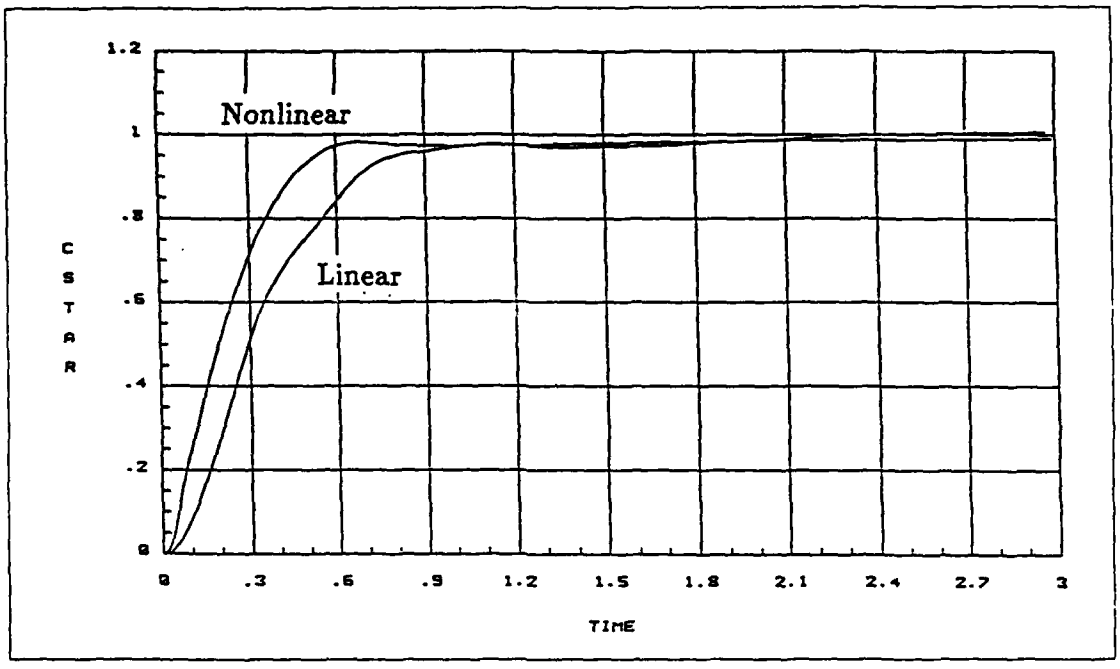

Figure 5.3. Response for 1g Command of Plant #15 and Nonlinear Aircraft

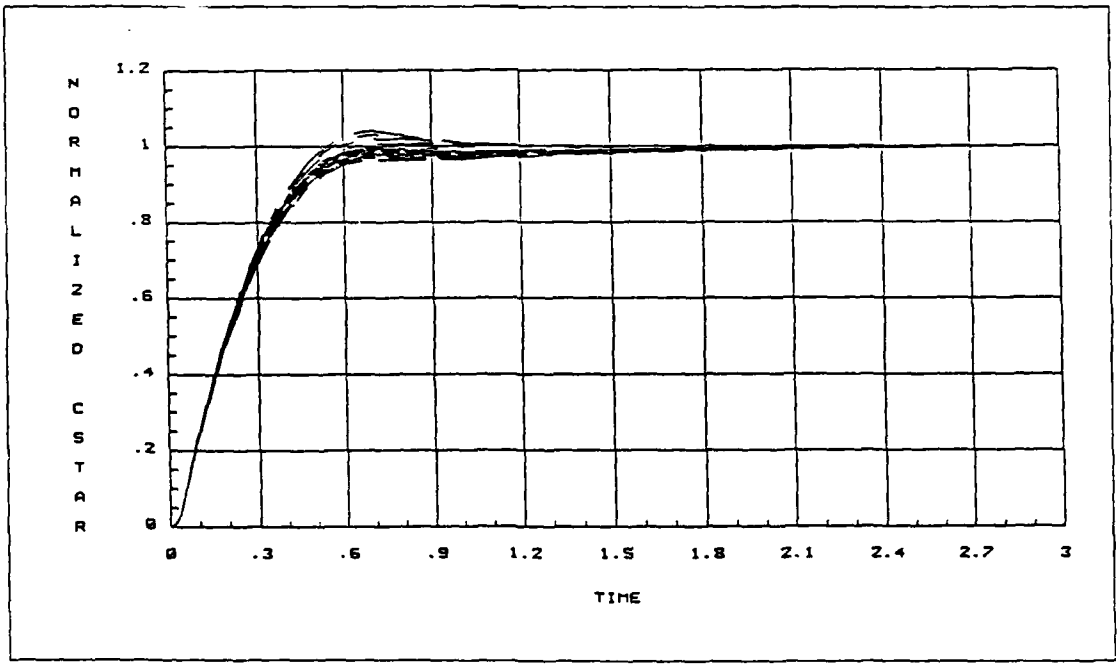

Figure 5.4. Normalized C^* Response at Nominal Flight Condition

The nonlinear gain factor, K_f, mentioned in Chapter IV enables the responses of Figure 5.4 to be normalized to commanded input rather than final value. Prior to the addition of this gain, the steady state error varied nonlinearly from one command to another.

It is desired to represent the inner loop SAS as a single linear plant at the nominal flight condition for synthesis of the outer loop of Chapter VI. Although the addition of the feedback greatly linearizes the aircraft response, the additional gain increases the validity of this approximation. The gain K_f is scheduled as a piece-wise linear function obtained by fitting data points with straight line approximations. Each data point is equal to the magnitude of the command divided by the steady state value. The function is specifically derived for 0.9M at 20,000 ft and is contained in Appendix C.

Expanding the Envelope. At the onset of the design, equivalent LTI plants are only obtained at the one nominal flight condition for 1g and 2g responses. Therefore, the design is only guaranteed to work over this range. To guarantee a larger flight envelope requires obtaining enough equivalent plants at various flight conditions to fully represent the nonlinear aircraft over that region of operation. However, the current set of plants P models much of the nonlinear characteristics already and may in fact be sufficient. This statement is further supported by the results of several hundred simulations consisting of step responses of various magnitudes and flight conditions.

The simulation envelope spans the region of 5,000 to 30,000 ft with speeds from 0.5 to 0.9M and commands up to 9g's, all simulations shown start trimmed for straight and level flight. Figure 5.5 shows the results for commands of 1g to 9g's normalized to final value, while representative results at 25 flight conditions are shown in Appendix C. The response for the maximum command at the nominal point is shown in Figures 5.6 and 5.7 where all angles are in degrees, rates are in

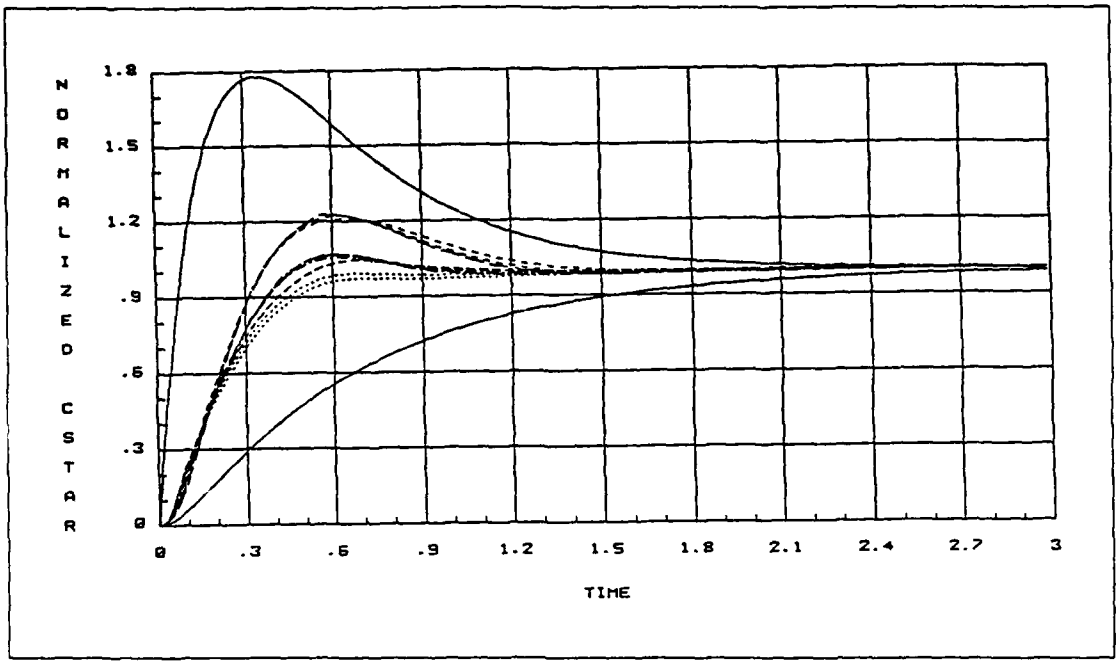

Figure 5.5. Normalized C^* Responses for 1-9g Commands at Nominal

deg/sec, altitude in feet, and true air speed in ft/sec.

The decision as to whether or not a particular response at each flight condition is included in the envelope is made by checking the normalized response against the specified tracking bounds of Figure 3.2 page 3-4. This envelope is shown in Figure 5.8 with a sampling of these limits in Table 5.1. Each loci of points represents the maximum command resulting in an acceptable response for a given altitude as airspeed is varied. It is felt that the major constraint on the operating region is due to aerodynamics and not the controller. The decreasing maneuverability of the aircraft with dynamic pressure, along with the decrease in available thrust at higher altitudes, explain the results well.

Two comments on generating the acceptable response envelope require clarification. First, the responses are normalized to their final value not commanded value. Therefore, the envelope does not suggest that the commanded C^* can be maintained at every flight condition. Second, several responses at 0.5M violated

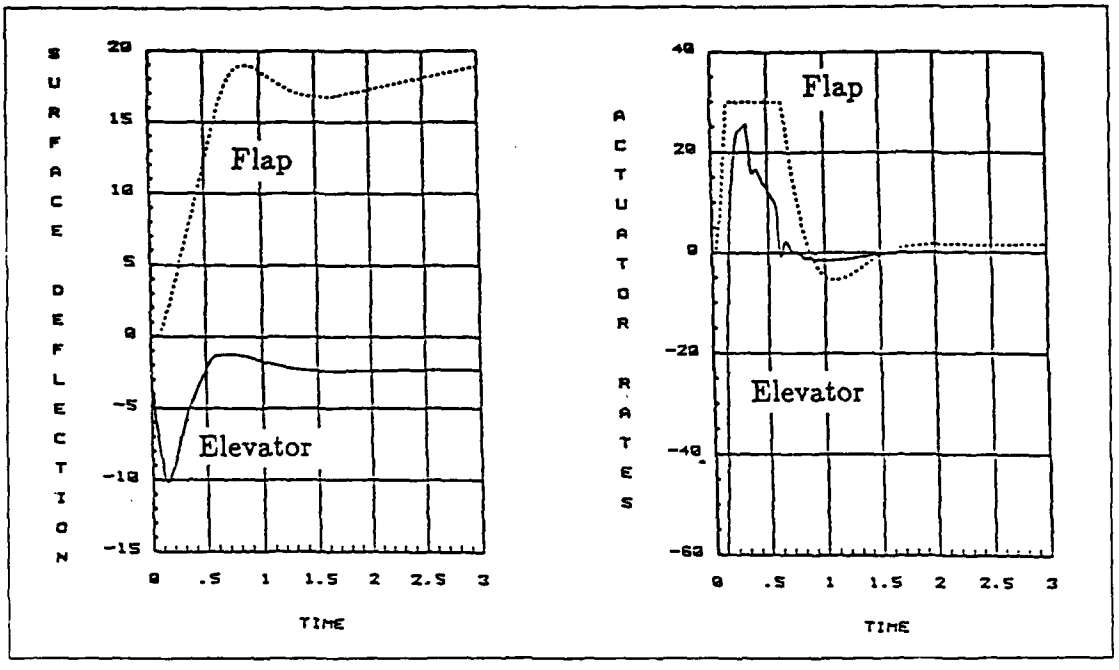

Figure 5.6. Surface Deflections and Rates for 9g Command at Nominal

Altitude (ft)	Mach Number				
	0.5	0.6	0.7	0.8	0.9
5,000	7.3	9.0	9.0	9.0	9.0
10,000	5.9	9.0	9.0	9.0	9.0
15,000	4.7	6.5	9.0	9.0	9.0
20,000	3.7	5.0	7.6	9.0	9.0
30,000	2.0	3.3	4.2	4.2	7.9

Table 5.1. Maximum Commands in g's for Acceptable Responses

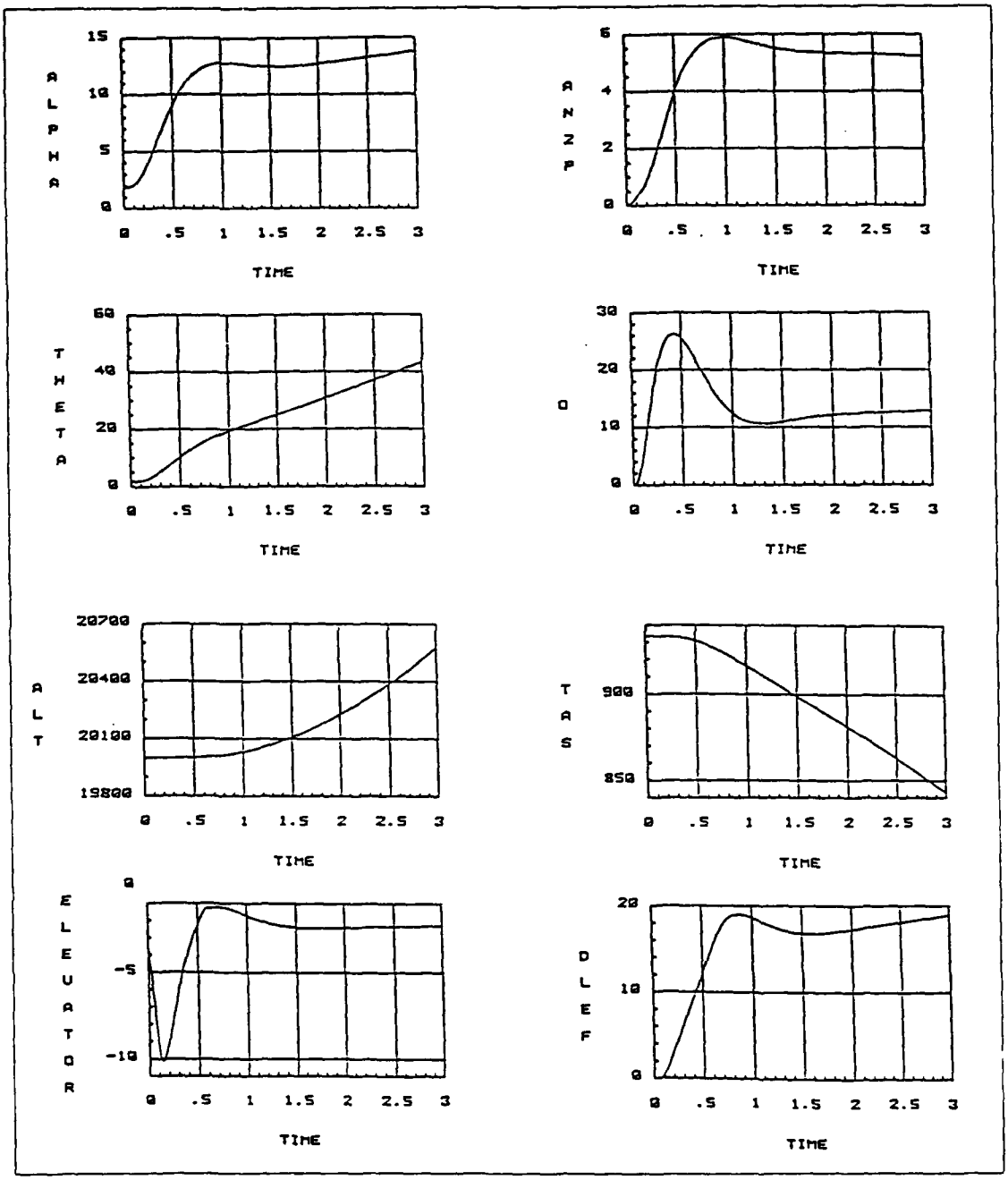

Figure 5.7. Aircraft Response to 9g Command at Nominal

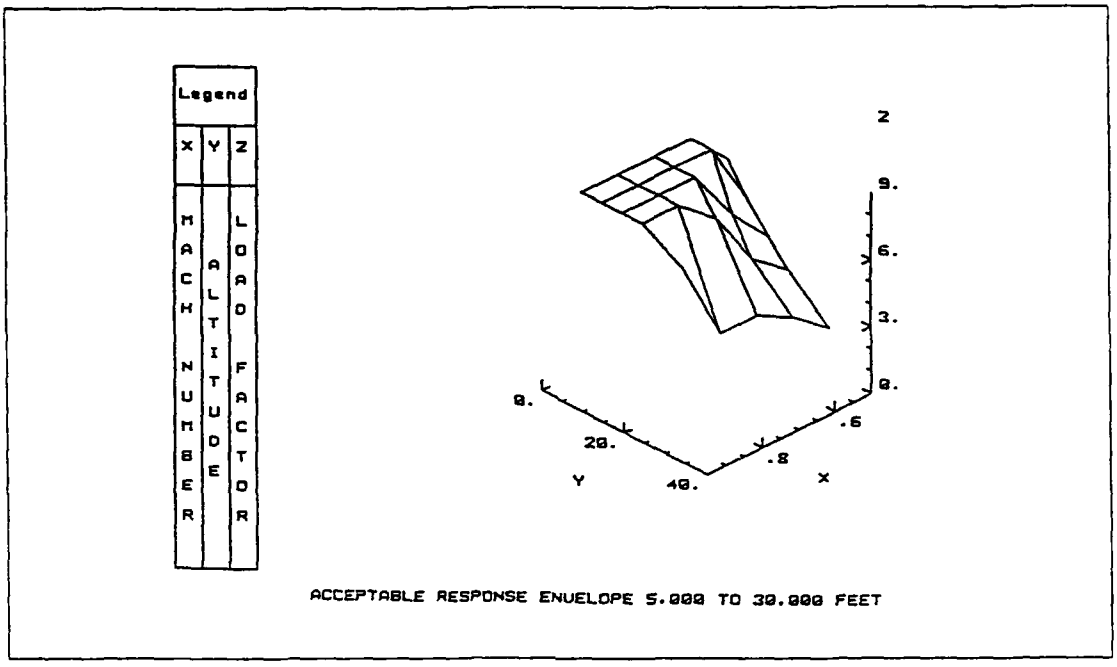

Figure 5.8. Flight Envelope of Acceptable SAS Responses

the bounds for small commands, then achieved acceptable responses for larger command up to the point of the maximum command listed in the envelope (see Appendix C). This is due to the slow prefilter chosen and can be eliminated by increasing the bandwidth of the prefilter. It should be noted that the slow responses occur while expanding the envelope and are not characteristic of the nominal flight condition.

Equivalent Inner Loop

As mentioned in the discussion of the nonlinear prefilter gain, it is desired to represent the designed SAS as a new equivalent linear plant. This simplifies the synthesis of the additional pilot compensation of Chapter VI.

The program used to generate the set P is used to obtain the equivalent plant as

$$P_e(s) = \frac{97.5870(s + 0.8703)(s^2 + 3.9438 \pm j10.3674)}{(s + 0.8352)(s^2 + 6.3252 \pm j8.8315)(s^2 + 8.7786 \pm j5.4357)} \tag{5.1}$$

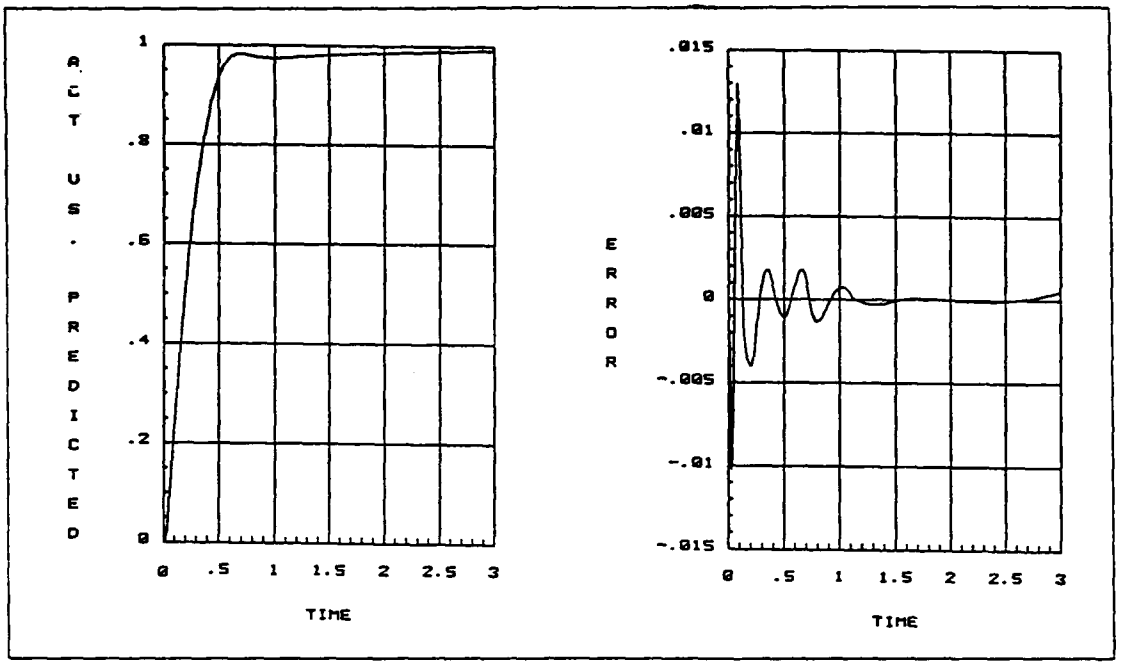

Figure 5.9. Outputs of $P_e(s)$ and YF-16 for Step Input

The time histories used are; the C^* response for a commanded 1g at the nominal flight condition, while the input is a unit step instead of the signals to the actuators. The response of both the nonlinear simulator and the equivalent SAS plant to a 1g step are shown along with the error in Figure 5.9.

Summary

This chapter presents the MATRIX$_X$ linear simulation of the SAS designed in Chapter IV as well as the reasons for modifying it. The modification is validated by comparing the resulting linear simulation with the nonlinear response. A nonlinear prefilter is then presented to better linearize the inner loop final values for use in the synthesis of Chapter VI. The robustness of the inner loop is demonstrated by nonlinear simulations that drastically expand the flight envelope. Finally, an equivalent LTI SAS plant is chosen to represent the design up to this point.

VI. Pilot Compensation

Introduction

This chapter presents the pilot compensation to be used in conjunction with the SAS designed in Chapter IV. The synthesis of this compensation is based upon obtaining a desirable response from the aircraft while reducing the workload of the pilot. The technique used is based upon the *Neal-Smith* pilot model for compensatory tracking. The compensation is designed on MATRIX$_X$ followed by nonlinear simulations in Fortran. A fourth order Padé approximation of a pure time delay is used in the Fortran simulations and the effects of this approximation are shown.

The Pilot Model

The form of the mathematical model used in the design of the remaining compensation is shown in Figure 6.1. The equivalent plant $P_e(s)$ is that of Eq (5.1) representing the SAS designed in Chapter IV. The model used to represent the pilot is that used in the technical report by Peter Neal and Rodger Smith [18] to predict pilot ratings for a longitudinal compensatory tracking task. The configuration of Figure 6.1 allows only a single degree of freedom, $F_p(s)$, to achieve the desired response.

The dynamic model representing the pilot is taken directly from the Neal-Smith report [18] as:

$$K_p e^{-0.3s}\left(\frac{\tau_{p_1}s+1}{\tau_{p_2}s+1}\right) \tag{6.1}$$

The pilot is represented by a variable gain K_p, a time delay, and a variable first order compensation network. The factors τ_{p_1} and τ_{p_2} represent the adaptive compensation provided by the pilot to accomplish a specific task. The time delay includes the time required for the pilot to sense a change in C^*, decide what action

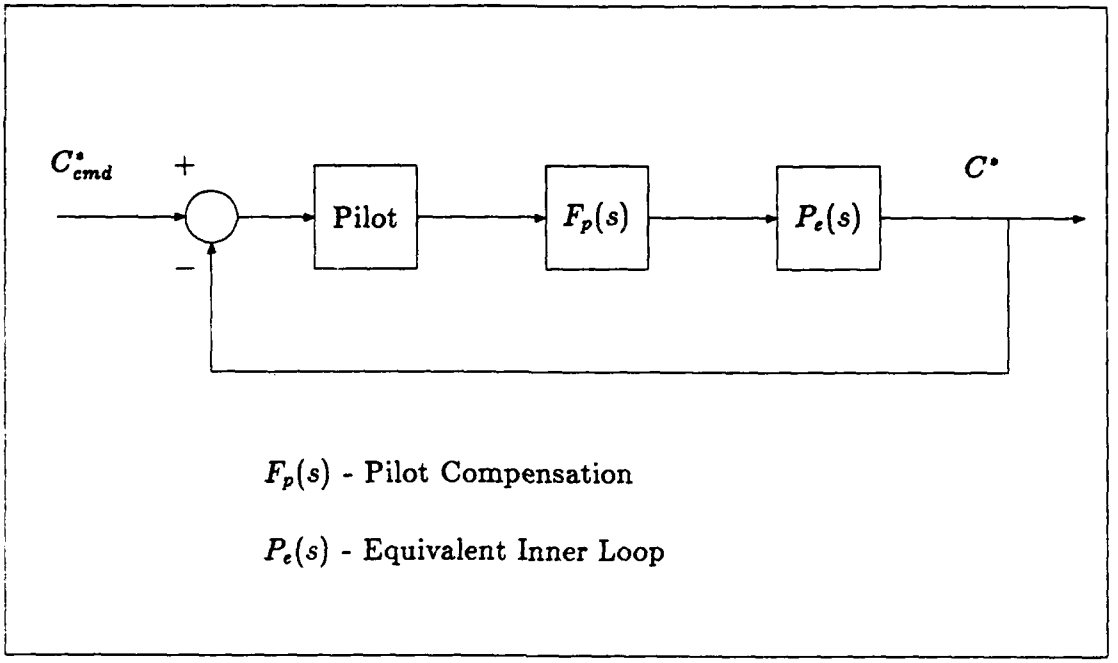

Figure 6.1. Form of Pilot Compensation

to take, and the neuromuscular lags [18]. The time delay of 0.3 seconds used may be excessive since the YF-16 uses a force stick and the displacement of the pilot's arm is negligible. The neuromuscular lags could therefore be neglected, but the objective is to present a synthesis technique so the value of 0.3 seconds is used throughout this thesis. The purely mental time delay of a human is closer to 0.2 seconds [15].

The block diagram of Figure 6.1 is considered a compensatory model in that the pilot operates only on the difference of commanded and actual C^*. It is obvious that in real life this is not the case, the pilot also uses many other inputs in determining the control that he applies. However, this model has been shown to adequately explain the more important aspects of tracking [18], and is relatively simple to analyze.

Transforming Analysis to Synthesis

The work in pilot modeling to date has been used to predict the pilot rating of a ***designed*** flight controller; if unacceptable results were predicted, modifications could be made to the prefilter [1]. The objective of this thesis is to take into account the prediction of pilot rating, given by the Neal-Smith criterion, and provide compensation a priori to give an acceptable predicted response.

The goal of this compensation is to minimize the additional compensation, or workload, required of the pilot to meet good closed loop performance requirements. The time delay in Eq (6.1) is inherent to the pilot, it is the gain K_p and the first order compensation network that must be generated by the pilot. Minimizing this compensation would enable the pilot to act only as a time delay giving, $K_p = 1$ and $\tau_{p_1} = \tau_{p_2} = 0$. The proposed synthesis technique is to perform a prediction analysis similar to that of Neal-Smith, while forcing an acceptable rating. The resulting pilot model may be of greater complexity than Eq (6.1) but must contain the time delay term. The resulting model is then equal to Pilot $\cdot$ $F_p(s)$ of Figure 6.1. Since it is desired that the pilot provide no additional lead-lag compensation, $F_p(s)$ is built into the control system and is set equal to the resulting pilot model obtained above excluding the time delay.

Synthesis of the Pilot Compensation $F_p(s)$

As outlined earlier, the design of $F_p(s)$ is based upon conducting a prediction of pilot rating using a modified Neal-Smith criterion. The modification is that the designer is free to model the pilot with any lead and/or lag compensation, instead of the "optimum" compensation presented in the technical report [18]. This freedom allows one to obtain an acceptable prediction in cases which would be impossible with Eq (6.1). This freedom must be weighted against achieving a practical compensator $F_p(s)$.

Pilot's View of Good Tracking Performance. The Neal-Smith report [18] gives an excellent explanation of converting "what the pilot sees" into usable tracking performance standards, to which the reader is referred. Sections 6.2 and 6.3 of the report are summarized below by presenting the performance standards along with definitions used in the technique [18]. All references to the closed loop are for $\frac{C^*}{C^*_{cmd}}$ of Figure 6.1.

Bandwidth (ω_{BW}): Bandwidth is defined as the frequency for which the phase angle of the *closed loop* is equal to $-90°$. It is a measure how quickly the pilot can move the aircraft's nose towards the target.

Droop: Droop is defined as the maximum excursion of the *closed loop* magnitude below the 0 dB line for frequencies less than ω_{BW}. In absence of large oscillations, droop is a measure of how slowly the aircraft settles down on target.

Standards of Performance: A minimum bandwidth ω_{BW} of 3.5 rad/sec for airspeeds above those causing wing buffet and a maximum droop of 3 dB.

PIO Tendency: The tendency for pilot induced oscillations is defined in terms of the Bode magnitude of any *closed loop* resonant peak that results from the pilot's efforts to achieve the performance standards.

Pilot Compensation: The pilot's physical and mental workload required to achieve the standard is defined in terms of the phase angle of his additional compensation at $\omega = \omega_{BW}$.

A visualization of the closed loop standards on bandwidth, droop along with a PIO limit of 3 dB are shown as closed loop contours on the Nichols chart of Figure 6.2.

In addition to the above standards of performance, this thesis proposes further constraints on the response. These modifications to the standards are gener-

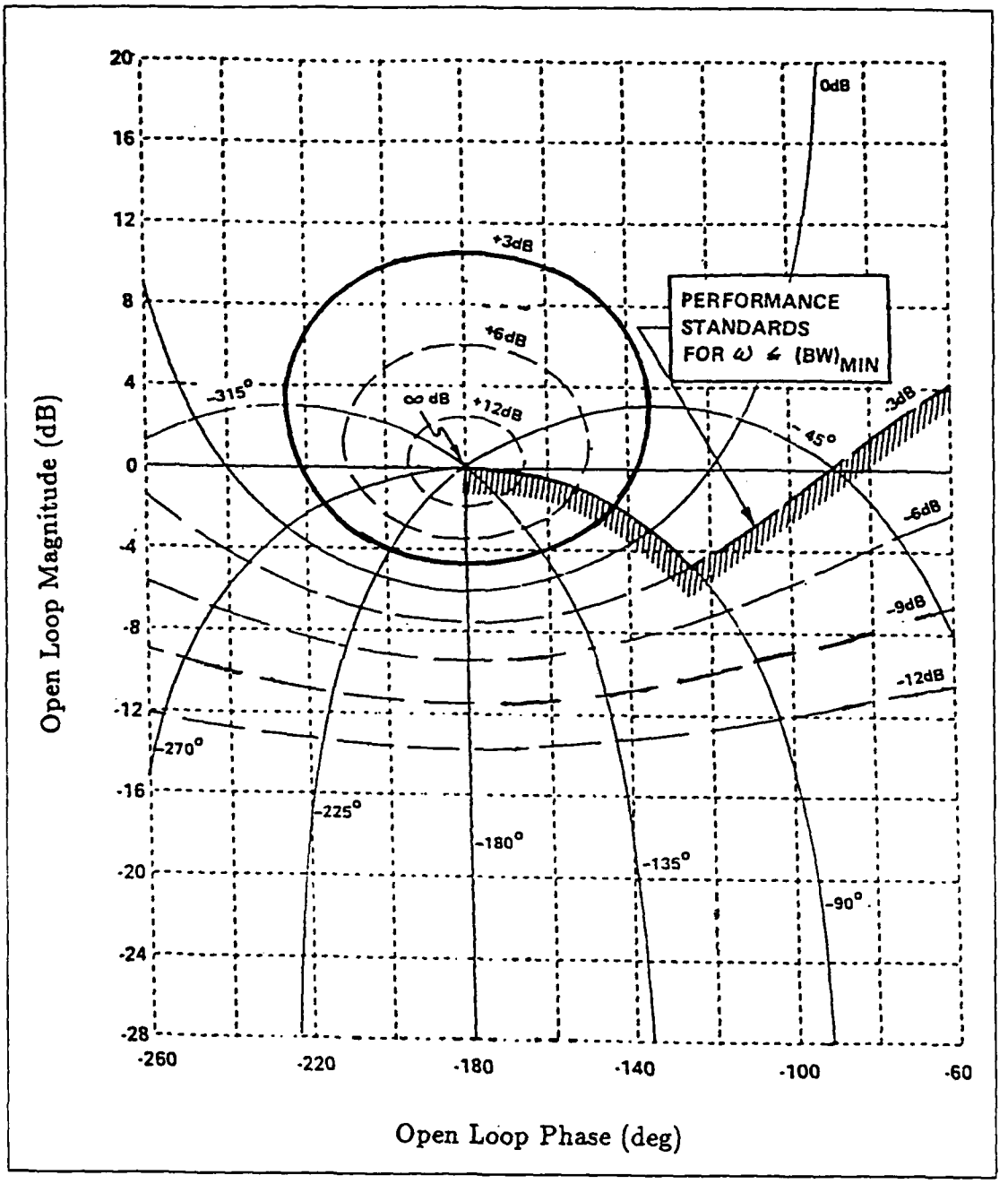

Figure 6.2. Nichols Chart Representation of Standards of Performance [15]

ated from analyzing the pilot comments of the reference report [18]. Their comments suggest that a response with an initial overshoot but no resulting undershoot of the final value is preferred. Such responses were consistently preferable to first order responses or those that oscillated about the final value like a pure second order response. The amount of undershoot is related to the amount of droop in the closed loop frequency response. With the above reasoning and the fact that the original 3 dB droop limit is chosen "somewhat arbitrarily" [18] it is decided to minimize the droop to nearly 0 dB.

Shaping the Response. Since it is desired to have the pilot act only as a time delay, the pilot model of Figure 6.1 is merely $e^{-0.3s}$ for the remainder of this analysis. The open loop transfer function for the technique is then defined as:

$$\text{Open Loop} = O(s) = e^{-0.3s} F_p(s) P_e(s) \tag{6.2}$$

With only a single degree of freedom the poles, zeros, and gain of $F_p(s)$ are used to shape the *closed loop* directly. Using the new specification of droop, the following is an outline of the shaping of $\frac{C^*}{C^*_{cmd}}$ on the Nichols chart (see Figure 6.2).

The response should "hug" the 0 dB M contour until crossing the closed loop phase angle contour of $-90°$ at a frequency of $\omega = \omega_{BW} = 3.5$ rad/sec. Once the standards are meet for $\omega \leq 3.5$ rad/sec the PIO tendency is the dominant factor. The Neal-Smith Criterion gives the maximum closed loop resonance resulting in a good rating as 3 dB. Therefore the 3 dB M contour is the dominant factor for $\omega > 3.5$ rad/sec.

The pilot model and $P_e(s)$ are fixed, thus a starting point in the design is the plot of the open loop response on the Nichols chart for $F_p(s) = 1$. However,the desired closed loop is to hug the 0 dB contour; therefore, the first try is to place a pole at the origin. The response for $F_p(s) = \frac{1}{s}$ is shown in Figure 6.3. This puts the open loop $O(j\omega)$ for $\omega = 3.5$ rad/sec at -12.1 dB and $-192°$. The compensator must contribute approximately 55° at this frequency.

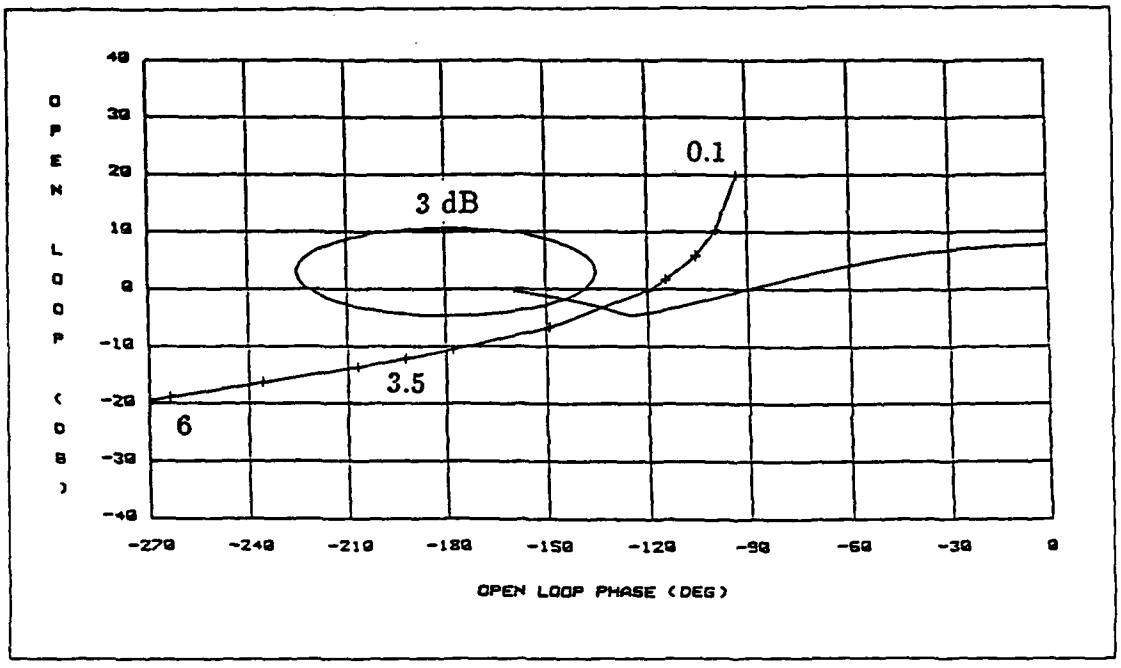

Figure 6.3. Starting Point for the Design of $F_p(s)$

The problems presented by the time delay are obvious in the figure. The characteristics of $e^{-0.3s}$ being $|1|\angle -0.3\omega$ rad. Having a gain of 0 dB at all frequencies but a phase angle contribution of $-0.3 \times \frac{180°}{\pi \text{ rad}} = -17.19$ deg/rad, for example $-1.719°$ at $\omega = 0.1$ rad/sec and $-171.9°$ at $\omega = 10$ rad/sec. These characteristics cause the open loop magnitude $|O(j\omega)|$ to be nearly horizontal for all frequencies above approximately 20 rad/sec. However, there is still room for improvement over the pilot's bandwidth of 0.5 to 10 rad/sec [18]. This near 0 dB/dec slope of the open loop can cause extreme gain sensitivity and high frequency resonant modes.

One example depicting both of these conditions is shown in Figure 6.4 which is taken directly from the Neal-Smith report. This figure shows the open loop $O(j\omega)$ frequency response for $0.6 \leq \omega <\approx 21$ rad/sec on the Nichols chart. The solid line is for $0.6 \leq \omega \leq 10$ rad/sec and the dotted line is for $15 \leq \omega <\approx 21$ rad/sec. The solid line shows the response over the pilot's bandwidth with a resonance of 1 dB at approximately 6.5 rad/sec. An increase of only 4 dB in the open loop produces

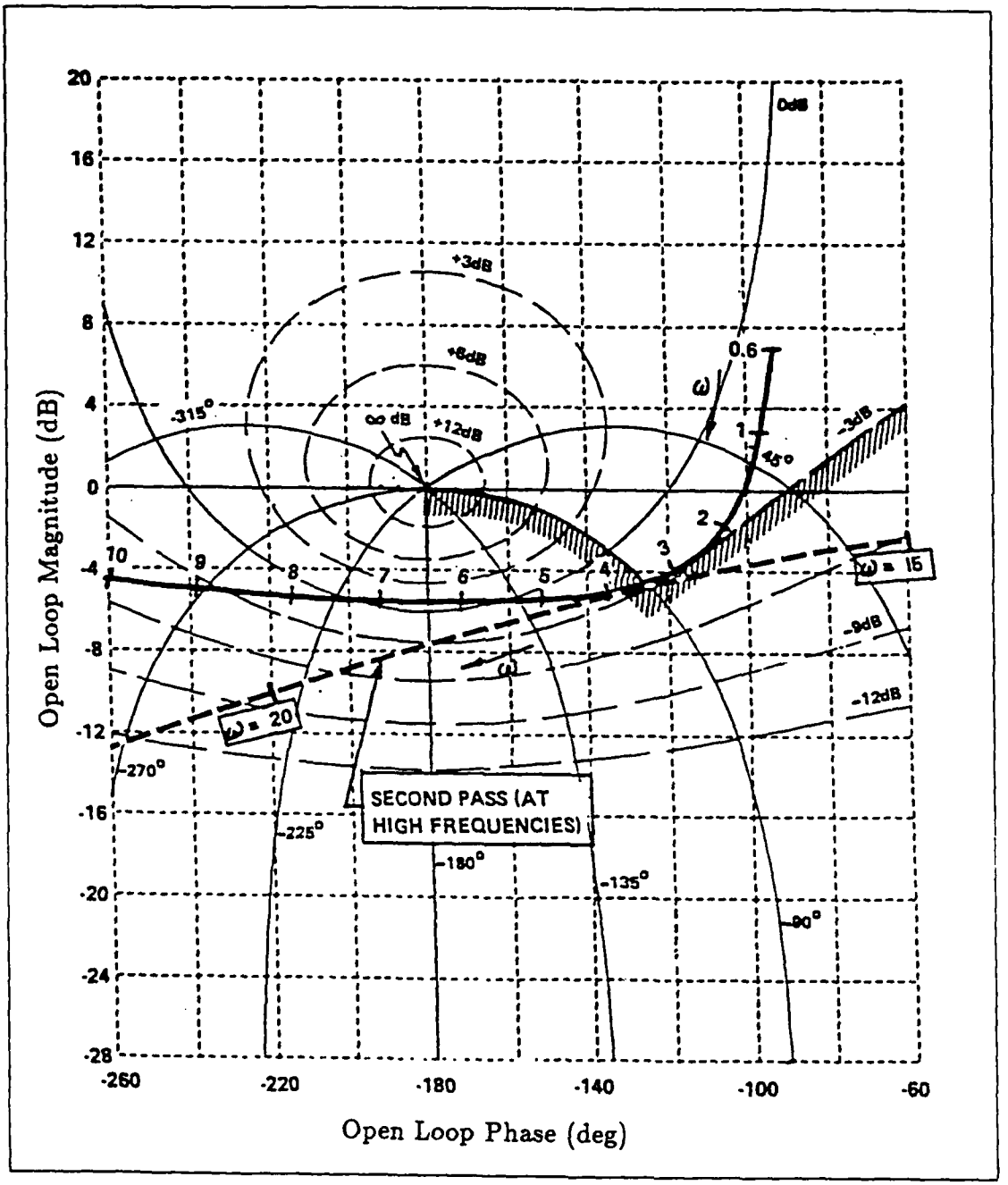

Figure 6.4. Response Showing Cause of High Frequency Resonance [15]

a resonance of 12 dB, representing a very lightly damped response. Visible in this frequency range is that the slope of the open loop function $O(j\omega)$ is positive between 7 and 15 rad/sec causing the high frequency resonance. This problem is seen by observing several points on the response of $O(j\omega)$ in Figure 6.4. The curve shows the closed loop magnitudes for $\omega_i \approx 10, 15, 17, 21$ rad/sec to be approximately $-5, -6, -2, -13$ dB respectively. The resonant peak in this frequency range represents a poorly damped mode at $\omega \approx 17$ rad/sec and can be seen in a Bode plot of the closed loop magnitudes for the above five frequencies. The pilot comments on the handling of the flight control system represented in Figure 6.4 of "difficulties in acquiring a target" and "oscillations about the target" are in agreement with the analysis. Therefore it is concluded that the slope of the open loop transfer function is to be kept negative until the magnitude is sufficiently small to avoid the above problems. However the phase required of the compensator may be so large that this is not possible, for such cases the slope is kept negative as long as possible while meeting low frequency specs.

In the attempt to minimize droop and PIO tendencies, while achieving some overshoot and a bandwidth of 3.5 rad/sec, the following compensator is chosen:

$$F_p(s) = \frac{761.5615(s^2 + 16.6s + 36)}{s(s^2 - 100s - 100^2)} \tag{6.3}$$

The system frequency response is shown in Figures 6.5 and 6.6.

Simulation of the Pilot Compensation

The MATRIX$_X$ linear time responses are used simultaneously with the Nichols chart in obtaining the final design. The step response is as desired, an initial 20 % overshoot with minimal undershoot. To acquire zero undershoot with a 20 % overshoot requires a reduction in bandwidth which is considered more undesirable than the undershoot. This is due to the amount of lead phase angle required to achieve a bandwidth $\omega_{BW} = 3.5$ rad/sec while maintaining a reasonable rate of decrease in the magnitude of $O(j\omega)$. The MATRIX$_X$ linear simulations using a pure delay

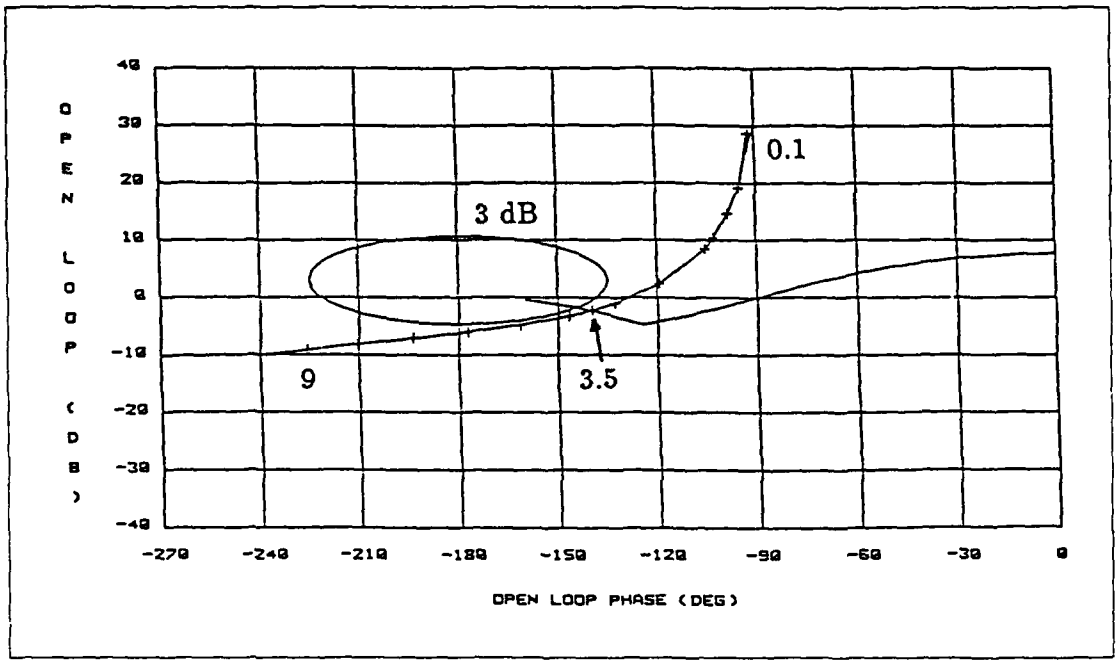

Figure 6.5. Response and Standards of Performance for Final Design

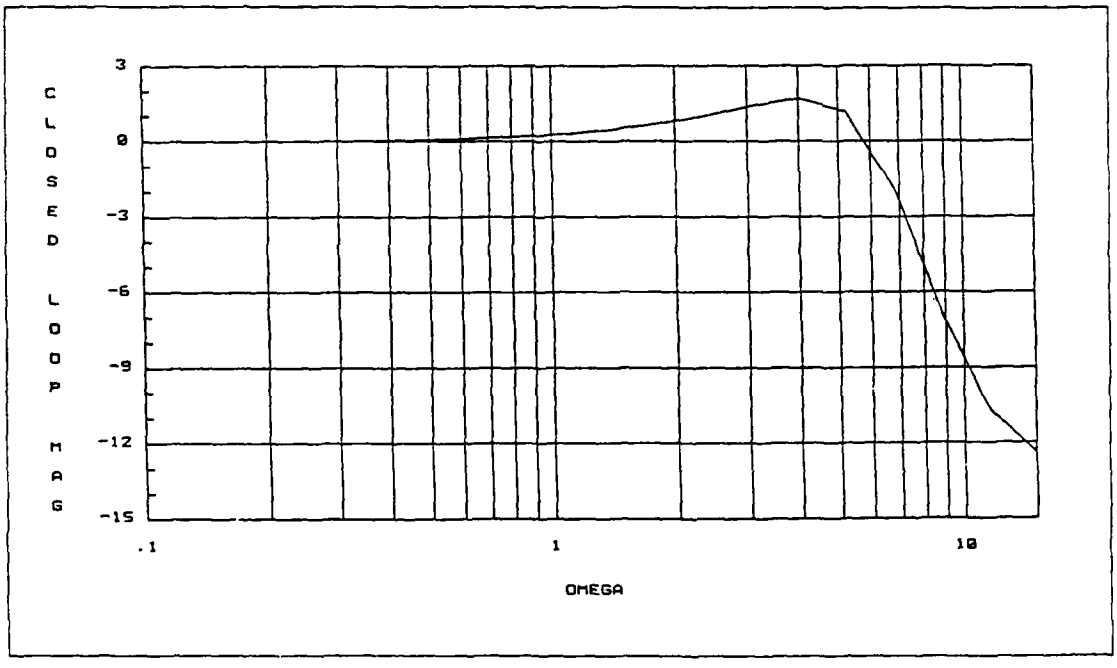

Figure 6.6. Closed Loop Frequency Response

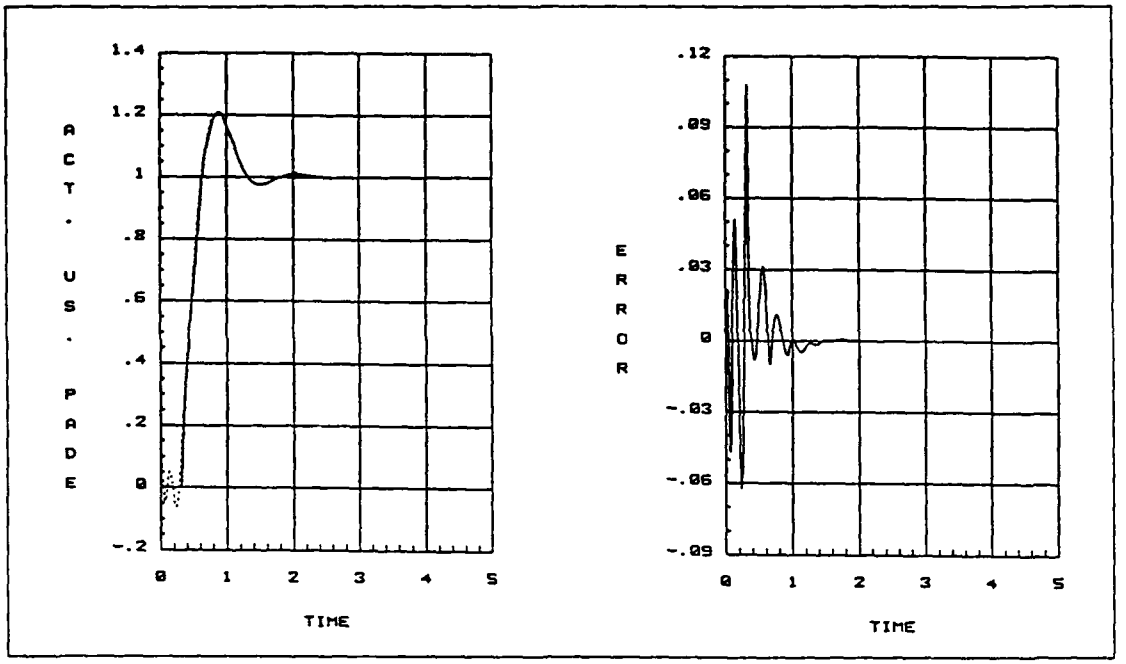

Figure 6.7. Effect of Using Padé Approximation

for the pilot model show zero output for the first 0.3 seconds with time specs of $t_p = 0.8$ sec and $t_s = 1.6$ sec.

Again the true test is that of the nonlinear simulation. Instead of writing the Fortran code to approximate the time delay it is decided to use a Padé approximation of the function e^{-s} (see Appendix D). Figure 6.7 shows the MATRIX$_X$ simulation of the design using both the time delay and a fourth order Padé approximation along with the error caused by using the approximation. Most of the error is during the first 0.3 seconds where the approximation has a nonminimum phase response while the delay has zero output. The approximation is judged to be sufficient and the nonlinear simulations begun.

The first nonlinear simulation is for a 1g step commanded initiated from straight and level flight at 0.9M and 20,000 ft. The response is shown in Figure 6.8 and is judged to be excellent, again 20 % overshoot with negligible undershoot and a small rise time after the initial time delay. The effects of the approximation's

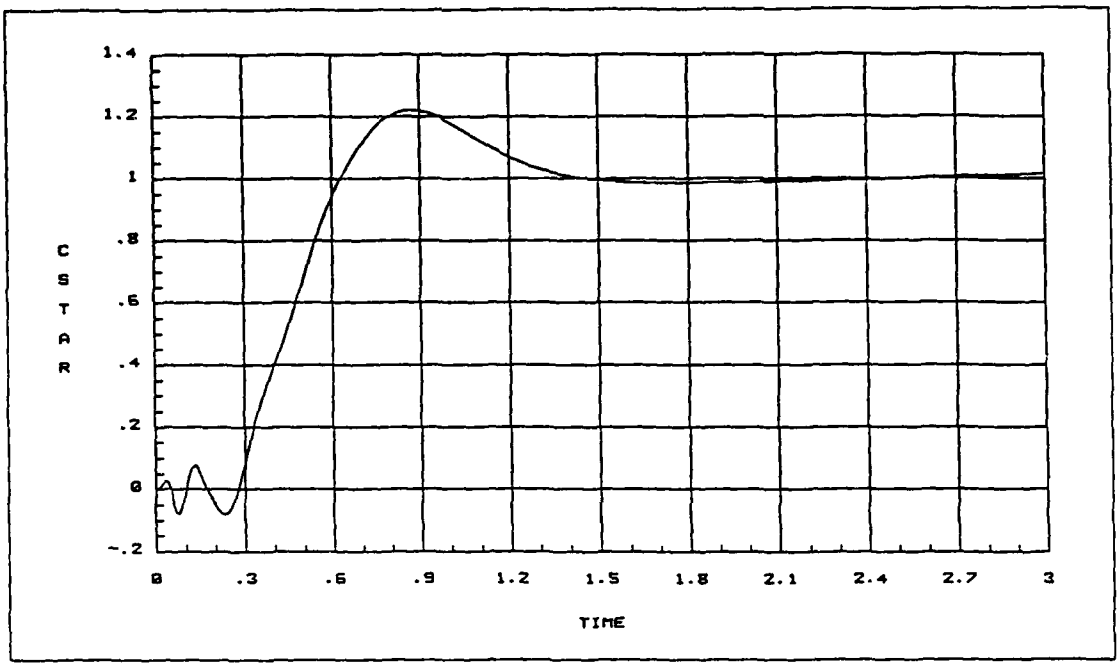

Figure 6.8. Nonlinear Response to $C^*_{cmd} = 1g$

nonminimum phase response on the aerodynamics are considered negligible due to their magnitude and duration. It is again noted that this nonminimum phase characteristic should be absent when a genuine time delay is used.

Next step is to answer the question of how to accomplish other simulations without voiding the standards of performance or pilot model proposed by the Neal-Smith report. Any pilot modeling must be constrained to a specific task [18]. The data for the Neal-Smith analysis was taken during fine tracking tasks, not for large acquisition commands. The decision is made to simulate 1g steps while varying the initial trim conditions. Additional simulations starting from coordinated turns trimmed to load factors of 2 to 5g's are found to give similar results as shown in Figure 6.9.

The question remains as to the sensitivity of the system to changes in the bandwidth while performing the same task. That is, what are the effects of this additional compensation when the pilot flies to achieve a bandwidth other than

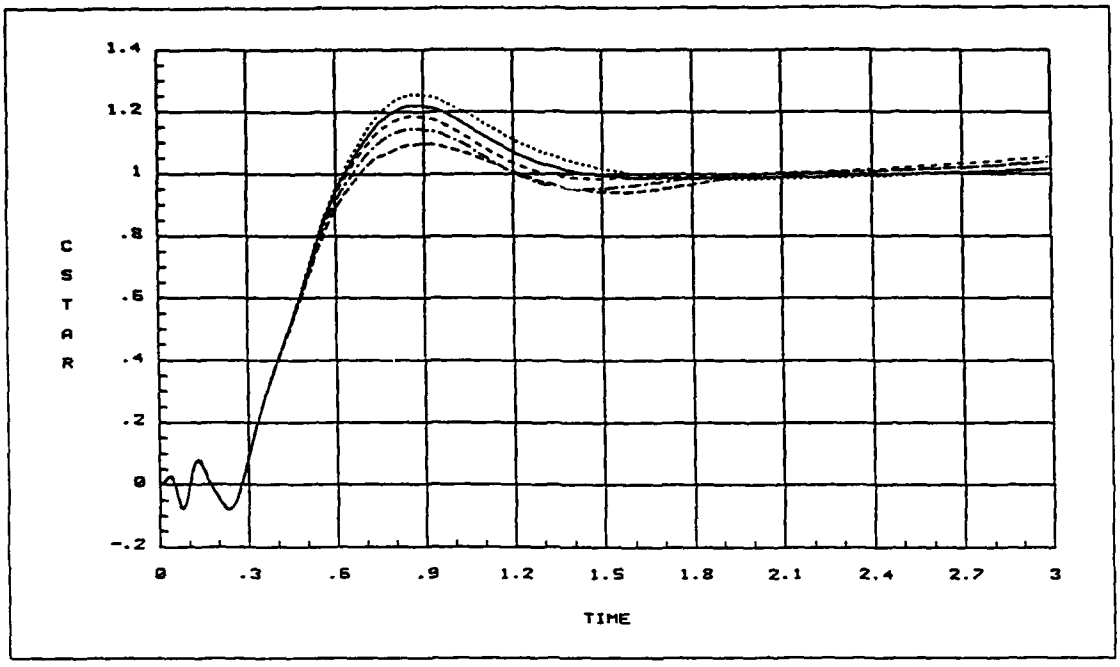

Figure 6.9. Simulations for Trimmed Load Factors of 1g to 5gs

3.5 rad/sec. This is accomplished by referring to Figure 6.5. If a reduction in bandwidth is desired, the pilot need only lower his gain, this has a stabilizing effect.

To increase the bandwidth the pilot must use gain, lead compensation, or a combination of the two. Pilots seem to have no problem with generating up to 25° of lead compensation and feel comfortable with doing so [18]. Without the compensation $F_p(s)$ the pilot may have used all this lead compensation and more, although the handling may have been judged good using the Neal-Smith Criterion. However this is based upon achieving a bandwidth of 3.5 rad/sec. To increase this bandwidth the pilot would have to use mostly gain, if he had used up his lead generating ability, which gives the gain sensitivity problem discussed with Figure 6.4. The addition of $F_p(s)$ allows the pilot to achieve a bandwidth of 3.5 rad/sec without generating any additional lead. This comfortable region of additional lead is then used to increase the bandwidth of the entire closed loop system avoiding the gain sensitivity problem.

Summary

This chapter presents the design of the outer loop of Figure 6.1, consisting of pilot compensation based upon the Neal-Smith Criteria. The objective of minimizing the compensation required of the pilot is accomplished by providing the compensation, to achieve a bandwidth of 3.5 rad/sec with a good response, with $F_p(s)$. This allows the pilot to act as a pure time delay. The nonlinear simulations presented, using a Padé approximation of the time delay, show excellent results for initial load factors of up to 5gs. Finally, a discussion of the effects of bandwidth show that the closed loop bandwidth for the tracking task has been increased.

VII. Conclusions and Recommendations

Discussion

This thesis demonstrates the application of Nonlinear Quantitative Feedback Theory to flight control design and presents a compensation design technique which reduces pilot work load. The nonlinear QFT technique is applied to the YF-16 aircraft which results in an inner loop SAS to control the output C^* and guarantees that the response lies within the bounds suggested by Tobie [20]. However, this inner loop design does not include the characteristics of the human pilot a priori, and such is the case with nearly all current preliminary flight control designs [1]. The characteristics of the human pilot are usually not dealt with until the man-in-the-loop simulation phase of final control system design. Waiting until this late point in the system's development to attack this problem is extremely cost inefficient in two ways. First, due to the high cost of such simulations delay must be keep to a minimum. Secondly, modifications to a system so far into it's development are very costly. Ignoring the inherent time delay of the human pilot results in extensive adjustments to the original design to achieve satisfactory pilot ratings.

Instead of fine tuning the design during this expensive phase of system design, an adjustment is made prior to these man-in-the-loop simulations with additional pilot compensation. This pilot compensation allows the controller to achieve good handling qualities predictions for simulations including the inherent time delay of the human pilot.

Extensive use of CAD tools, not included in this thesis, greatly reduces the calculations and book keeping required in the synthesis process. Listings of the Fortran code and MATRIX$_X$ routines may be made available through the following points of contact:

Convert Time Histories to Transfer Functions: Professor Isaac M. Horowitz, Department of Electrical Engineering and Computer Sciences, University of California at Davis.

MATRIX$_X$ Macros: Professor Constantine H. Houpis, Electrical and Computer Science Engineering Department, Air Force Institute of Technology, WPAFB Dayton Ohio.

Conclusions

Based upon the work performed on this thesis and the results obtained, the following conclusions are made.

1. A nonlinear plant can be represented by a set P of linear time-invariant plants for use in a design problem. The method of Chapter III is found to describe the nonlinear YF-16 rather well.
2. Nonlinear Quantitative Feedback Theory can be successfully applied to the synthesis of flight controllers resulting in fixed compensators that yield acceptable responses over a large range of nonlinear parameter variation.
3. Linear simulations are an effective design aid but final analysis of the control of the nonlinear plant must be performed using the nonlinear simulations. The linear simulations are invaluable for the insight that they provide but this insight can only be gained by comparing them to the nonlinear simulations.
4. Use of the MATRIX$_X$ routines in the synthesis process greatly reduces the workload and calculation errors, however they are written for this specific thesis. There is a definite need for a generic computer aided design (CAD) package to ease the design burden associated with QFT and to speed the design process.
5. It is possible to design compensation for the task of reducing pilot workload and therefore increasing the system bandwidth. The technique developed

in this thesis will work for other tasks. It is necessary to emphasize that the closed loop performance requirements are task specific, and the expected performance is expected to vary depending on the particular task.

Recommendations

After completion of the of the stability augmentation system design for the YF-16 and the pilot compensation, followed by analyzing the simulation results, one task remains to be completed. The technique must be validated by actual man-in-the-loop simulations such as on AFIT's SIMSTAR hybrid computer. The real-time, full flight envelope simulator is nearing completion [2,16]. An original objective of this thesis effort was to include such simulations; however, upgrades to the system have prevented it. Beyond this immediate suggested task, three distinct areas for future study are proposed.

1. Extend the nonlinear SISO plant to that of the nonlinear MIMO plant with an emphasis on survivability and on acceptable responses while experiencing various surface failure conditions. Such work is underway based upon linearized plant models; however, using the nonlinear plant should make the results more realistic.

2. Expand the area of pilot compensation. Given any existing flight controller, use the developed technique for a variety of pilot tasks, where each task has different performance requirements. The controller can be adapted for a given task and a new compensator designed. Included in this research should be the ability to perform real-time man-in-the-loop simulations such as on AFIT's SIMSTAR F-16 simulator. This type of simulation can validate the technique proposed in this thesis by comparing handling qualities ratings for the same aircraft before and after the implementation of the pilot compensation for different tasks.

3. Develope a generic interactive CAD package devoted to QFT. Many useful routines have been developed by researchers for their work; however, their objective is to complete a specific design. Therefore these routines are written for the specific problem at hand with no time to check out other possibilities that can arise in other situations. A full time effort devoted solely to such a CAD package will be a step in the right direction.

Summary

This chapter reviews the design and results of this thesis. Recommendations are made for future projects in nonlinear QFT, pilot compensation, and development of a QFT CAD package.

Appendix A. *Equivalent LTI Plants*

The following are the LTI equivalents of the nonlinear plant response, outlined in Chapter III.

C^* Transfer Functions for 1g Responses

Plant #1: fit with 2,4

$$\frac{C^*(s)}{e_{\delta e}(s)} = \frac{-7.8130(s+2.2038)(s+11.2499)}{(s+1.4401)(s+2.535 \pm j3.0232)(s+54.9636)}$$

Plant #2: fit with 1,3

$$\frac{C^*(s)}{e_{\delta e}(s)} = \frac{-12.1501(s+4.4432)}{(s+2.1664 \pm j3.1576)(s+23.6823)}$$

Plant #3: fit with 2,4

$$\frac{C^*(s)}{e_{\delta e}(s)} = \frac{-5.3139(s+3.6184)(s+4.4139)}{(s+1.6627 \pm j2.5911)(s+5.7862 \pm j4.8427)}$$

Plant #4: fit with 2.4

$$\frac{C^*(s)}{e_{\delta e}(s)} = \frac{-5.0612(s+2.4154 \pm j2.1172)}{(s+1.6203 \pm j2.6521)(s+4.8324 \pm j3.3295)}$$

Plant #5: fit with 3,5

$$\frac{C^*(s)}{e_{\delta e}(s)} = \frac{-5.305(s+0.3668)(s+2.7128)(s+37.5146)}{(s+0.3301)(s+1.816 \pm j2.9212)(s+9.2333 \pm j14.9602)}$$

Plant #6: fit with 3,5

$$\frac{C^*(s)}{e_{\delta e}(s)} = \frac{-8.4862(s+1.4992)(s+3.5374 \pm j9.092)}{(s+1.1349)(s+3.158 \pm j3.5824)(s+4.2219)(s+70.153)}$$

Plant #7: fit with 4,6

$$\frac{C^*(s)}{e_{\delta e}(s)} = \frac{-7.557(s+0.4904)(s+4.88271 \pm j17.0975)(s+6.3816)}{(s+0.4382)(s+2.4838 \pm j2.973)(s+6.8833 \pm j13.8218)(s+29.3342)}$$

Plant #8: fit with 3,5

$$\frac{C^*(s)}{e_{\delta e}(s)} = \frac{-5.6663(s+0.2243)(s+2.4005)(s+27.2064)}{(s+0.1912)(s+1.6578 \pm j2.9563)(s+8.197 \pm j12.3188)}$$

C^* Transfer Functions for 2g Responses

Plant #9: fit with 2,4

$$\frac{C^*(s)}{e_{\delta e}(s)} = \frac{-7.0856(s+1.3909)(s+15.8178)}{(s+0.8592)(s+2.8374 \pm j2.3273)(s+35.7299)}$$

Plant #10: fit with 2,4

$$\frac{C^*(s)}{e_{\delta e}(s)} = \frac{-7.2503(s+3.587 \pm j3.1188)}{(s+1.5046 \pm j2.3305)(s+4.7352 \pm j5.9231)}$$

Plant #11: fit with 3,5

$$\frac{C^*(s)}{e_{\delta e}(s)} = \frac{-7.3788(s+0.9628)(s+3.7751 \pm j6.8517)}{(s+0.653)(s+3.0254)(s+3.8841 \pm j3.815)(s+19.3303)}$$

Plant #12: fit with 2,4

$$\frac{C^*(s)}{e_{\delta e}(s)} = \frac{-8.9094(s+0.977 \pm j2.4645)}{(s-0.8337 \pm j2.5676)(s+3.0528)(s+7.6762)}$$

Plant #13: fit with 3,5

$$\frac{C^*(s)}{e_{\delta e}(s)} = \frac{-6.0796(s+1.1201 \pm j3.2202)(s+9.4709)}{(s+0.9523)(s+1.0421 \pm j3.0456)(s+10.2039 \pm j8.8792)}$$

Plant #14: fit with 3,5

$$\frac{C^*(s)}{e_{\delta e}(s)} = \frac{-8.8134(s+0.6449)(s+7.0771 \pm j6.0902)}{(s+0.4816)(s+2.8856 \pm j2.2334)(s+9.6376 \pm j10.1537)}$$

Plant #15: fit with 4,6

$$\frac{C^*(s)}{e_{\delta e}(s)} = \frac{-10.164(s+0.3891)(s+1.946 \pm j20.3273)(s+3.0283)}{(s+0.3002)(s+1.7901 \pm j2.1313)(s+3.4594 \pm j16.0937)(s+19.2338)}$$

Validation of the LTI Transfer Functions

The following figures validate the set P of LTI plants used to represent the nonlinear YF-16. Each plot on the left contains two outputs. One being the actual output of the YF-16 simulator, the other the output of the LTI plant for the same input signal to the elevator's actuators. Each plot on the right is the error between the LTI response and that of the YF-16.

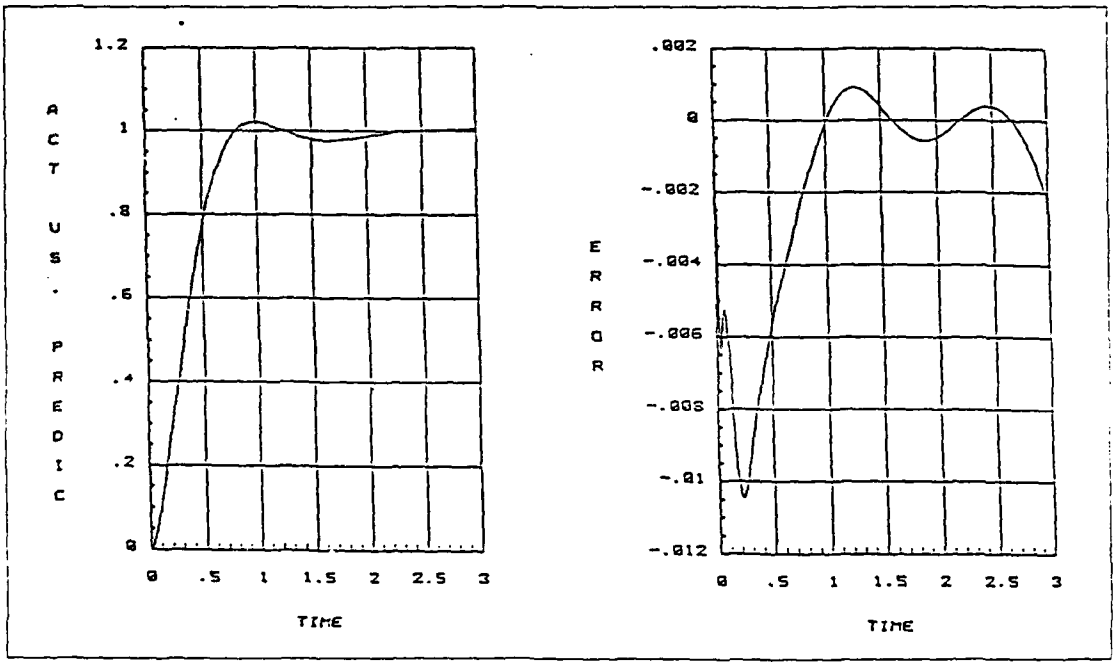

Figure A.1. Outputs of LTI Plant #1 and of YF-16 for the Same Input

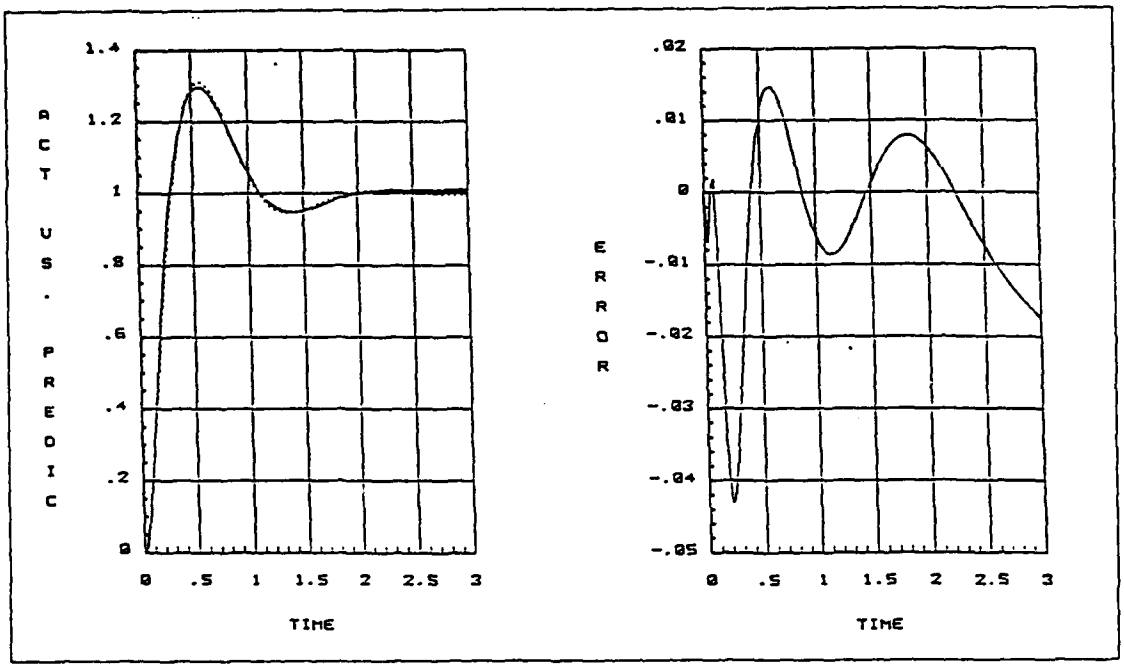

Figure A.2. Outputs of LTI Plant #2 and of YF-16 for the Same Input

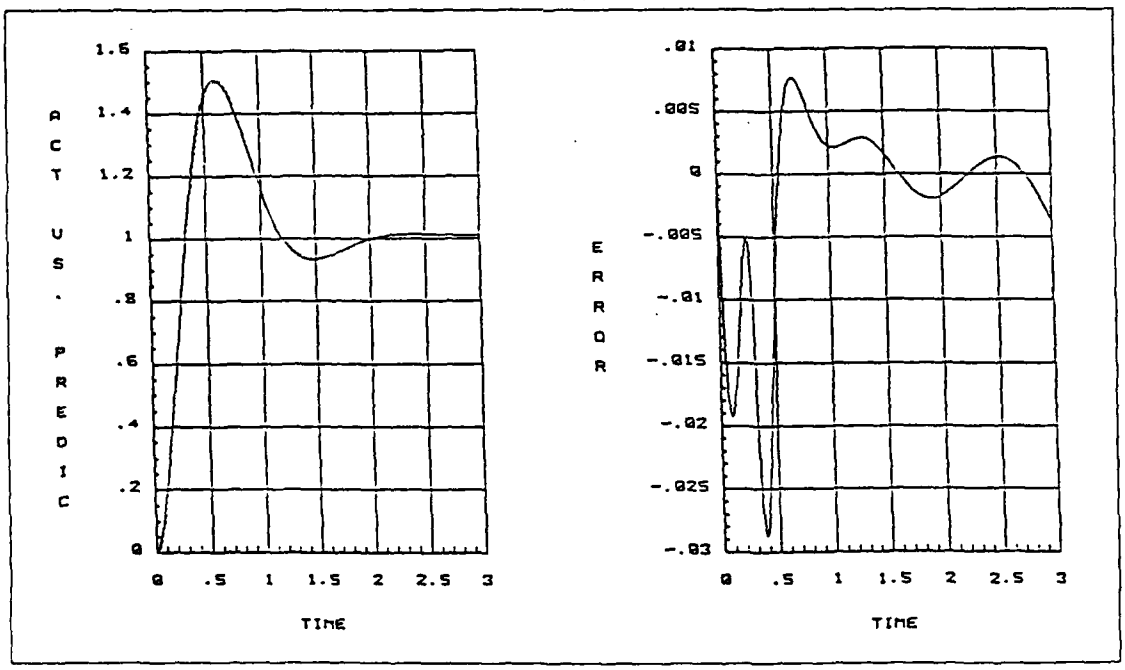

Figure A.3. Outputs of LTI Plant #3 and of YF-16 for the Same Input

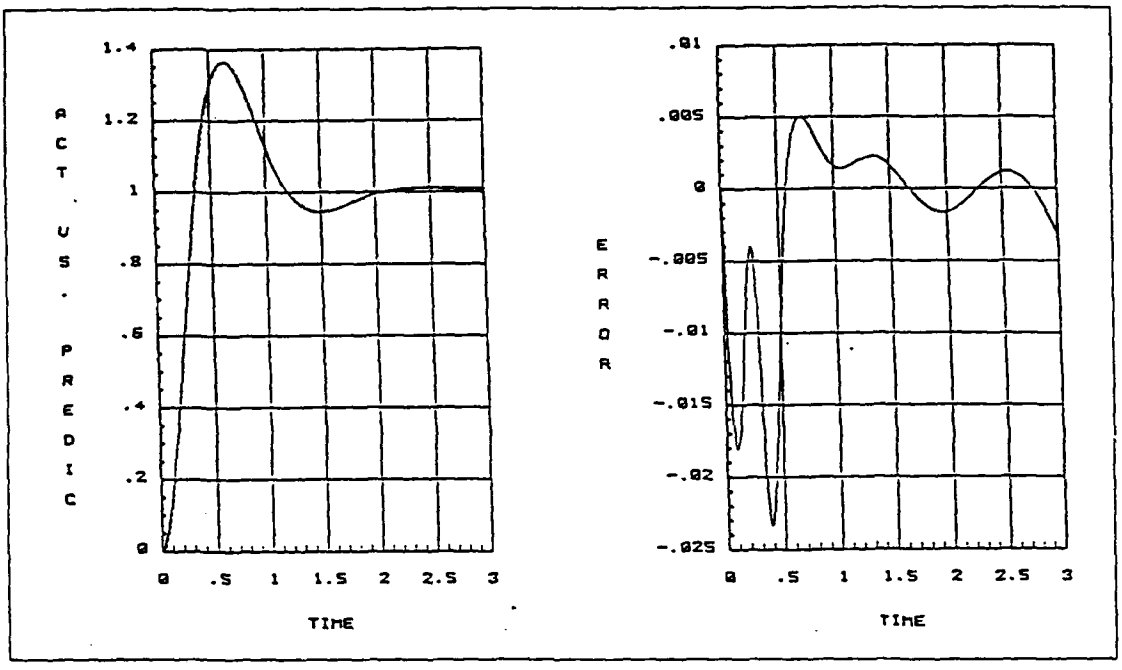

Figure A.4. Outputs of LTI Plant #4 and of YF-16 for the Same Input

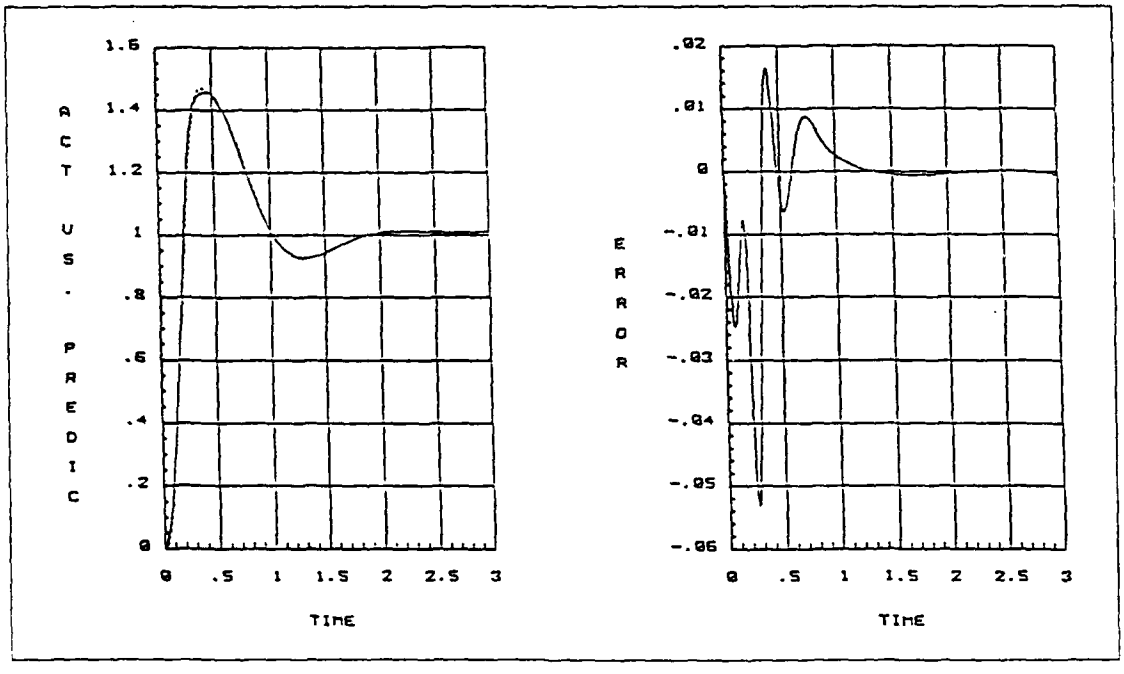

Figure A.5. Outputs of LTI Plant #5 and of YF-16 for the Same Input

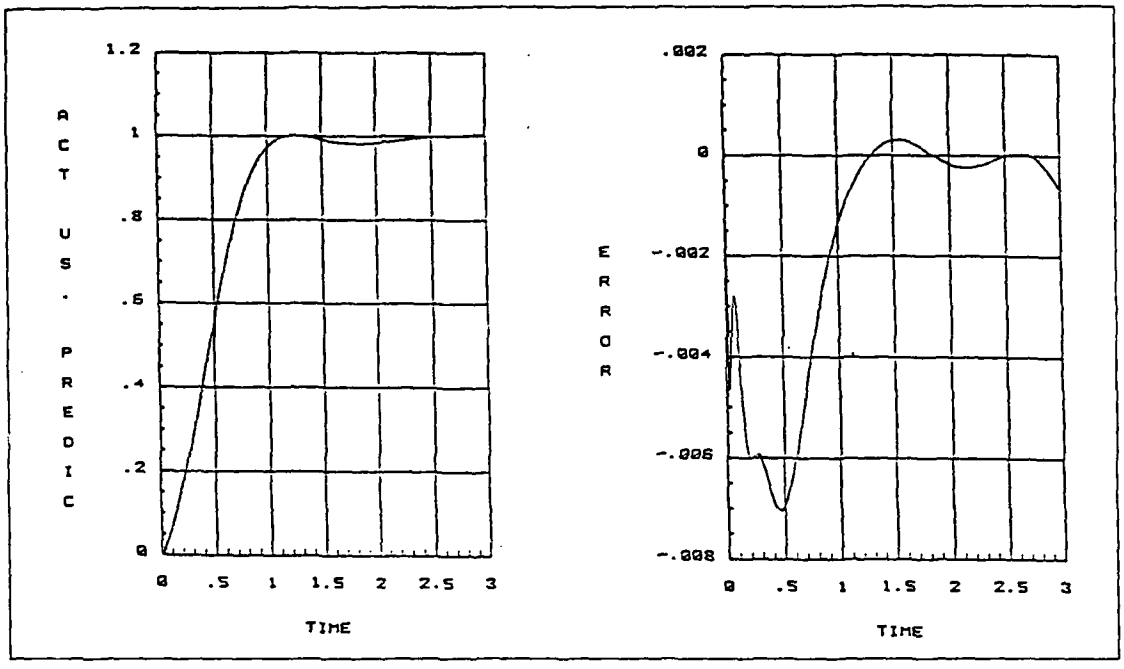

Figure A.6. Outputs of LTI Plant #6 and of YF-16 for the Same Input

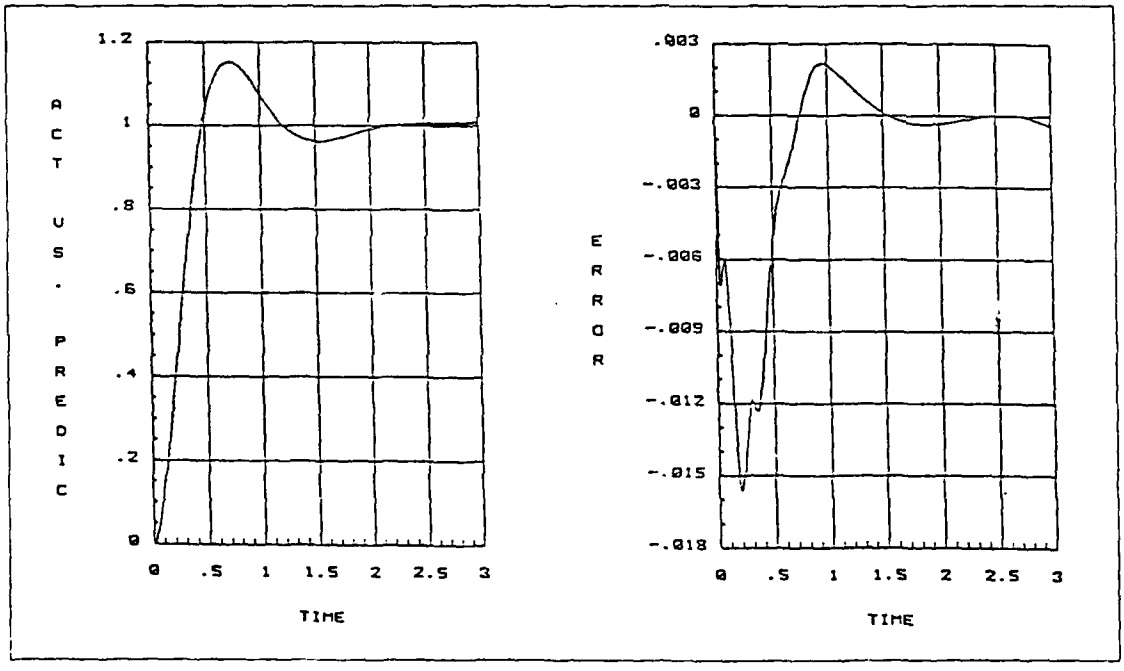

Figure A.7. Outputs of LTI Plant #7 and of YF-16 for the Same Input

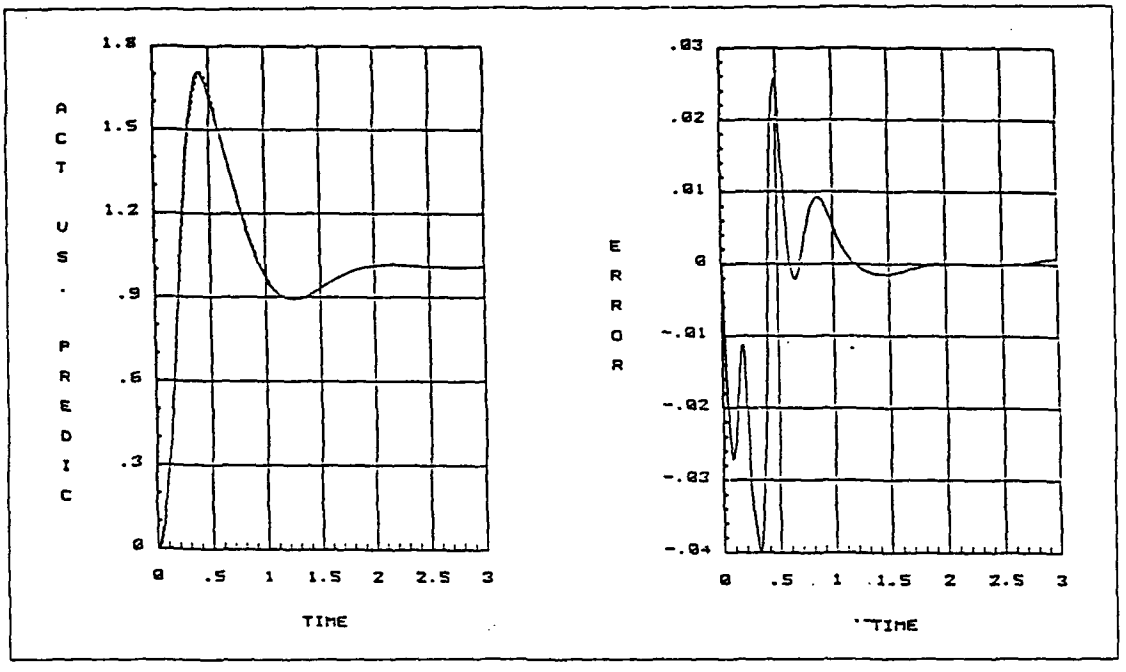

Figure A.8. Outputs of LTI Plant #8 and of YF-16 for the Same Input

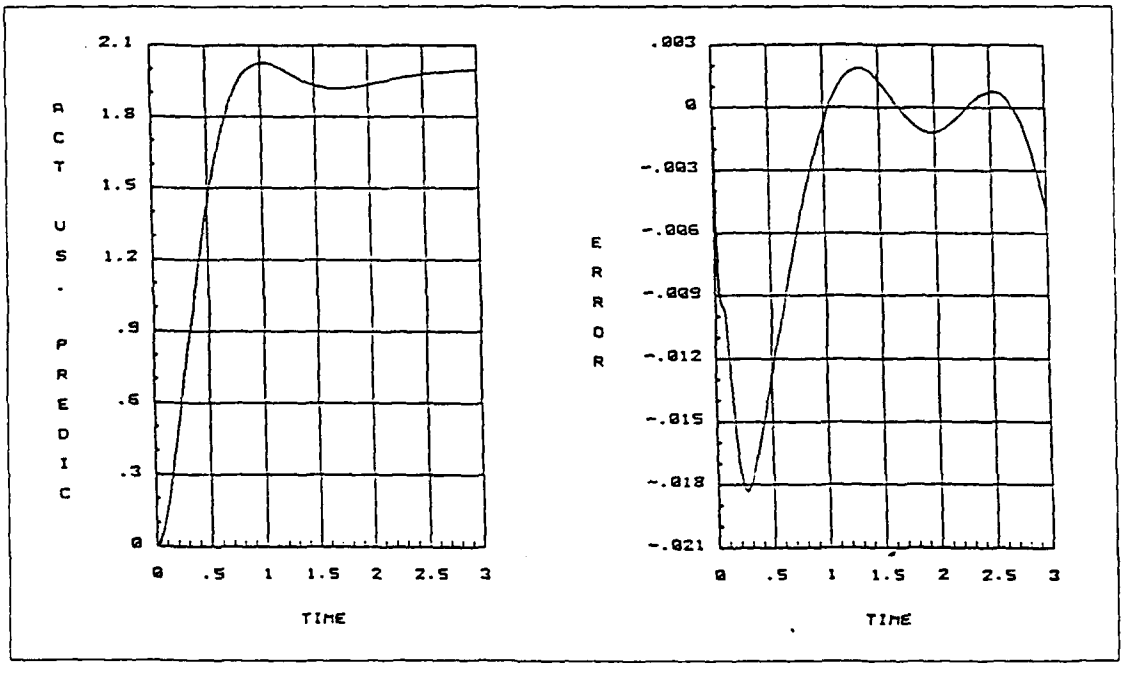

Figure A.9. Outputs of LTI Plant #9 and of YF-16 for the Same Input

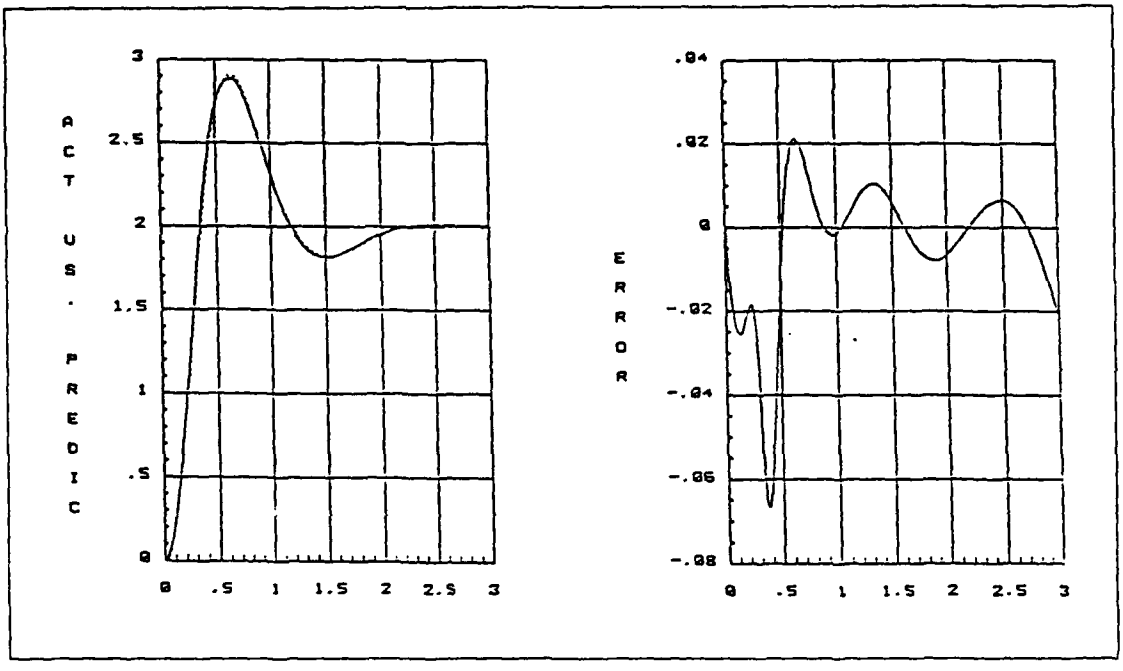

Figure A.10. Outputs of LTI Plant #10 and of YF-16 for the Same Input

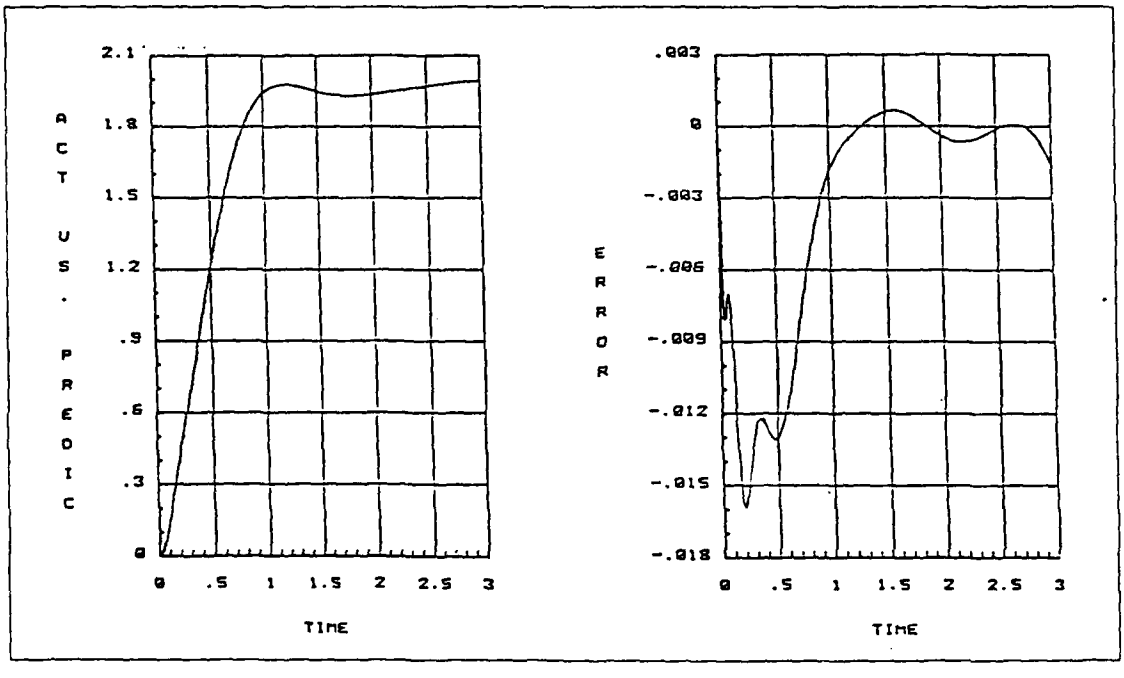

Figure A.11. Outputs of LTI Plant #11 and of YF-16 for the Same Input

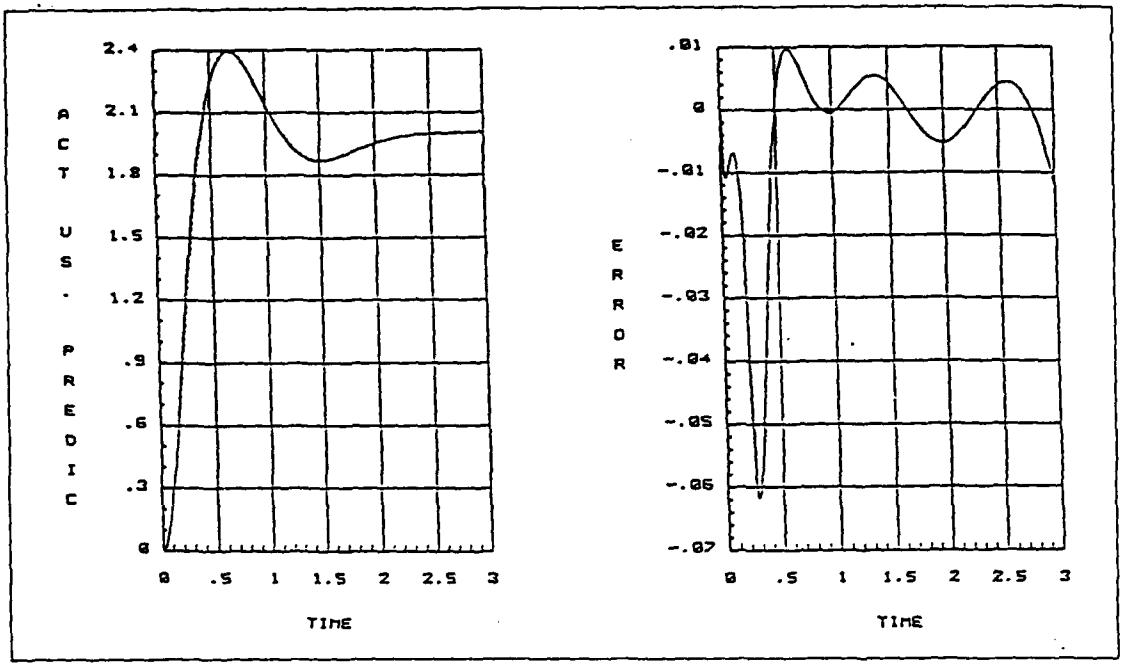

Figure A.12. Outputs of LTI Plant #12 and of YF-16 for the Same Input

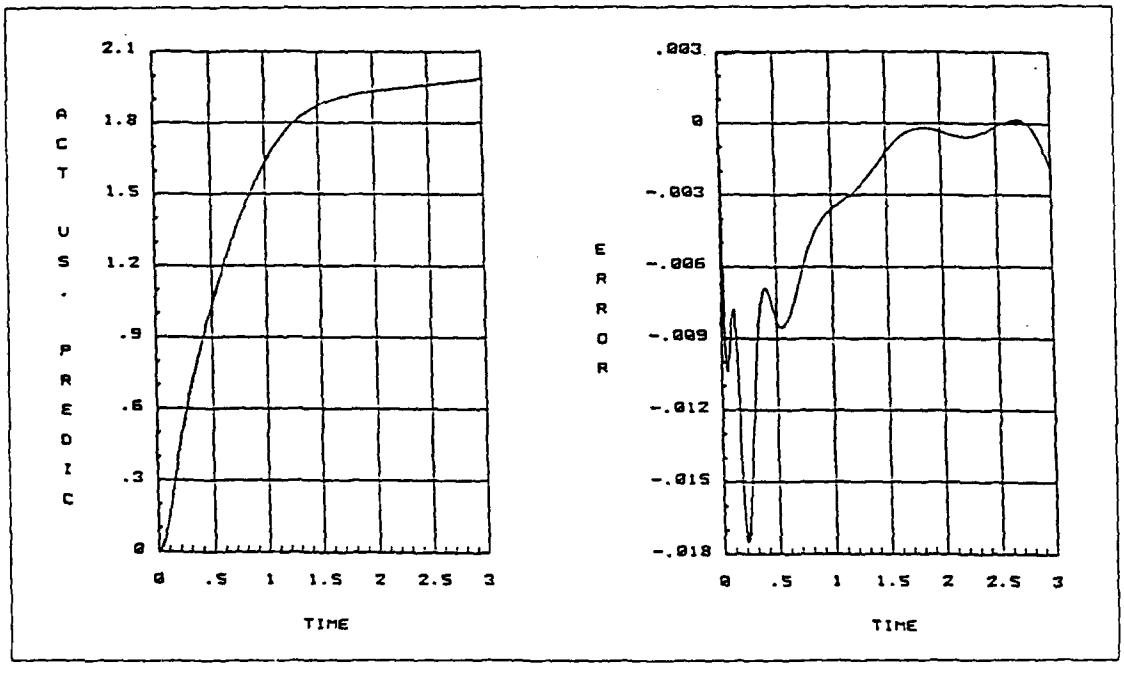

Figure A.13. Outputs of LTI Plant #13 and of YF-16 for the Same Input

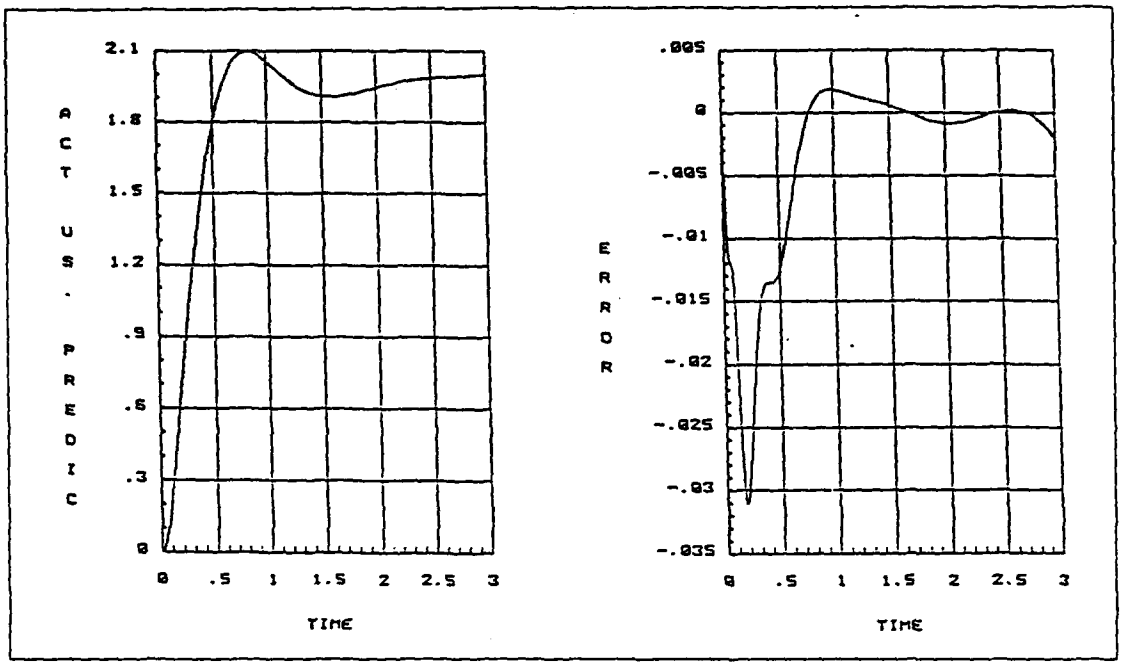

Figure A.14. Outputs of LTI Plant #14 and of YF-16 for the Same Input

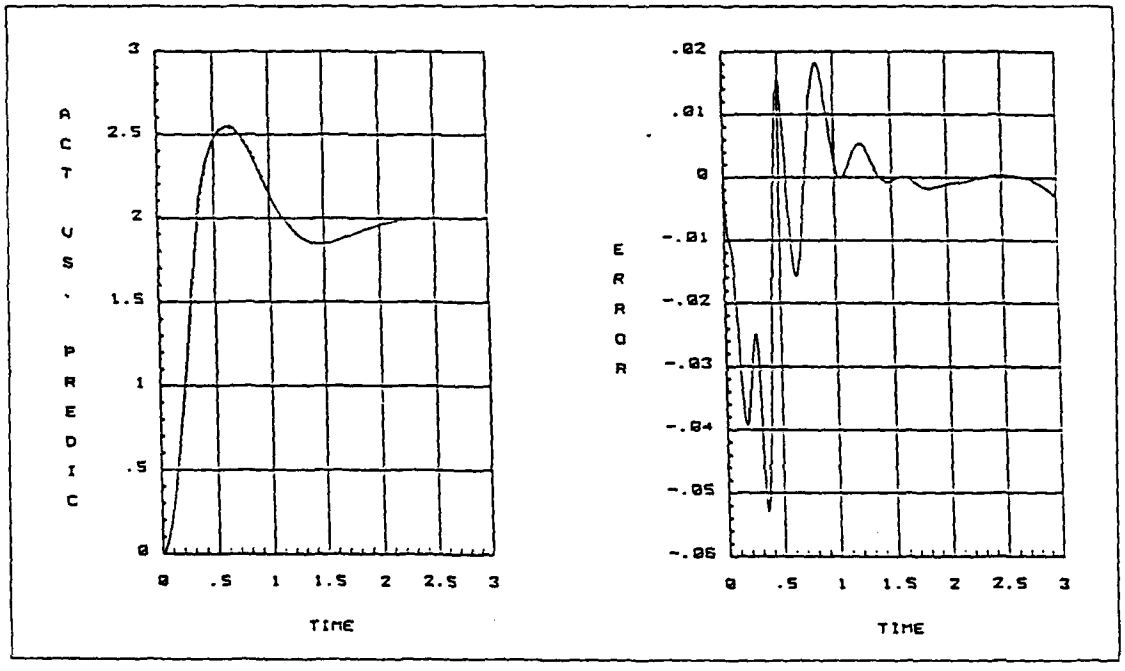

Figure A.15. Outputs of LTI Plant #15 and of YF-16 for the Same Input

Appendix B. *Boundary Data*

This appendix contains the data required to generate the tracking bounds on the nominal loop transmission of Chapter IV. The additional boundary on the 2g responses is presented along with the tabulated allowable magnitude variation for 1g and 2g command bounds. The plant templates representing $P(j\omega)$ for the frequencies used in generating the boundaries are also included.

Frequency Domain Tracking Bounds:

It is shown in Figure B.1 that the 2g responses used in generating the equivalent LTI plant set do not fully populate the envelope of acceptable responses. In order to make the amount of uncertainty more realistic an additional upper bound is placed on these outputs. The 2g responses superimposed upon the 2g boundaries are shown in Figure B.2, the lower boundary is the same for 1g and 2g responses.

The transfer functions representing the envelope bounds are displayed below while the allowable magnitude variations vs. frequency are presented in Tables B.1 and B.2.

1G Upper fit

$$\frac{15.8965s + 14.3414}{s^2 + 8.0691s + 14.3165} = \frac{15.8965(s + 0.9022)}{(s + 5.4349)(s + 2.6342)}$$

2G Upper fit

$$\frac{7.4435s + 11.3600}{s^2 + 4.2224s + 11.1403} = \frac{7.4435(s + 1.5262)}{(s + 2.1112 \pm 2.5852j)}$$

Lower fit for both cases

$$\frac{19.2109}{s^2 + 13.6822s + 19.2703} = \frac{19.2109}{(s + 12.088)(s + 1.5942)}$$

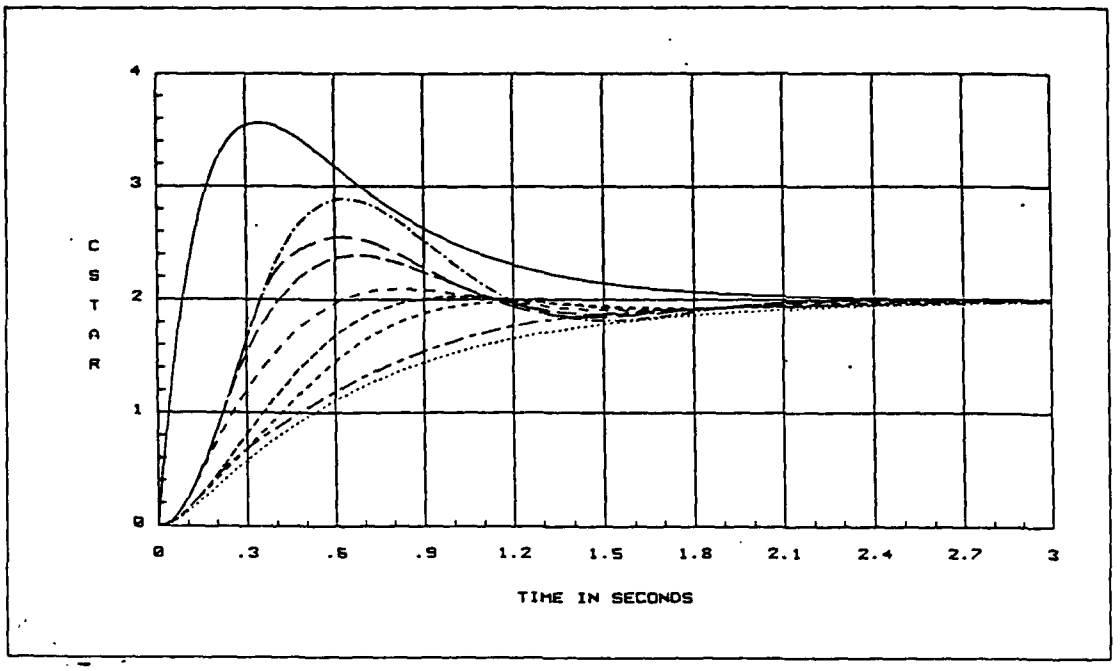

Figure B.1. 2g Responses within Original 1g Envelope

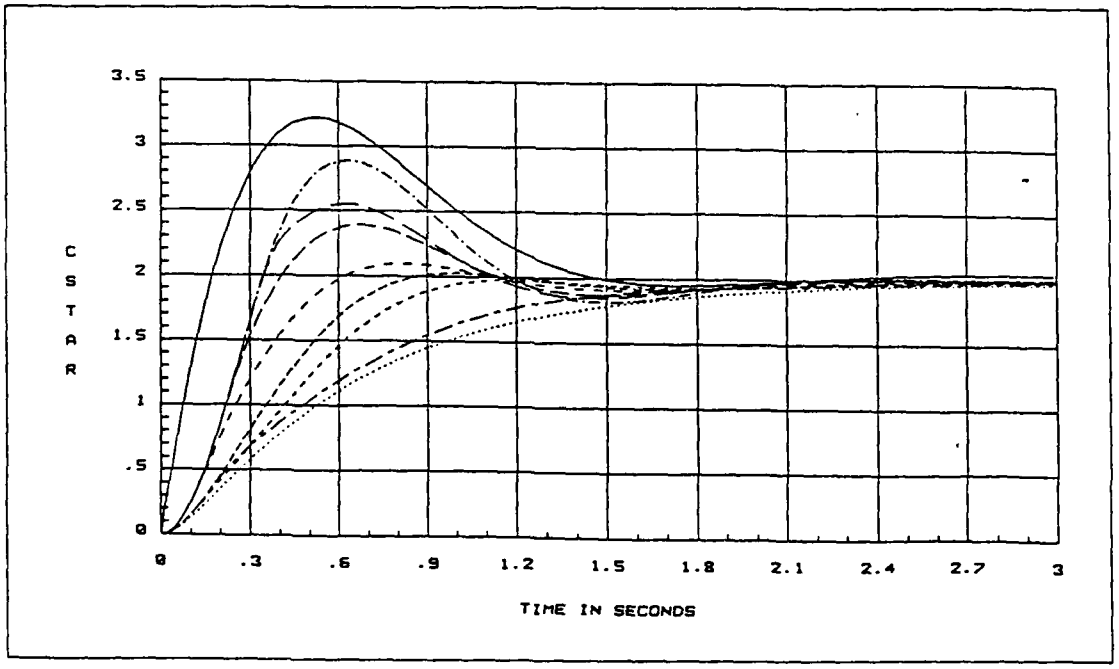

Figure B.2. 2g Responses within 2g Envelope

ω (Rad/sec)	Upper Mag dB	Lower Mag db	$\delta_R(\omega)$ dB
0.1	0.0604	-0.0442	0.1045
0.5	0.9880	-0.4417	1.4298
1.0	2.7661	-1.4975	4.2636
2.5	5.7770	-5.5986	11.3756
3.0	6.0609	-6.8583	12.9192
5.0	5.7344	-11.0619	16.7962
8.0	3.9240	-15.7846	19.7086
10.0	2.6459	-18.3495	20.9954
15.0	-0.1477	-23.5948	23.4470
18.0	-1.5395	-26.1905	24.6510
20.0	-2.3699	-27.7500	25.3801
50.0	-10.0150	-42.5389	32.5239

Table B.1. Allowed Variation in Magnitude vs. Frequency (1g Bounds)

ω (Rad/sec)	Upper Mag dB	Lower Mag db	$\delta_R(\omega)$ dB
0.1	0.1898	-0.0442	0.2340
0.5	0.6493	-0.4417	1.0911
1.0	1.8435	-1.4975	3.3409
2.5	5.4556	-5.5986	11.0542
3.0	5.8017	-6.8583	12.6599
5.0	3.7549	-11.0619	14.8168
8.0	-0.2971	-15.7846	15.4876
10.0	-2.3227	-18.3495	16.0268
15.0	-5.9656	-23.5948	17.6292
18.0	-7.5839	-26.1905	18.6066
20.0	-8.5146	-27.7500	19.2354
50.0	-16.5322	-42.5389	26.0068

Table B.2. Allowed Variation in Magnitude vs. Frequency (2g Bounds)

Plant Templates

The plant templates for the frequencies in Tables B.1 and B.2 are shown in Figures B.3 through B.5 and are all the same scale.

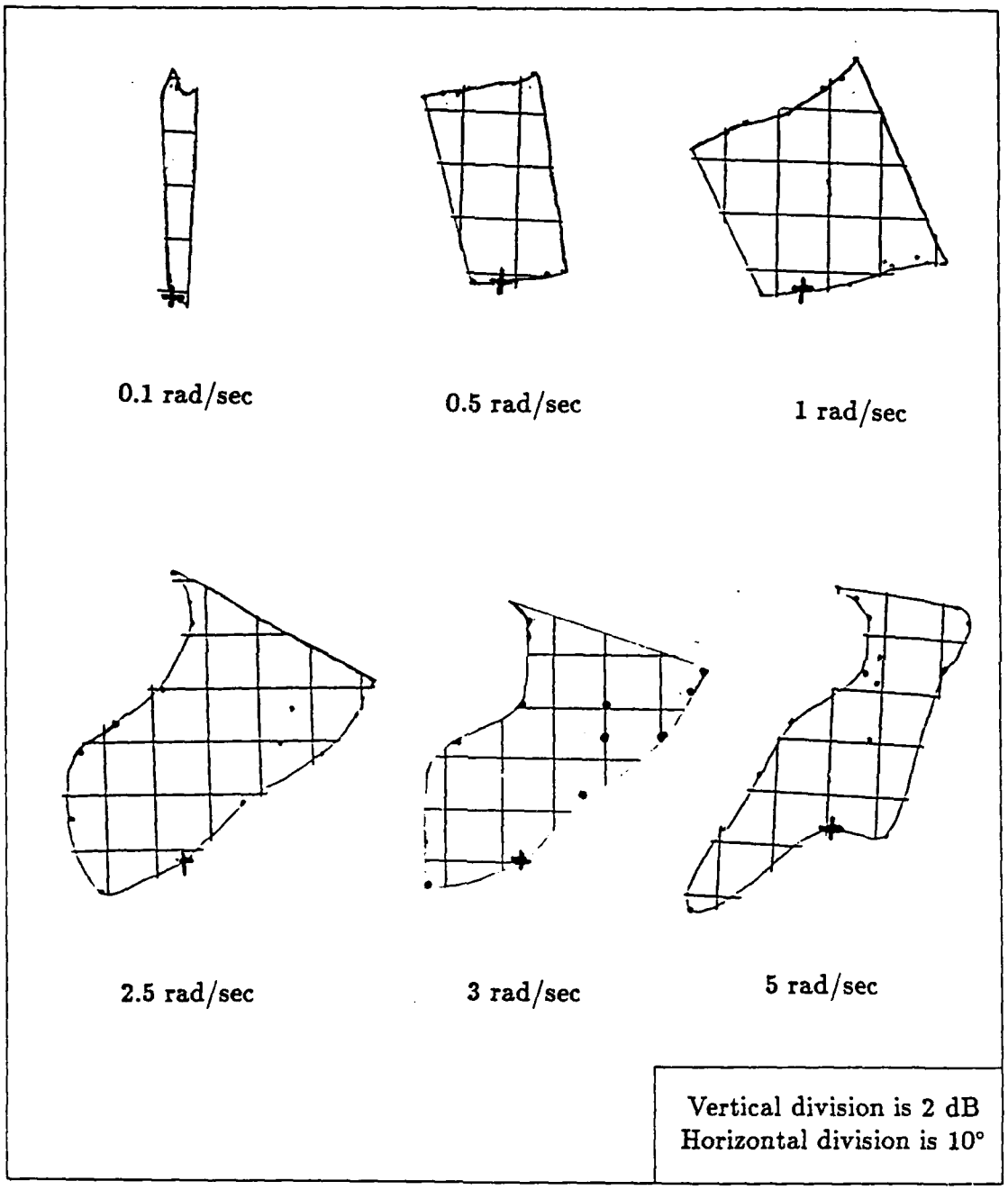

Figure B.3. Plant Templates for $0.1 \leq \omega \leq 5$ rad/sec

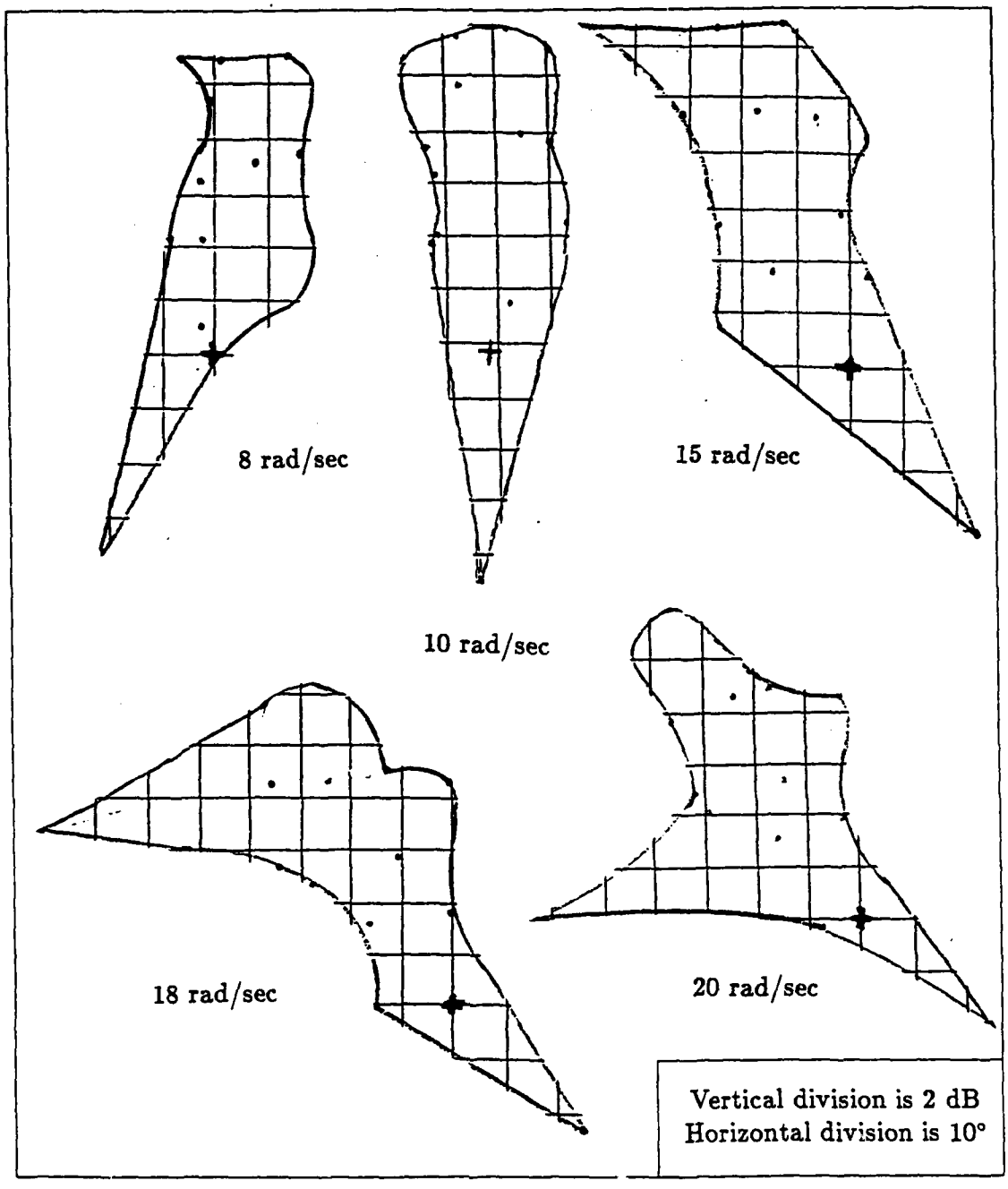

Figure B.4. Plant Templates for $8 \leq \omega \leq 20$ rad/sec

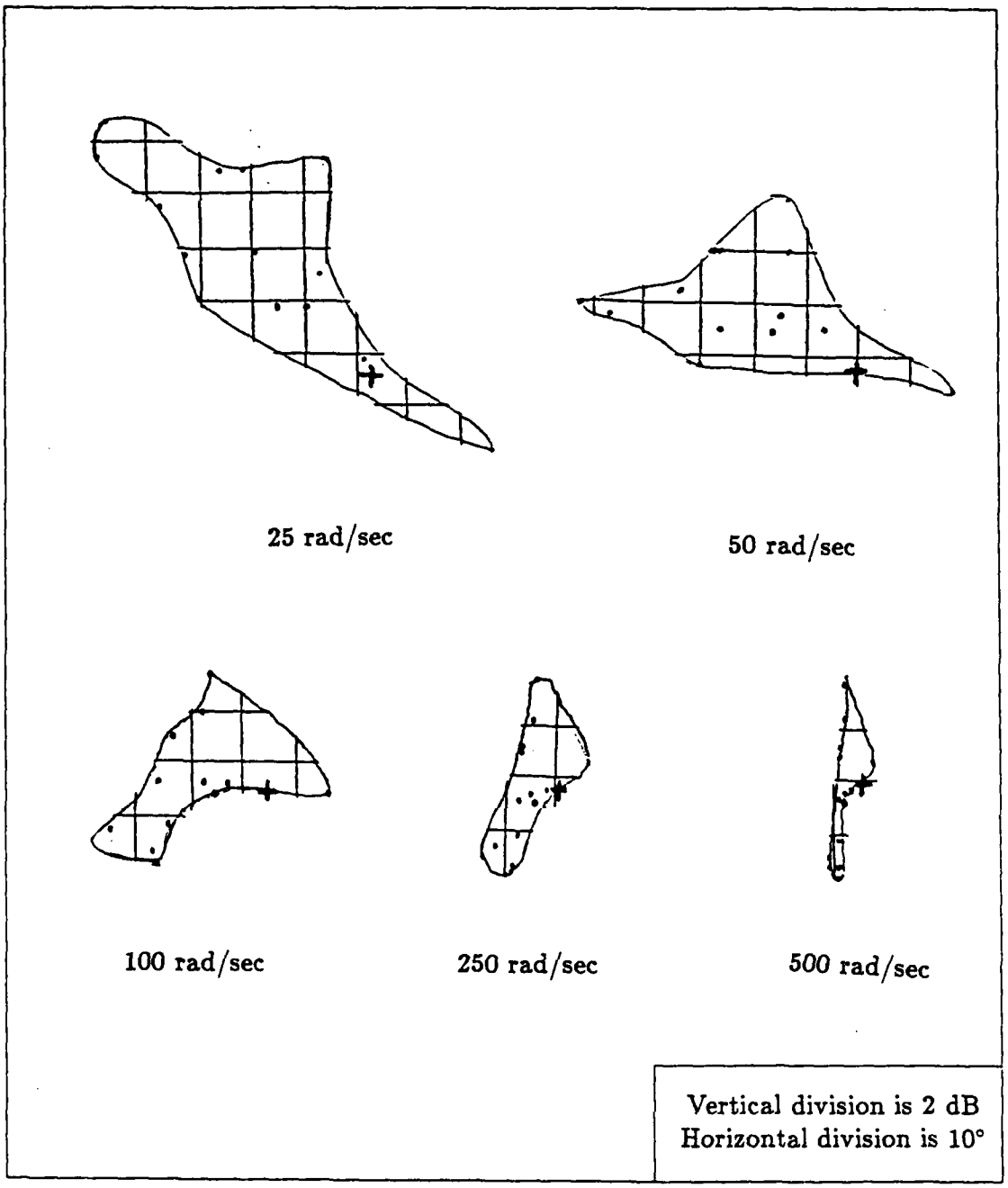

Figure B.5. Plant Templates for $25 \leq \omega \leq 500$ rad/sec

Appendix C. *Simulation of the Stability Augmentation System*

This appendix presents the scheduling of the prefilter gain K_f vs. commanded input, along with the normalized responses of the SAS at the flight conditions listed in Chapter V.

Generation of the Nonlinear Prefilter

As described in Chapter V, a nonlinear prefilter is designed to better linearize the final values of the response at the nominal point of 0.9M and 20,000 ft. The discrete data points for K_f in Figure C.1 are obtained by applying step commands of strength 0.1g to 3.0 g every 0.1g, and at 4g to 8g every 1g. These points are then approximated by the continuous line in the figure. This peace-wise gain function is then programed in Fortran for use in the nonlinear YF-16 simulations.

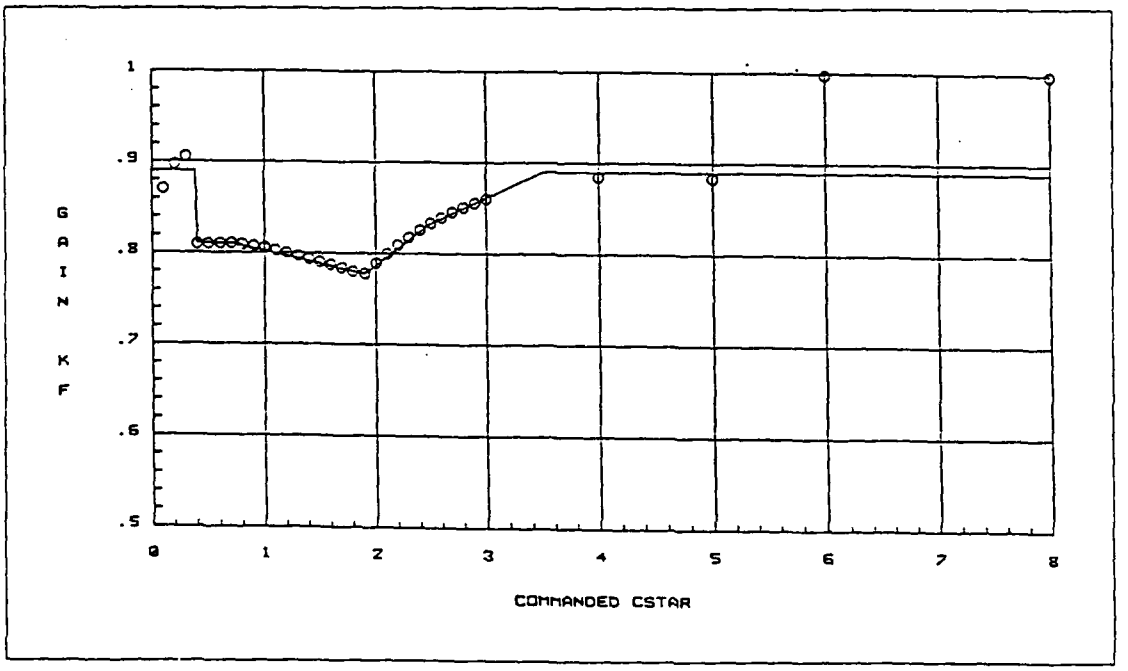

Figure C.1. Scheduling of the Prefilter Gain K_f

Results of Expanding the Envelope

The following figures are representative of the nonlinear simulations run on the inner loop SAS. The 25 flight conditions shown are the same as the tabulated data used to present the acceptable envelope of Chapter V. The responses in each figure are shown superimposed upon the normalized tracking bounds. The responses shown are only up to the maximum command resulting in an acceptable response in increments of 1g. When this maximum command is not an integer, the maximum acceptable response is also included. For example Figure C.2 contains the normalized responses at 5,000 ft and 0.5M with a maximum acceptable command of 7.3g, the traces are those for commands of 1g ,2g ,3g ,4g ,5g ,6g ,7g ,7.3g.

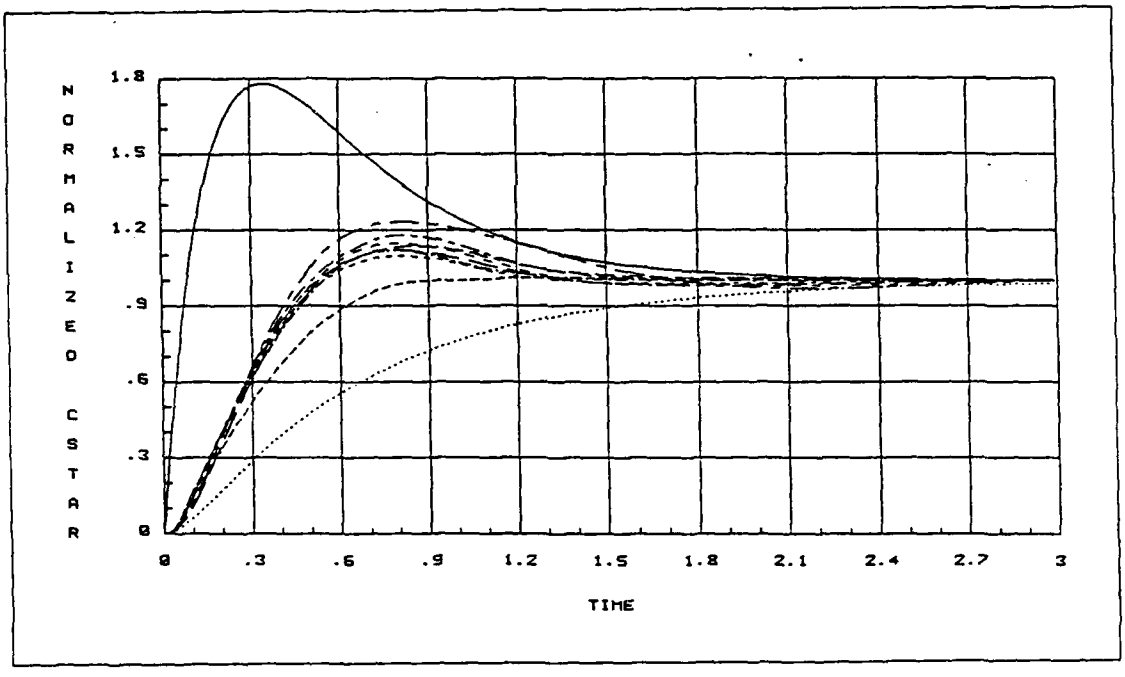

Figure C.2. Normalized Response at 5,000 ft 0.5M

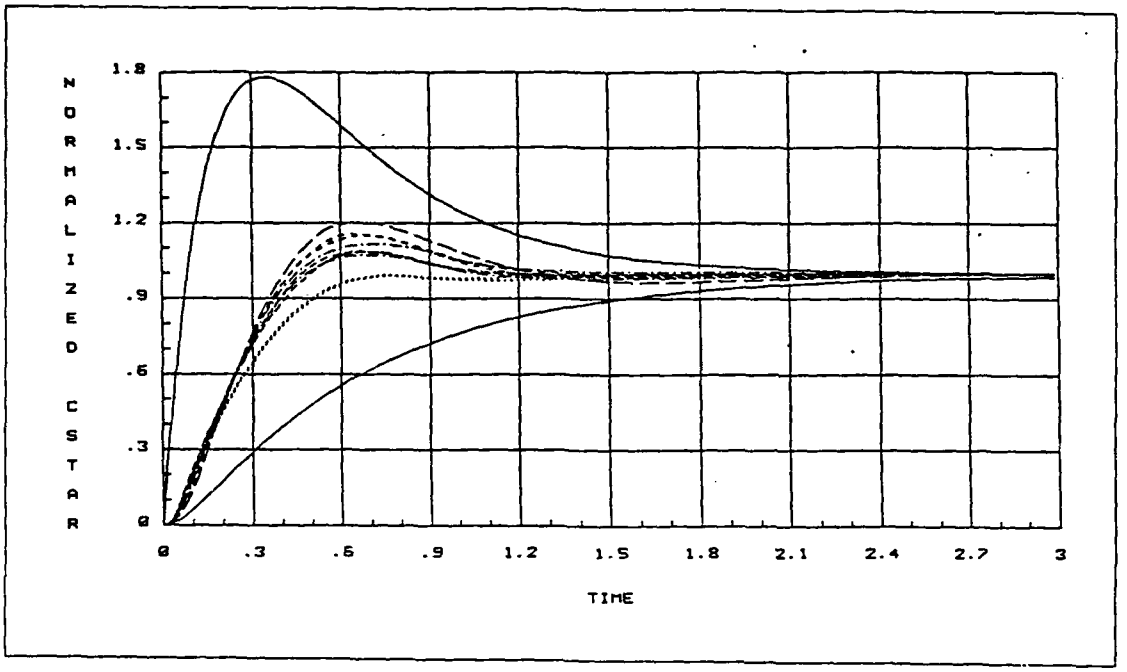

Figure C.3. Normalized Response at 5,000 ft 0.6M

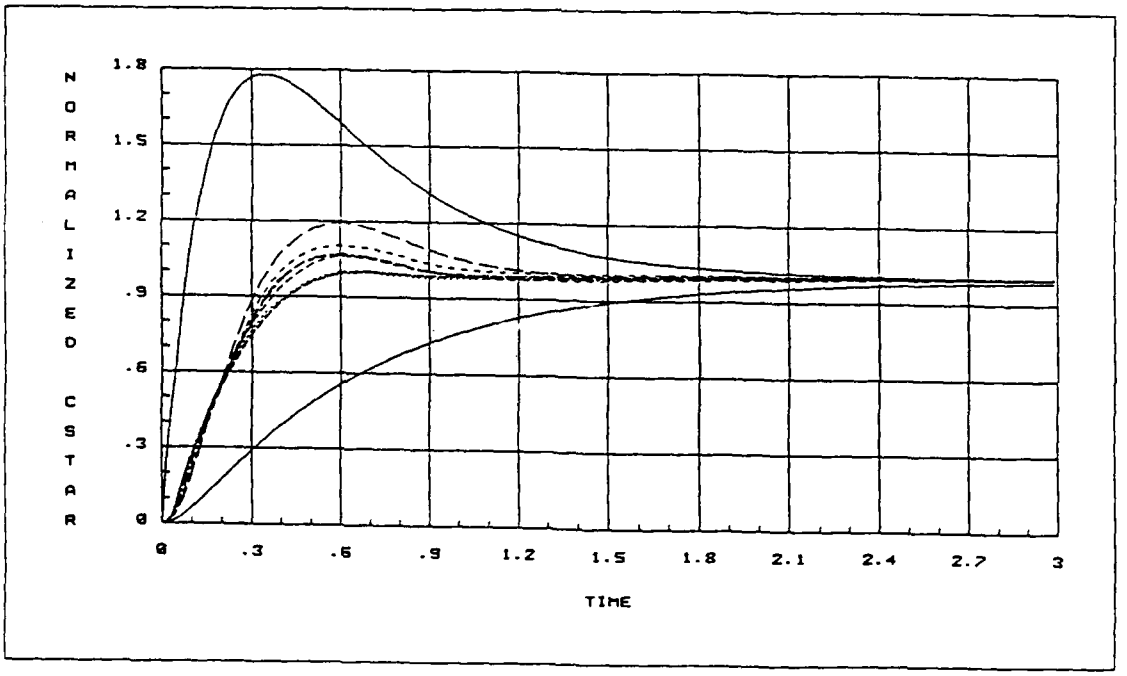

Figure C.4. Normalized Response at 5,000 ft 0.7M

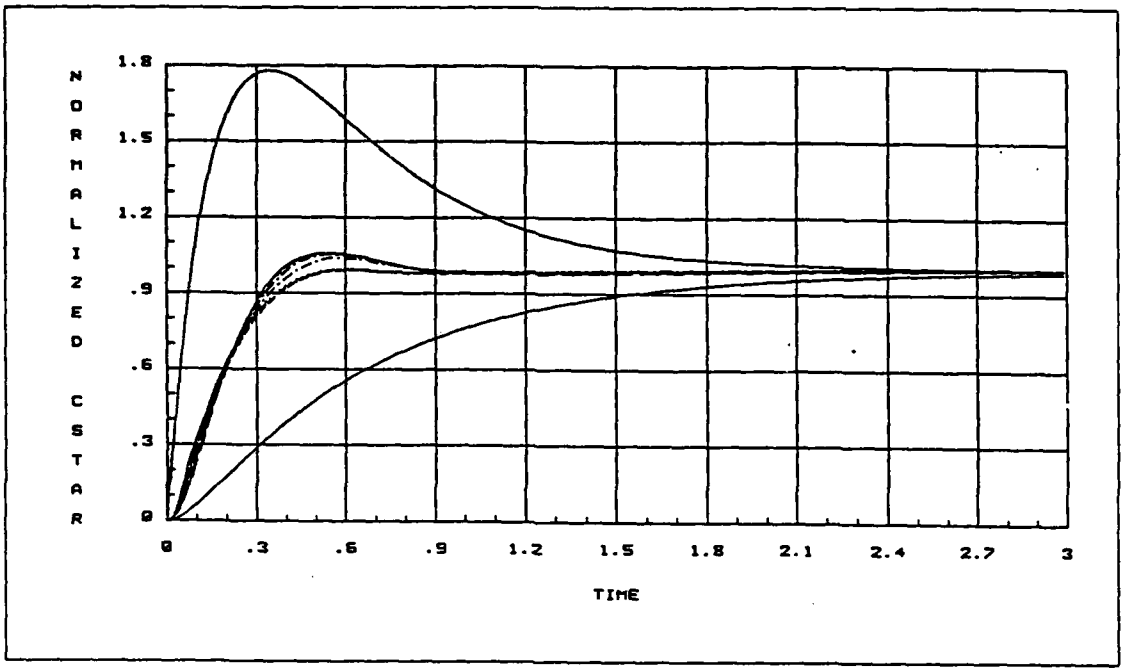

Figure C.5. Normalized Response at 5,000 ft 0.8M

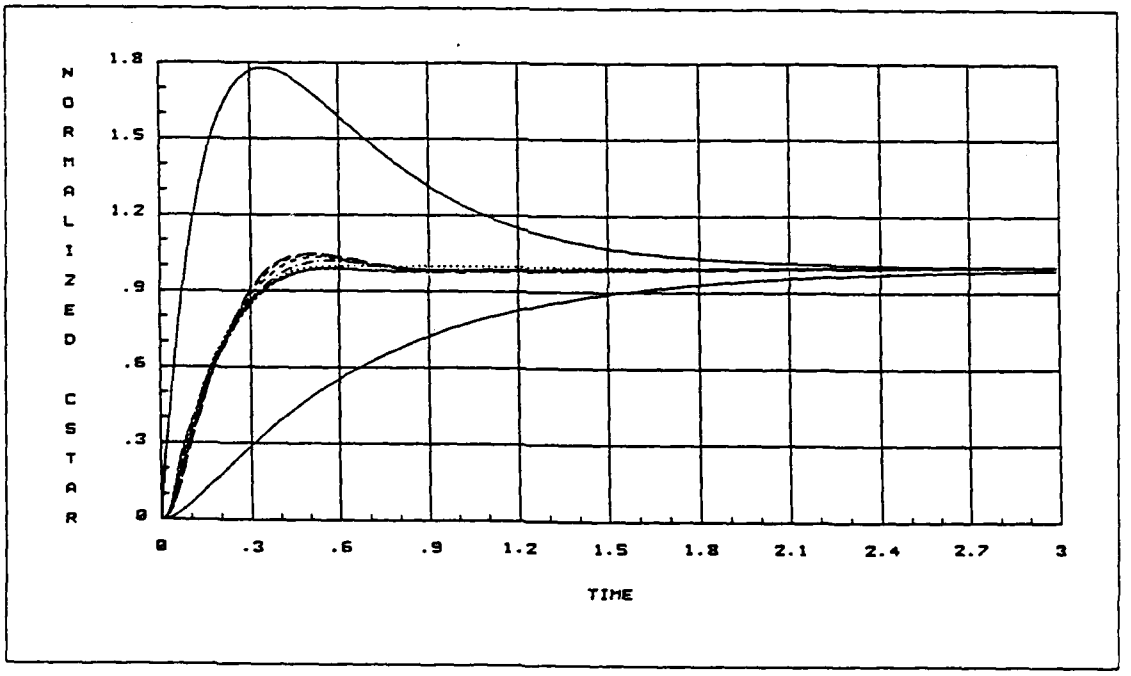

Figure C.6. Normalized Response at 5,000 ft 0.9M

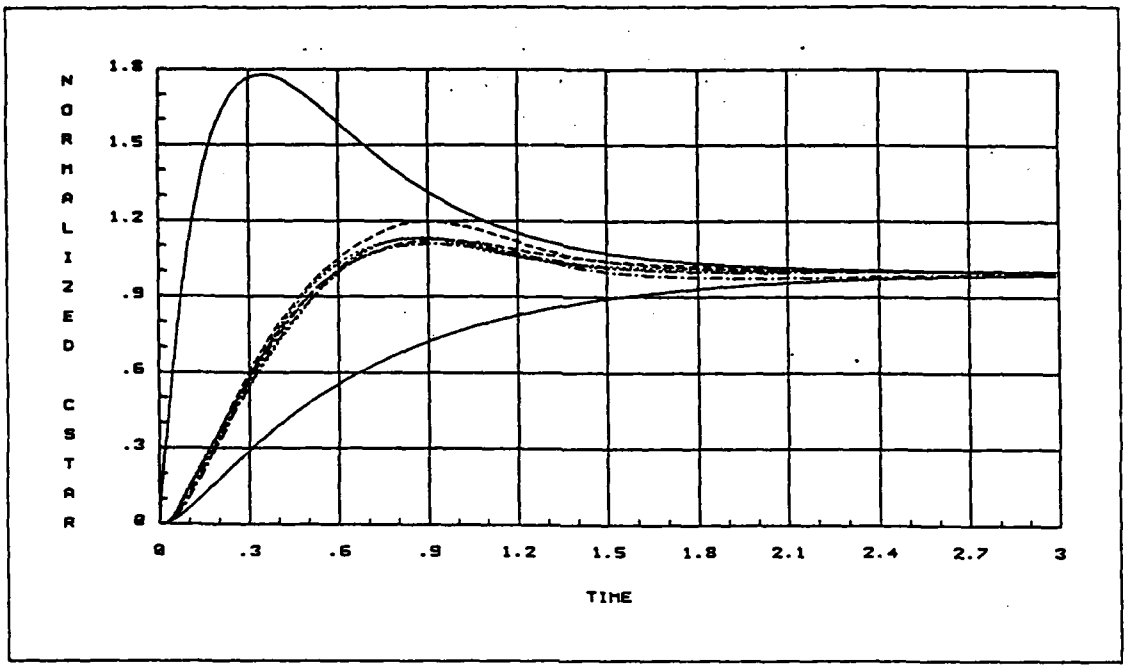

Figure C.7. Normalized Response at 10,000 ft 0.5M

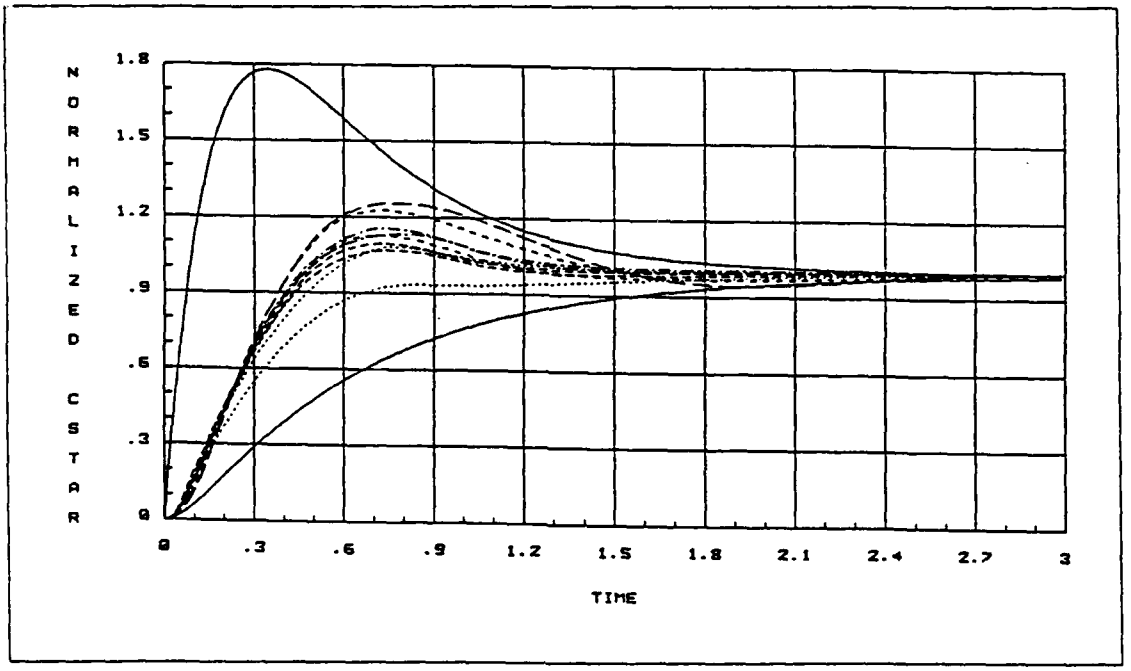

Figure C.8. Normalized Response at 10,000 ft 0.6M

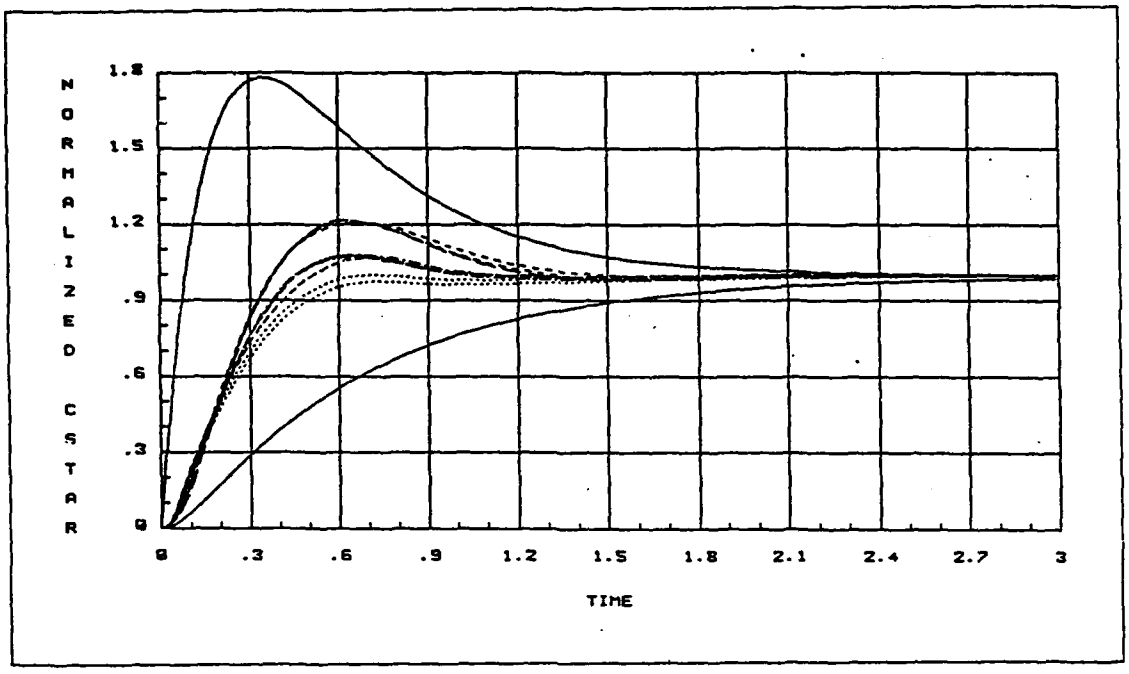

Figure C.9. Normalized Response at 10,000 ft 0.7M

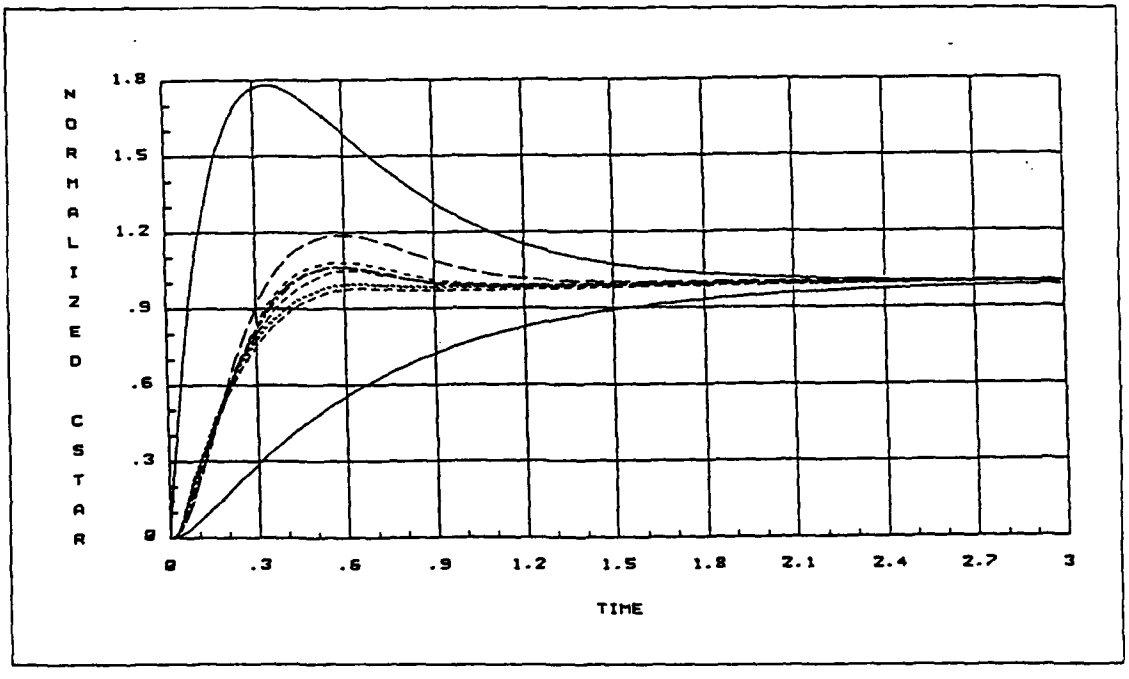

Figure C.10. Normalized Response at 10,000 ft 0.8M

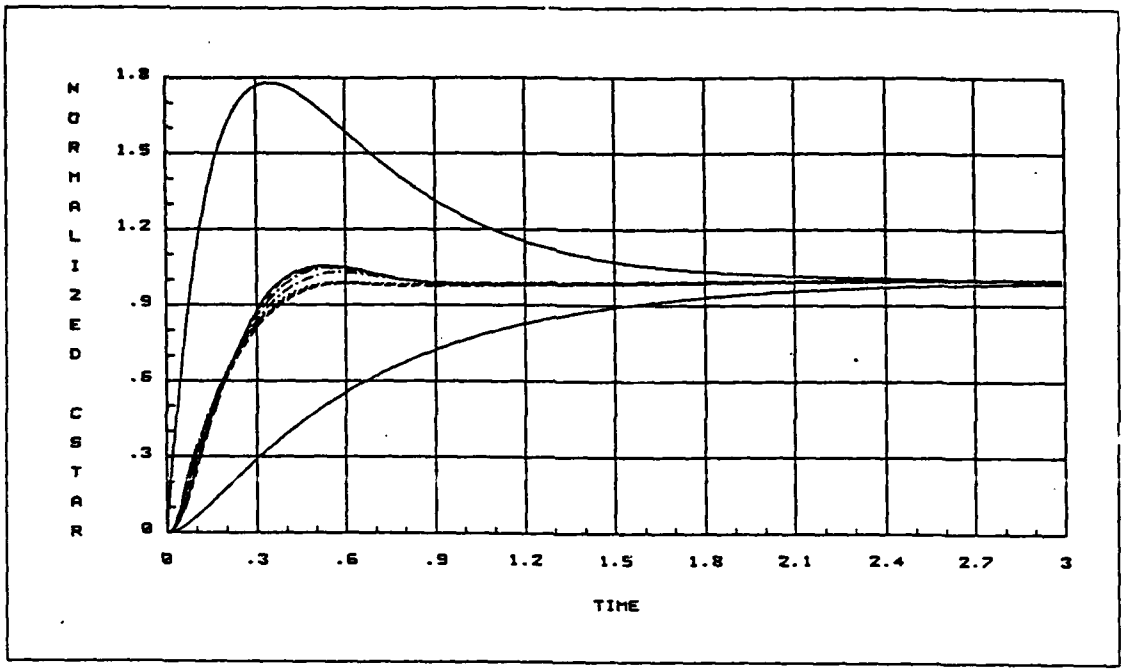

Figure C.11. Normalized Response at 10,000 ft 0.9M

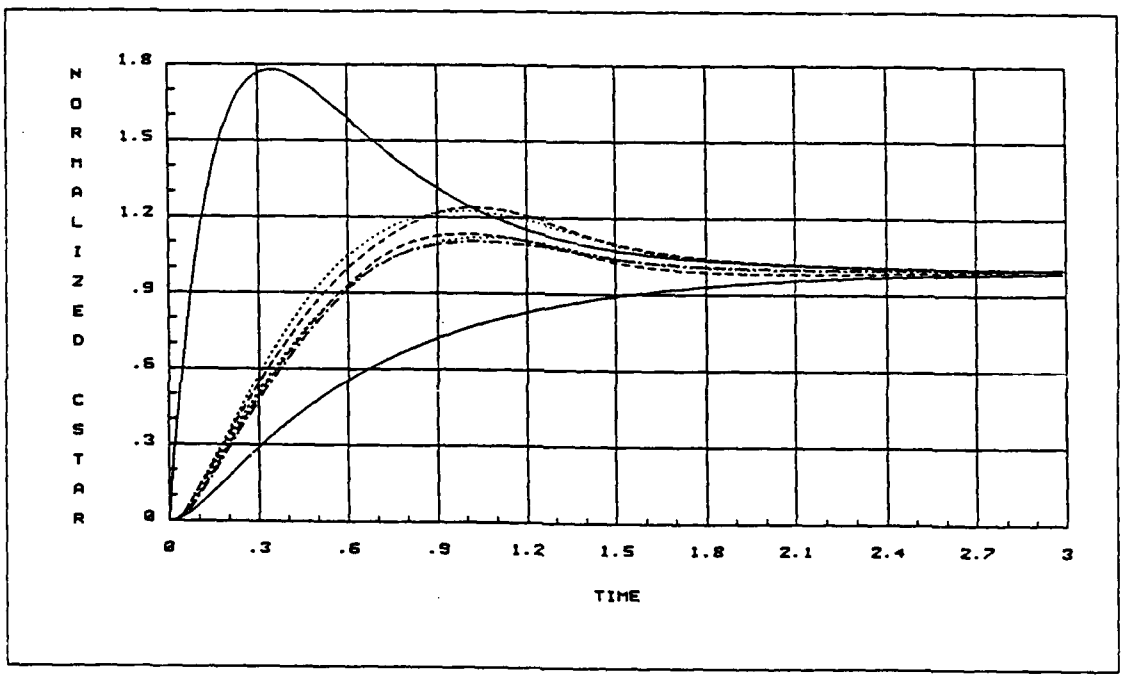

Figure C.12. Normalized Response at 15,000 ft 0.5M

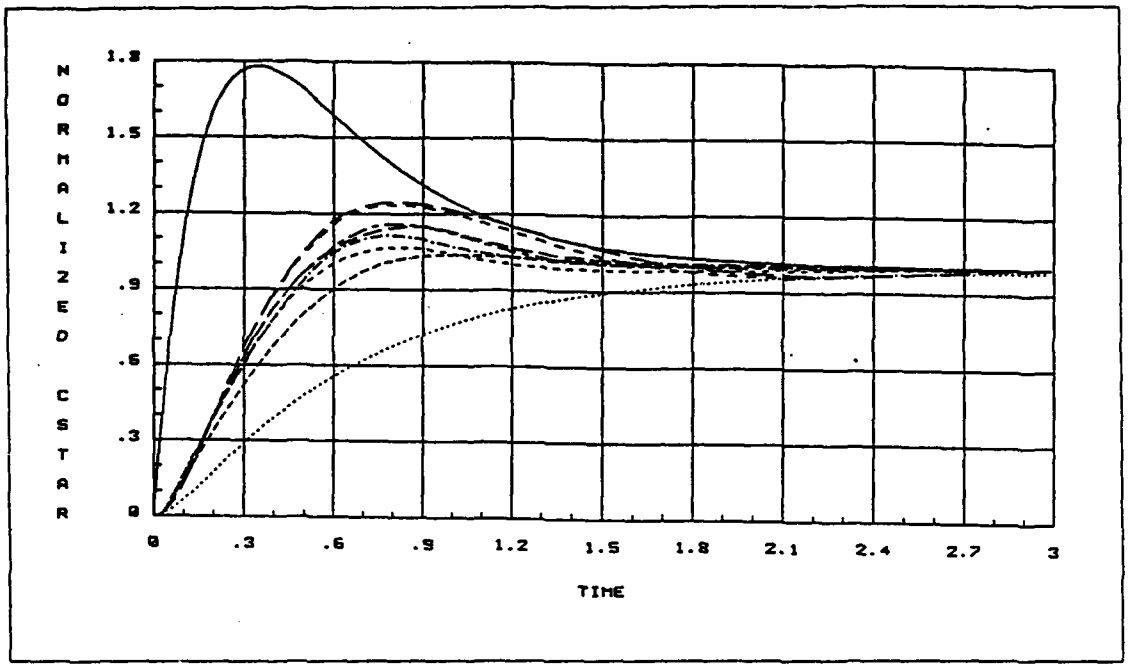

Figure C.13. Normalized Response at 15,000 ft 0.6M

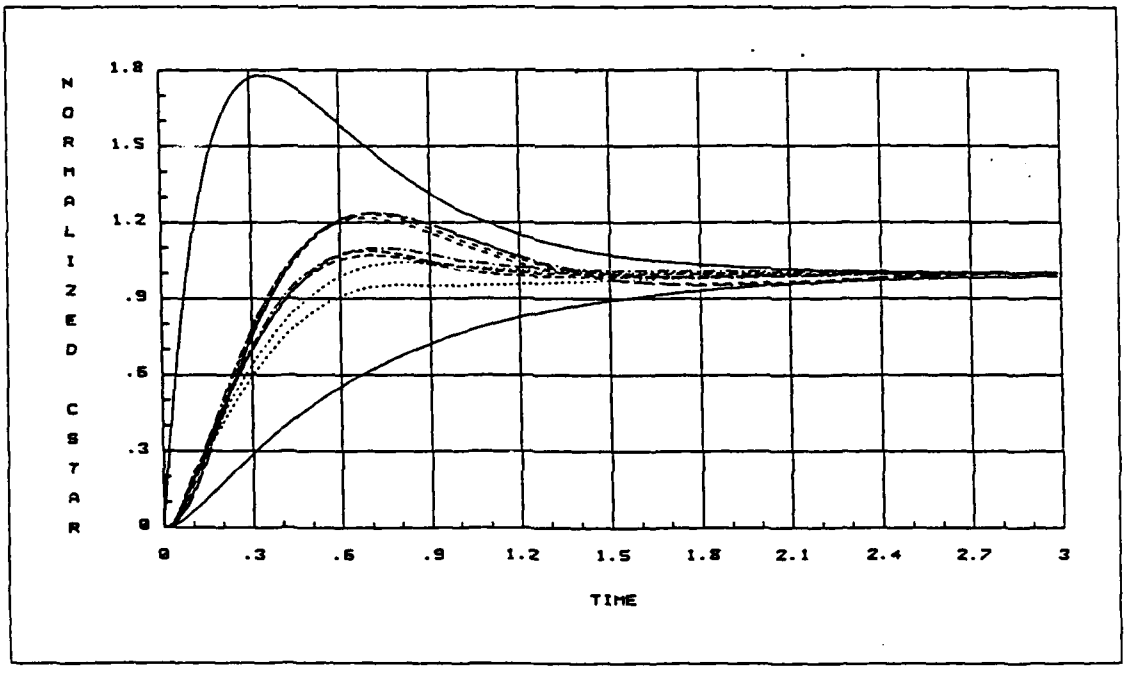

Figure C.14. Normalized Response at 15,000 ft 0.7M

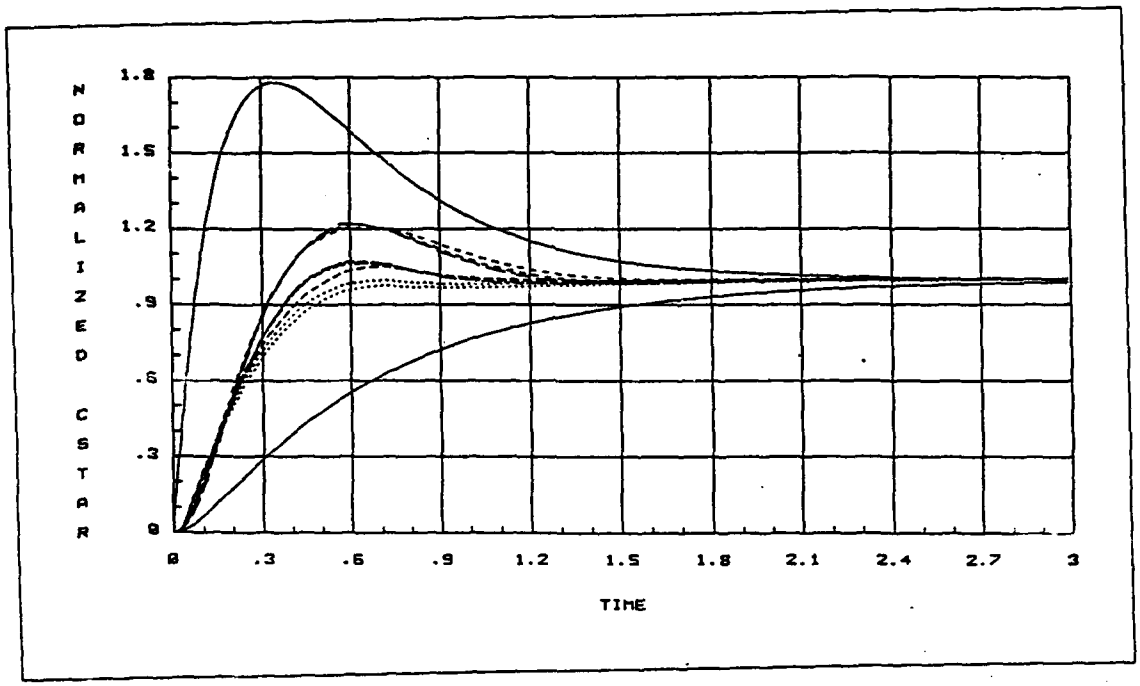

Figure C.15. Normalized Response at 15,000 ft 0.8M

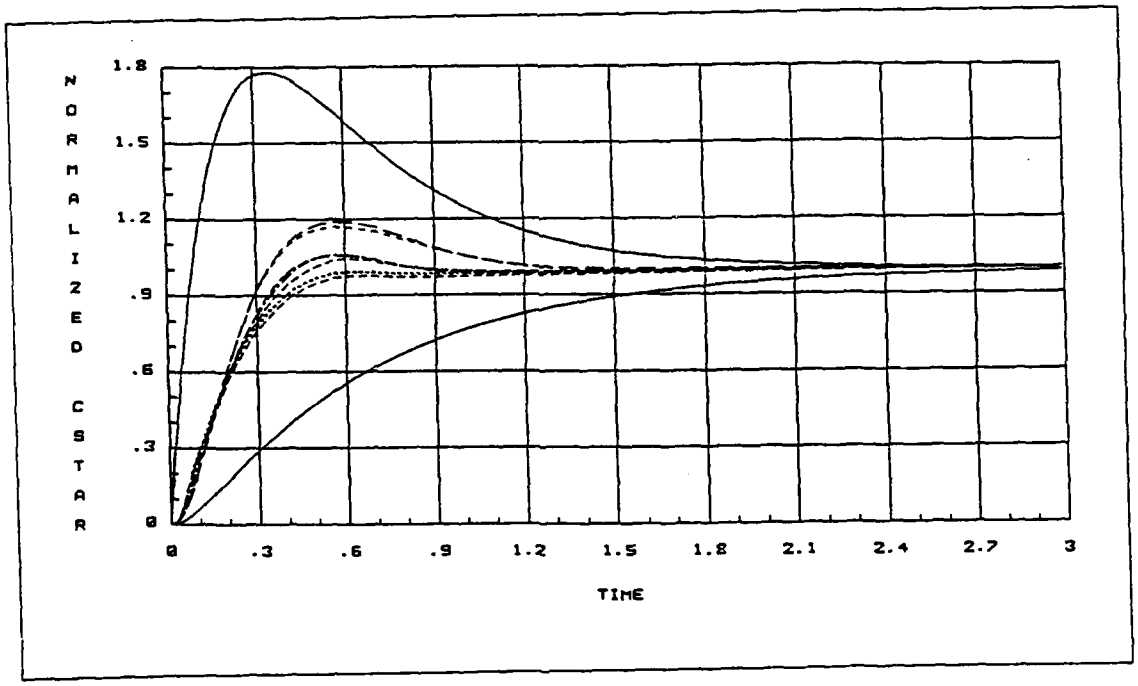

Figure C.16. Normalized Response at 15,000 ft 0.9M

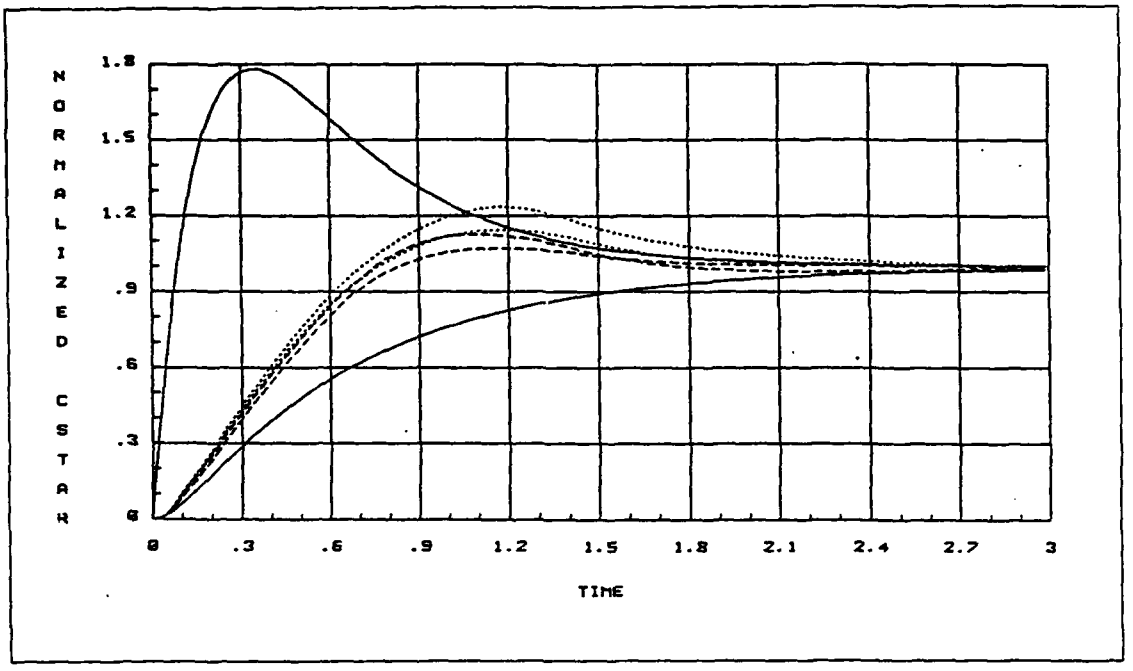

Figure C.17. Normalized Response at 20,000 ft 0.5M

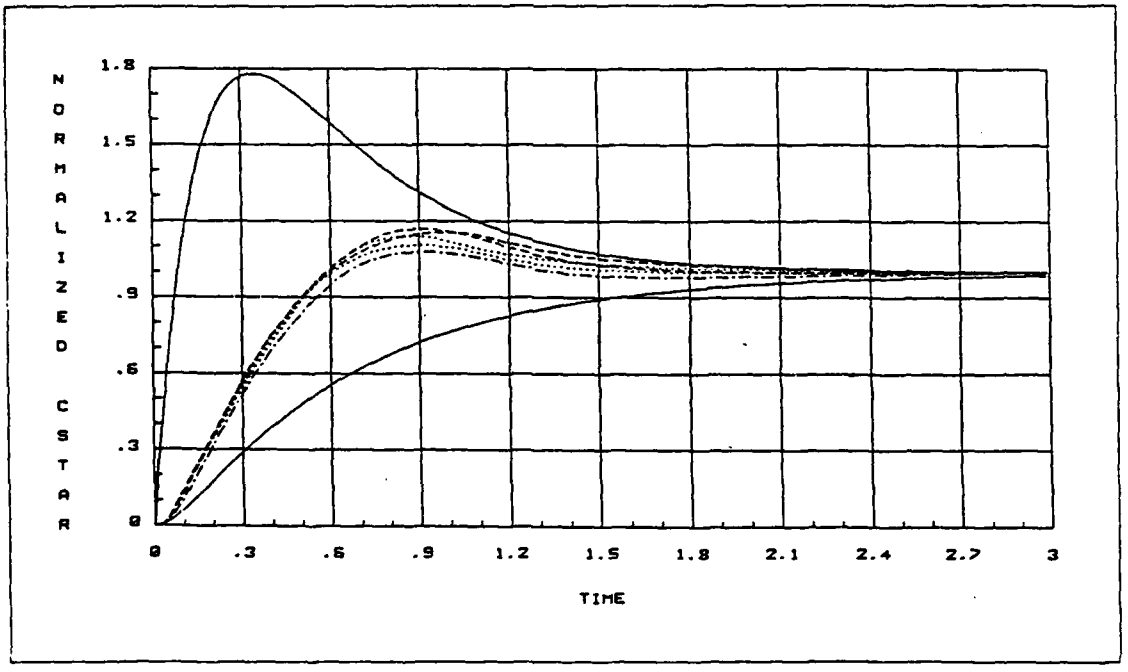

Figure C.18. Normalized Response at 20,000 ft 0.6M

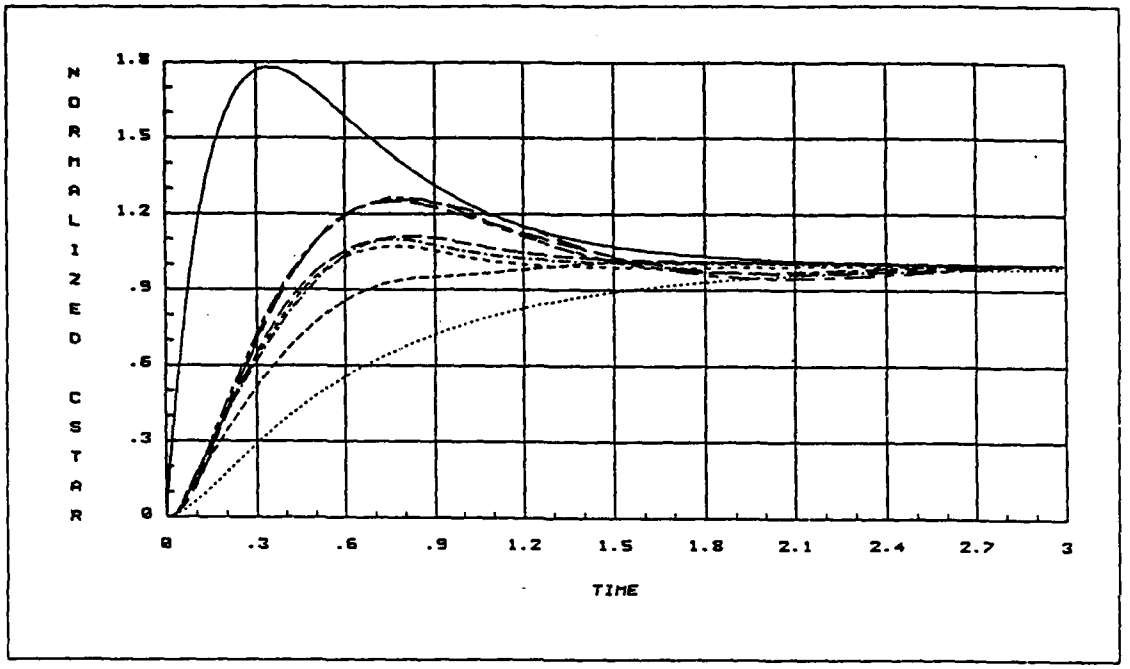

Figure C.19. Normalized Response at 20,000 ft 0.7M

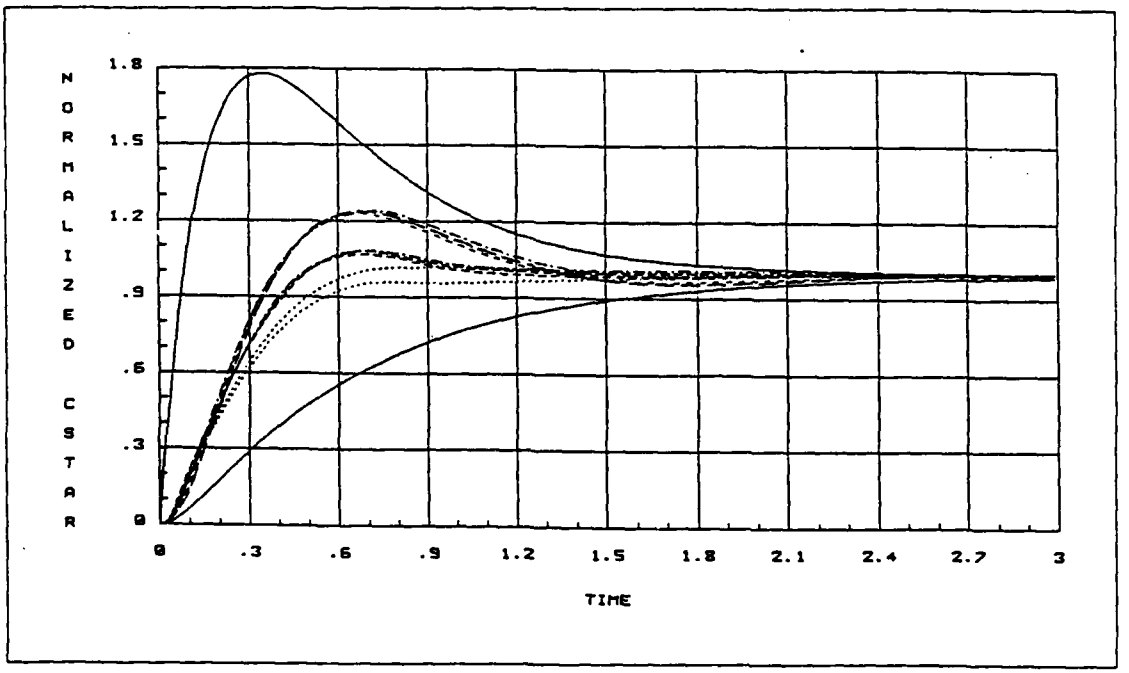

Figure C.20. Normalized Response at 20,000 ft 0.8M

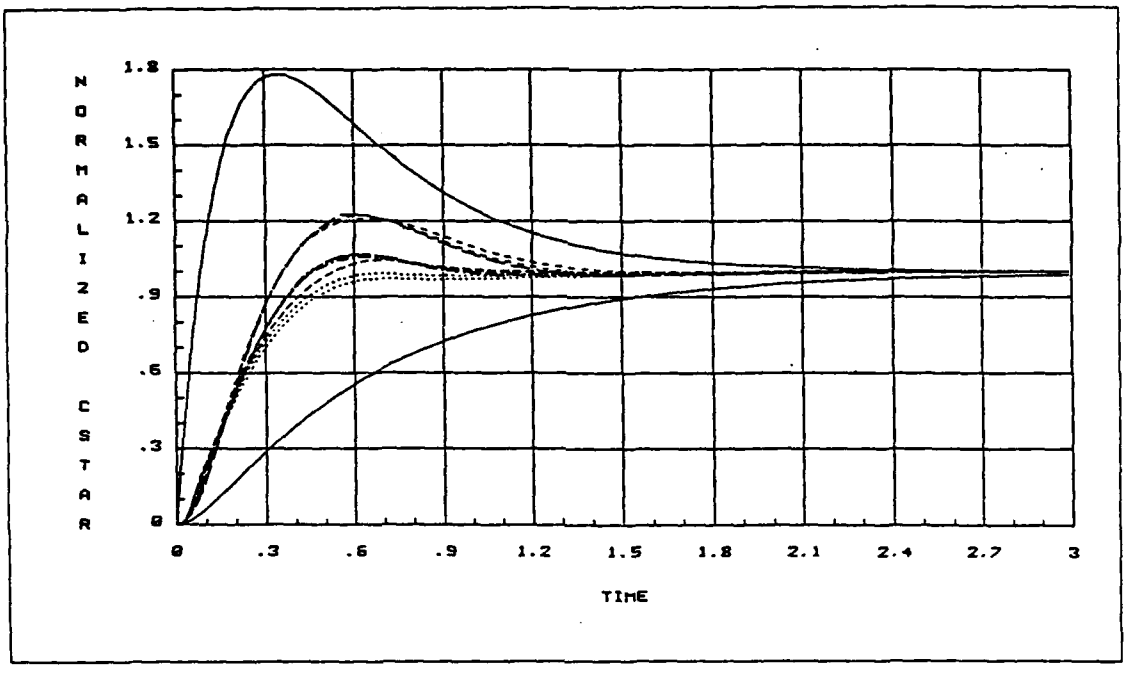

Figure C.21. Normalized Response at 20,000 ft 0.9M

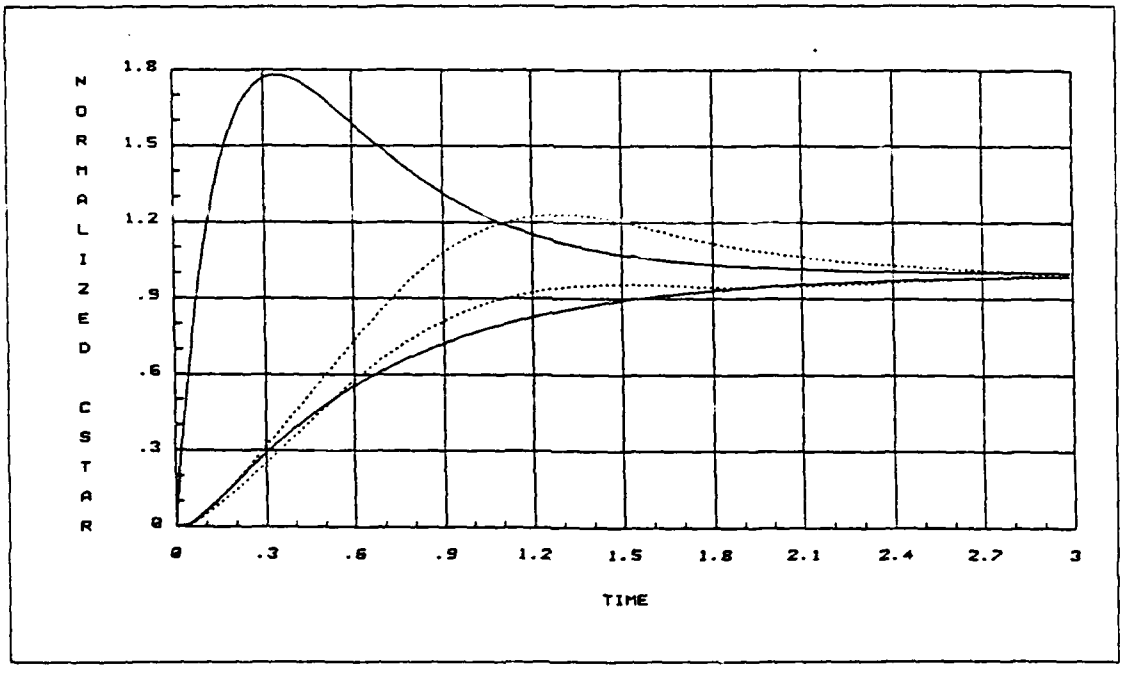

Figure C.22. Normalized Response at 30,000 ft 0.5M

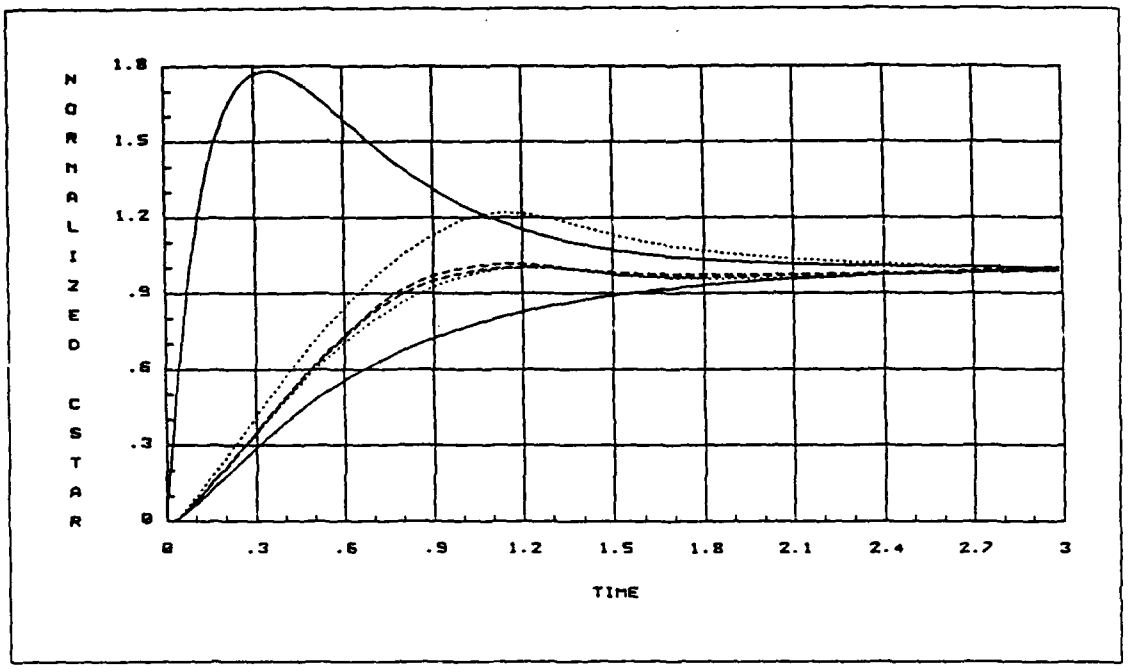

Figure C.23. Normalized Response at 30,000 ft 0.6M

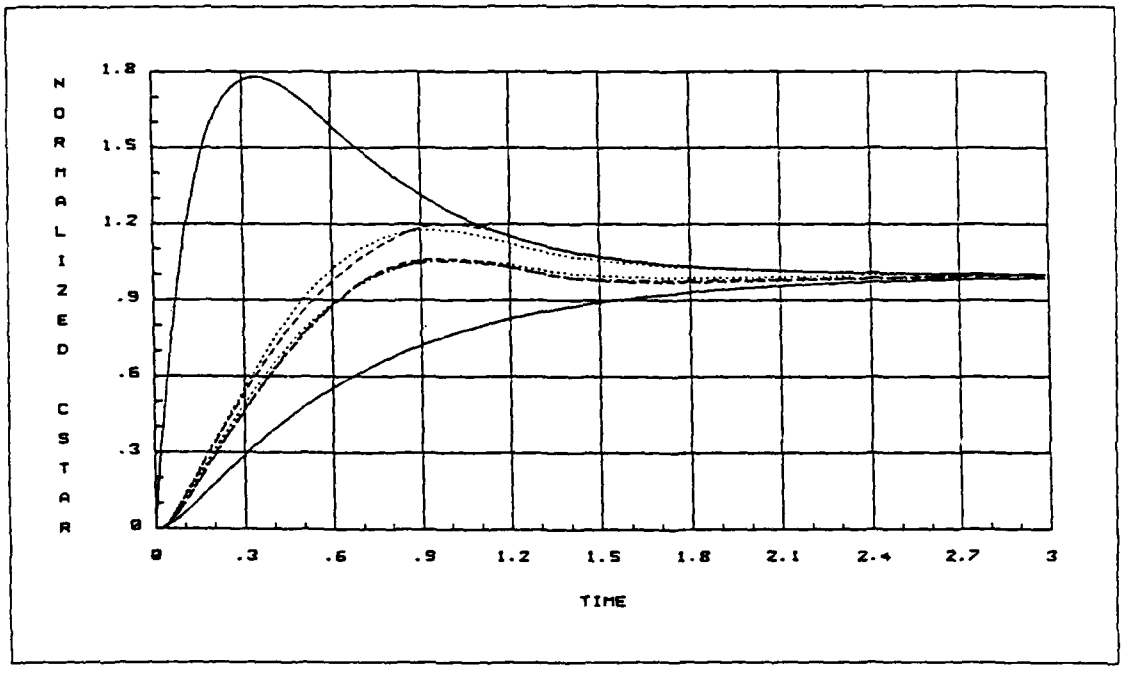

Figure C.24. Normalized Response at 30,000 ft 0.7M

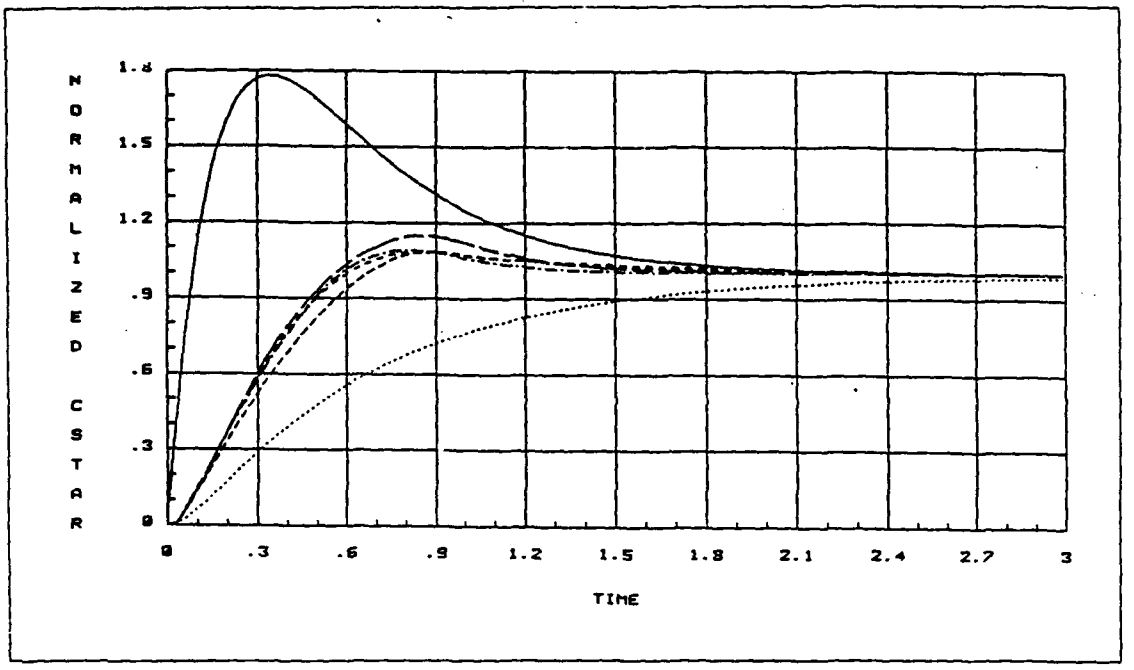

Figure C.25. Normalized Response at 30,000 ft 0.8M

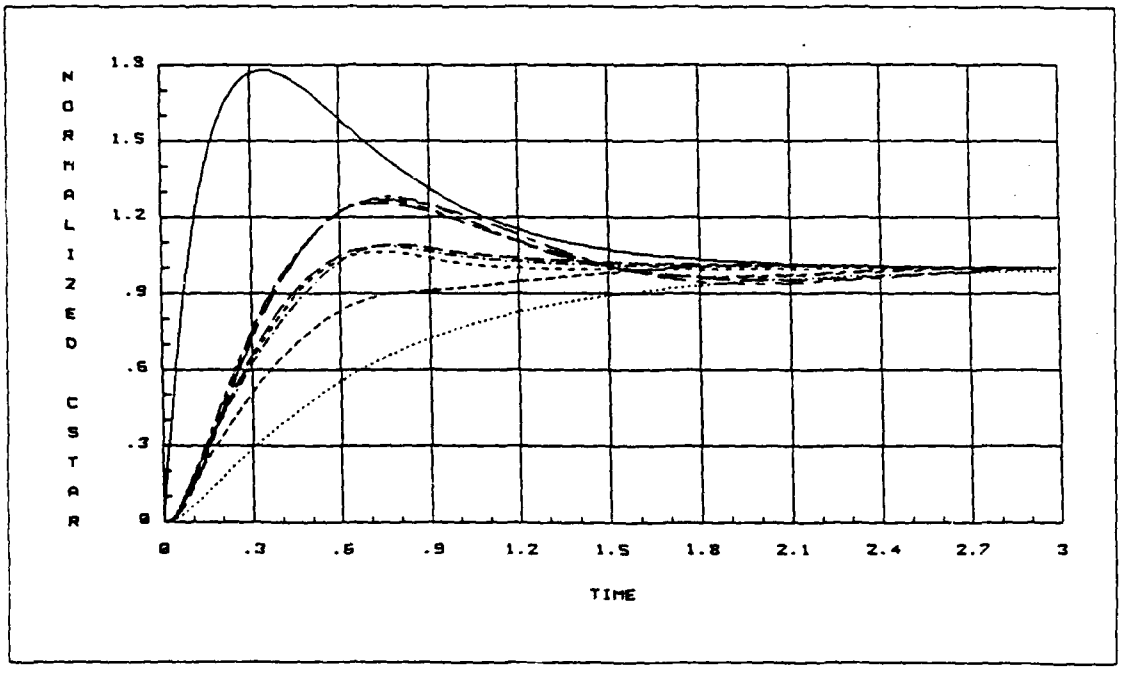

Figure C.26. Normalized Response at 30,000 ft 0.9M

Appendix D. *Fourth Order Padé Approximation*

The following Padé method is taken directly from an appendix of a digital control systems text [11] and applied to the function $e^{-\tau s}$ to obtain an approximation of a pure time delay.

The General Padé Method

The Padé method produces rational-fraction approximations of the form

$$F(x) = \frac{A_m(x)}{B_m(x)} \qquad m = 0, 1, 2, \ldots \tag{D.1}$$

for the differentiable power series

$$d(x) = c_0 + c_1 x + c_2 x^2 + c_3 x^3 + \cdots \tag{D.2}$$

where $c_0 \neq 0$ and $F(x) \approx g(x)$. $A_m(x)$ and $B_m(x)$ are polynomials of the form

$$A_m(x) = a_0 + a_1 x + a_2 x^2 + a_3 x^3 + \cdots + a_m x^m \tag{D.3}$$

$$B_m(x) = b_0 + b_1 x + b_2 x^2 + b_3 x^3 + \cdots + b_m x^m \tag{D.4}$$

where, for this discussion, the coefficients a_i and b_j are finite values other than zero.

Let

$$\mathbf{a} = \begin{bmatrix} a_0 \\ a_1 \\ a_2 \\ \vdots \\ a_m \end{bmatrix} \tag{D.5}$$

$$\mathbf{b} = \begin{bmatrix} b_0 \\ b_1 \\ b_2 \\ \vdots \\ b_m \end{bmatrix} \tag{D.6}$$

$$\mathbf{C_{p,q}} = \begin{bmatrix} c_q & c_{q-1} & \cdots & c_{q-p} \\ c_{q+1} & c_q & \cdots & c_{q-p+1} \\ \cdots & \cdots & \cdots & \cdots \\ c_{q+p-1} & c_{q+p-2} & \cdots & c_{q-1} \end{bmatrix} \qquad (D.7)$$

where the elements of Eq (D.1) whose subscripts are negative, that is $i - j < 0$, are all zero.

The coefficients of Eqs (D.3) and (D.4) may be solved from the following matrix equations:

$$\mathbf{C_{m,m+1}b} = \mathbf{0} \qquad (D.8)$$

$$\mathbf{C_{m+1,0}b} = \mathbf{a} \qquad (D.9)$$

The matrices $\mathbf{C_{m,m+1}}$ and $\mathbf{C_{m+1,0}}$ are obtained from Eq (D.7), where for the former $p = m$ and $q = m + 1$ and for the latter $p = m + 1$ and $q = 0$. Note that $\mathbf{a}$ and $\mathbf{b}$ are $(m + 1) \times 1$ vectors, $C_{m,m+1}$ is an $m \times (m + 1)$ matrix and $C_{m+1,0}$ is an $(m + 1) \times (m + 1)$ matrix.

The Approximation

The power series of e^x where $x = \tau s$ is expanded in a MacLaurin series about zero, resulting in

$$d(x) = e^x = 1 + x + \frac{x^2}{2!} + \frac{x^3}{3!} + \frac{x^4}{4!} + \cdots \qquad (D.10)$$

$d(x)$ is to be approximated by the fourth order rational fraction

$$F(x) = \frac{a_0 + a_1 x + a_2 x^2 + a_3 x^3 + a_4 x^4}{b_0 + b_1 x + b_2 x^2 + b_3 x^3 + b_4 x^4} \qquad (D.11)$$

where $m = 1, c_0 = c_1 = 1, c_2 = \frac{1}{2}, c_3 = \frac{1}{6}$, etc. From Eq (D.7) the following are obtained:

$$\mathbf{C_{4,5}} = \begin{bmatrix} c_5 & c_4 & c_3 & c_2 & c_1 \\ c_6 & c_5 & c_4 & c_3 & c_2 \\ c_7 & c_6 & c_5 & c_4 & c_3 \\ c_8 & c_7 & c_6 & c_5 & c_4 \end{bmatrix}$$

$$\mathbf{C}_{5,0} = \begin{bmatrix} c_0 & 0 & 0 & 0 & 0 \\ c_1 & c_0 & 0 & 0 & 0 \\ c_2 & c_1 & c_0 & 0 & 0 \\ c_3 & c_2 & c_1 & c_0 & 0 \\ c_4 & c_3 & c_2 & c_1 & c_0 \end{bmatrix}$$

Inserting these matrices into Eqs (D.8) and (D.9) results in for Eq (D.8)

$$\mathbf{C}_{4,5}\mathbf{b} = \begin{bmatrix} \frac{1}{5!} & \frac{1}{24} & \frac{1}{6} & \frac{1}{2} & 1 \\ \frac{1}{6!} & \frac{1}{5!} & \frac{1}{24} & \frac{1}{6} & \frac{1}{2} \\ \frac{1}{7!} & \frac{1}{6!} & \frac{1}{5!} & \frac{1}{24} & \frac{1}{6} \\ \frac{1}{8!} & \frac{1}{7!} & \frac{1}{6!} & \frac{1}{5!} & \frac{1}{24} \end{bmatrix} \begin{bmatrix} b_0 \\ b_1 \\ b_2 \\ b_3 \\ b_4 \end{bmatrix} = \mathbf{0} \qquad (D.12)$$

There are only 4 equations and 5 unknowns, setting $b_0 = 1$ Eq (D.12) becomes

$$\begin{bmatrix} 5 & 20 & 60 & 120 \\ 6 & 30 & 120 & 360 \\ 7 & 42 & 210 & 840 \\ 8 & 56 & 336 & 1680 \end{bmatrix} \begin{bmatrix} b_0 \\ b_1 \\ b_2 \\ b_3 \\ b_4 \end{bmatrix} = \begin{bmatrix} -1 \\ -1 \\ -1 \\ -1 \\ -1 \end{bmatrix} \qquad (D.13)$$

Solving for $\mathbf{b}$ gives

$$\mathbf{b} = \begin{bmatrix} 1 \\ \frac{-1}{2} \\ \frac{3}{28} \\ \frac{-1}{84} \\ \frac{1}{1680} \end{bmatrix}$$

Inserting the values of $\mathbf{C_{m+1,0}}$ and $\mathbf{b}$ into Eq (D.9) results in

$$\begin{bmatrix} 1 & 0 & 0 & 0 & 0 \\ 1 & 1 & 0 & 0 & 0 \\ \frac{1}{2} & 1 & 1 & 0 & 0 \\ \frac{1}{6} & \frac{1}{2} & 1 & 1 & 0 \\ \frac{1}{24} & \frac{1}{6} & \frac{1}{2} & 1 & 1 \end{bmatrix} \begin{bmatrix} 1 \\ \frac{-1}{2} \\ \frac{3}{28} \\ \frac{-1}{84} \\ \frac{1}{1680} \end{bmatrix} = \begin{bmatrix} a_0 \\ a_1 \\ a_2 \\ a_3 \\ a_4 \end{bmatrix}$$

Solving for $\mathbf{a}$ gives

$$\mathbf{a} = \begin{bmatrix} 1 \\ \frac{1}{2} \\ \frac{3}{28} \\ \frac{1}{84} \\ \frac{1}{1680} \end{bmatrix}$$

Inserting the values of $\mathbf{a}$, $\mathbf{b}$ and $x = \tau s$ into Eq (D.11) yields

$$F(x) = \frac{s^4 + \frac{20}{\tau}s^3 + \frac{180}{\tau^2}s^2 + \frac{840}{\tau^3}s + \frac{1680}{\tau^4}}{s^4 - \frac{20}{\tau}s^3 + \frac{180}{\tau^2}s^2 - \frac{840}{\tau^3}s + \frac{1680}{\tau^4}} \approx e^{\tau s} \qquad (D.14)$$

For the pilot model of Chapter VI the time delay of $\tau = -0.3$ gives the approximation used in the nonlinear simulations as

$$\begin{aligned} e^{-0.3s} &\approx \frac{s^4 - 66.667s^3 + 2000s^2 - 3.111 \times 10^4 s + 2.0741 \times 10^5}{s^4 + 66.667s^3 + 2000s^2 + 3.111 \times 10^4 s + 2.0741 \times 10^5} \\ &\approx \frac{(s - 14.03 \pm j17.7)(s - 19.31 \pm j5.78)}{(s + 14.03 \pm j17.7)(s + 19.31 \pm j5.78)} \end{aligned} \qquad (D.15)$$

Bibliography

1. Barfield, Finley Head Control Engineer AFTI/F-16. Personal interviews. Flight Dynamics Labs, Wright-Patterson AFB, OH 28 January through December 1988.
2. Dameron, Capt Gary G. *A Real-Time Simulator for Man-in-the-Loop Testing of Aircraft Control Systems (SIMTACS-RT).* MS thesis, AFIT/GE/ENG/88D-8. School of Engineering, Wright-Patterson AFB OH, December 1988.
3. D'Azzo, John J. Unpublished lecture notes from EENG 640, Automatic Control I. School of Engineering, Air Force Institute of Technology, Wright-Patterson AFB OH, Winter 1988.
4. East, D. J. "A New Approach to Optimal Loop Synthesis," *International Journal of Control, 34:* 731-748 (1981).
5. Hamilton, 2Lt Steve W. *QFT Digital Controller for an Unmanned Research Vehicle with an Improved Method for Choosing the Control Weightings.* MS thesis, AFIT/GE/ENG/87D-22. School of Engineering, Wright-Patterson AFB OH, December 1987.
6. Horowitz, Isaac M. "Improvement in Quantitative Nonlinear Feedback Design by Cancellation," *International Journal of Control, 34:* 547-560 (1981).
7. Horowitz, Isaac M. and Moshe Breiner. "Quantitative Synthesis of Feedback Systems with Uncertain Nonlinear Multivariable Plants," *International Journal of Systems Science, 12:* 539-563 (1981).
8. Horowitz, Isaac M. *et al. Research in Advanced Flight Control Design*, 1 June 1977 - 31 May 1979. Contract AFOSR-77-3355. Rehovot Israel: Dept of Applied Mathematics The Weizmann Institute of Science, January 1980 (AD-A082424).
9. Horowitz, Isaac M. and Uri Shaked. "Superiority of Transfer Function Over State-Variable Methods in Linear Time-Invariant Feedback System Design," *IEEE Transactions on Automatic Control, 20:* 84-97 (February 1975).
10. Horowitz, Isaac M. "Synthesis of Feedback Systems with Nonlinear Time-Varying Uncertain Plants to Satisfy Quantitative Performance Specifications, " *Proceedings of the IEEE, 64:* 123-130 (January 1976).
11. Horowitz, Isaac M. "The Singular-G Method for Unstable Non-Minimum-Phase Plants," *International Journal of Control, 49:* 533-541 (1986).
12. Houpis, Constantine H. and Gary B. Lamont. *Digital Control Systems Theory, Hardware, Software.* New York: McGraw Hill Book Company, 1988.
13. Houpis, Constantine H. *Quantitative Feedback Theory*, AFWAL-TR-86-3107. Dayton OH: AFWAL/FIGL, January 1987.

14. Houpis, Constantine H. Unpublished lecture notes from EENG 743, Literature Study in Current Control Topics. School of Engineering, Air Force Institute of Technology, Wright-Patterson AFB OH, Winter 1988.

15. Kabrisky, Matthew. Unpublished lecture notes from EENG 548, Human Factors Engineering. School of Engineering, Air Force Institute of Technology, Wright-Patterson AFB OH, Fall 1988.

16. Kassan, 2Lt Mark W. *F-16 Simulator for Man-in-the-Loop Testing of Aircraft Control Systems (SIMTACS).* MS thesis, AFIT/GE/ENG/87D-30. School of Engineering, Wright-Patterson AFB OH, December 1987.

17. Krishnan, K. R. and A. Cruickshanks. "Frequency-domain Design of Feedback Systems for Specified Insensitivity of Time-domain Response to Parametric Variation," *International Journal of Control, 25:* 609-620 (1977).

18. Neal, T. Peter, and Rogers E. Smith. *An In-Flight Investigation to Develop Control System Design Criteria for Fighter Airplanes,* AFFDL-TR-70-74, Vol. I, Air Force Flight Dynamics Laboratory: Wright-Patterson AFB Ohio, December 1970.

19. Quinlivan, Richard P. *Multimode Flight Control Definition Study: Final Report*, 29 March 1971 - 29 March 1972. Contract F33615-71-C-1485. Binghamton NY: G.E. Aerospace Instruments and Control System Department, May 1972.

20. Tobie, H. N., E. M. Elliott, and L.G. Malcom. *A New Longitudinal Handling Qualities Criterion,* National Aerospace Electronics Conference, Dayton Ohio, 16-18 May 1966.

21. Yaniv, O., Department of Electrical Engineering, Tel Aviv University. Personal interview. AFIT School of Engineering, Dayton OH, December 1987.

Vita

Lieutenant Thomas J. Kobylarz was born on [redacted] He graduated from high school in Ewing Twp., New Jersey in 1981 and attended the United States Air Force Academy from which he received the degree of Bachelor of Science in Electrical Engineering in May 1986. Upon graduation he received a regular commission in the Air Force and attended undergraduate pilot training at Laughlin AFB Texas from July 1986 to May 1987. In June of 1987 he entered the School of Engineering, Air Force Institute of Technology studying for a Masters Degree in Electrical Engineering.

Lieutenant Kobylarz is a member of the Tau Beta Pi and Eta Kappa Nu honor societies. Following his graduation from AFIT he will be assigned to the 4950th Test Wing, WPAFB Ohio.

[redacted]

UNCLASSIFIED
SECURITY CLASSIFICATION OF THIS PAGE

REPORT DOCUMENTATION PAGE

Form Approved
OMB No. 0704-0188

1a. REPORT SECURITY CLASSIFICATION UNCLASSIFIED	1b. RESTRICTIVE MARKINGS
2a. SECURITY CLASSIFICATION AUTHORITY	3. DISTRIBUTION/AVAILABILITY OF REPORT Approved for public release; distribution unlimited
2b. DECLASSIFICATION/DOWNGRADING SCHEDULE	
4. PERFORMING ORGANIZATION REPORT NUMBER(S) AFIT/GE/ENG/88D-19	5. MONITORING ORGANIZATION REPORT NUMBER(S)
6a. NAME OF PERFORMING ORGANIZATION School of Engineering 6b. OFFICE SYMBOL (If applicable) AFIT/ENG	7a. NAME OF MONITORING ORGANIZATION
6c. ADDRESS (City, State, and ZIP Code) Air Force Institute of Technology Wright-Patterson AFB, OH 45433-6583	7b. ADDRESS (City, State, and ZIP Code)
8a. NAME OF FUNDING/SPONSORING ORGANIZATION AF Wright Aeronautical Lab 8b. OFFICE SYMBOL (If applicable) AFWAL/FDCX	9. PROCUREMENT INSTRUMENT IDENTIFICATION NUMBER
8c. ADDRESS (City, State, and ZIP Code) Wright-Patterson AFB, OH 45433	10. SOURCE OF FUNDING NUMBERS PROGRAM ELEMENT NO. / PROJECT NO. / TASK NO. / WORK UNIT ACCESSION NO.
11. TITLE (Include Security Classification) See box 19	
12. PERSONAL AUTHOR(S) Thomas J. Kobylarz, B.S.E.E. 1 Lt, USAF	
13a. TYPE OF REPORT MS Thesis 13b. TIME COVERED FROM _____ TO _____	14. DATE OF REPORT (Year, Month, Day) 1988 December 15. PAGE COUNT 113
16. SUPPLEMENTARY NOTATION	

17. COSATI CODES			18. SUBJECT TERMS (Continue on reverse if necessary and identify by block number)
FIELD	GROUP	SUB-GROUP	Quantitative Feedback Theory, Nonlinear Systems, Pilot Compensation, Pilot Modeling, Man-in-the-loop, Neal-Smith
01	04		

19. ABSTRACT (Continue on reverse if necessary and identify by block number)

Title: FLIGHT CONTROLLER DESIGN WITH NONLINEAR AERODYNAMICS, LARGE PARAMETER UNCERTAINTY, AND PILOT COMPENSATION

Thesis Chairman: Dr. Constantine H. Houpis
Professor of Electrical Engineering

Approved for Public Release IAW AFR 190-1
10 Jan 89

20. DISTRIBUTION/AVAILABILITY OF ABSTRACT ☒ UNCLASSIFIED/UNLIMITED ☐ SAME AS RPT. ☐ DTIC USERS	21. ABSTRACT SECURITY CLASSIFICATION UNCLASSIFIED
22a. NAME OF RESPONSIBLE INDIVIDUAL Dr. Constantine H. Houpis	22b. TELEPHONE (Include Area Code) (513) 255-2024 22c. OFFICE SYMBOL AFIT/ENG

DD Form 1473, JUN 86 *Previous editions are obsolete.* SECURITY CLASSIFICATION OF THIS PAGE

UNCLASSIFIED

Nonlinear Quantitative Feedback Theory (QFT), developed by Dr. Isaac Horowitz, is used to design a flight control system for the YF-16 aircraft. Upon completing this stability augmentation system (SAS) additional compensation is added to reduce pilot workload while improving handling qualities.

The YF-16 uncertain plant is simulated with C^* (a blend of normal acceleration at pilot station and pitch rate) as the controlled output. The simulation includes the full six degree of freedom nonlinear dynamic equations of motion and aerodynamic data throughout the entire subsonic flight envelope. A technique is presented which enables the uncertain nonlinear YF-16 to be represented as a set of linear time-invariant plants which is equivalent to the nonlinear plant with respect to the set of acceptable outputs. Once this set of plants is obtained, a linear QFT controller is synthesized yielding fixed compensation which is extremely insensitive to varying flight conditions.

Given the aircraft and resulting flight controller, additional compensation is generated which accounts for the man-in-the-loop. The Neal-Smith pilot model for a compensatory tracking task is used to develope a technique which allows the designer to synthesize compensation which minimizes pilot workload, increases system bandwidth, and improves handling qualities ratings. The presented technique is applicable to other aircraft and pilot tasks, possessing a similar pilot model, given the desired standards of performance. This technique can be used at the earliest stages of flight control design phase thus saving time and money over the current practice.

Simulations in the time and frequency domains demonstrate that the desired performance is attained. Further work with real-time man-in-the-loop simulations should be accomplished to expand the area of pilot compensation.